TITANIA-SILICA GEL-GLASSES

BY

YEU-CHYI CHENG

A DISSERTATION PRESENTED TO THE GRADUATE SCHOOL
OF THE UNIVERSITY OF FLORIDA
IN PARTIAL FULFILLMENT OF THE REQUIREMENTS
FOR THE DEGREE OF DOCTOR OF PHILOSOPHY

UNIVERSITY OF FLORIDA

1991

Dedicated to My Family

ACKNOWLEDGEMENTS

It is really difficult for me to acknowledge everyone who helped me through the completion of this work.

I am grateful to Professor Larry L. Hench, supervisory committee chairman, for his continual advice and support, and for the freedom he has given me during the course of this research.

I would like to thank Drs. Joseph Simmons, David E. Clark, Brij M. Moudgil and Dinesh O. Shah for their invaluable advice and discussion, and for serving as the members of my supervisory committee.

Special thanks go to Dr. Jon K. West for his invaluable discussion and support during this research.

Thanks are also extended to Guy P. Latorre and Al G. Fosmoe II at the AMRC for their assistance in the laboratory.

Financial support from the Air Force Office of Scientific Research under contract #F49620-88-C-0073 is also greatly appreciated.

TABLE OF CONTENTS

Page

ACKNOWLEDGEMENTS iii

LIST OF TABLES vii

LIST OF FIGURES viii

ABSTRACT xv

CHAPTERS

I INTRODUCTION 1

1.1 Sol-Gel Processing 3

1.2 Objectives of This Study 10

II LITERATURE REVIEW 13

2.1 Introduction 13

2.2 Sol-gel procedure for Making Titania-Silica Glasses 15
2.2.1 Co-Hydrolysis 15
2.2.2 Pre-Hydrolysis 18
2.2.3 Colloidal Sol-Gel Process 21

2.3 Characterization of Sol-Gel Derived TiO_2-SiO_2 Glass 24
2.3.1 Chemical Analysis 24
2.3.2 Thermal Characterization 25
2.3.3 Structural Characterization 29
2.3.4 Physical Properties 37
2.3.5 Spectroscopy 40

2.4 Summary 44

III EXPERIMENTAL PROCEDURES 47

3.1 Sol Preparation 47

3.2 Gelation and Aging 49

3.3 Drying 54

3.4 Characterization Techniques 54
3.4.1 Thermal Analysis 54
3.4.2 Structural Analysis 58
3.4.3 Physical Property Characterization 59
3.4.4 Chemical Analysis 60
3.4.5 Spectroscopy Characterization 60

IV THERMAL CHARACTERIZATION 63

4.1 Thermogravimetric Analysis 63

4.2 Dilatometry 74
4.2.1 Effect of Thermal Treatment 76
4.2.2 Effect of Adsorbed Water 76
4.2.3 Effect of Atmosphere 90
4.2.4 Effect of Heating Rate 93
4.2.5 Effect of Titania Content 103

V PHYSICAL AND CHEMICAL CHARACTERIZATION 107

5.1 Structural Analysis 107
5.1.1 X-Ray Diffraction 108
5.1.2 Density 111
5.1.2.1. Effect of titania content 111
5.1.2.2 Effect of sintering atmosphere 117
5.1.3 Characterization of Texture 118
5.1.3.1. Gas adsorption analysis 118
5.1.3.1.1 Characterization of dried gels ... 118
5.1.3.1.2 Densification 125
5.1.3.2 Topological analysis 141
5.1.3.3 Calculation of viscosity of titania-silica glasses 156

5.2 Physical Properties 162

5.3 Composition and Spectroscopy Characterization . 170
5.3.1 Composition of Gel-Glasses 173
5.3.2 X-ray Photoelectron Spectroscopy 173
5.3.3 Fourier Transform Infrared Spectroscopy ... 180
5.3.4 Raman Spectroscopy 202
5.3.5 UV/VIS/NIR Spectroscopy 206

VI QUANTUM CALCULATIONS 215

6.1 Introduction 215

6.2 Structure of the Titania Doped Silica 220

6.3 Quantum Calculations of UV-Cutoff for Titania-Silica 229

6.4 Quantum Calculations of Water Adsorption onto Titania-Silica 229

VII CONCLUSIONS AND FUTURE DIRECTIONS 235
REFERENCES 241
BIOGRAPHICAL SKETCH 250

LIST OF TABLES

Table		Page
2.1	Thermal expansion of titania-silica	28
2.2	Density of titania-silica glass	32
5.1	Neutron activation analysis of titania-silica gels	174
5.2	Results of XPS investigations	179
5.3	Results from high pressure IR study	199
5.4	UV/VIS/NIR peak assignment	208
6.1	INDO energies of titanium doped structures	221
6.2	Bond distance of ring structure	226
6.3	Bond angle of ring structure	227
6.4	Dilation of titanium doped silica structure	232

LIST OF FIGURES

Figure		Page
1.1	Schematic illustration of sol-gel processing	11
2.1	Thermal expansion of titania-silica glasses (a) prepared by colloidal sol-gel method	30
2.1	Thermal expansion of titania-silica glasses (b) prepared by flame hydrolysis method	31
2.2	Vicker hardness of titania-silica gels as a function of temperature	38
2.3	Refractive index and density for gel-glasses with various titania contents	39
2.4	Infrared spectra of the glasses and precipitated crystals of the titania-silica system	41
3.1	Schematic illustration of the sol-gel processing of 5% titania-silica gel monoliths	48
3.2	Variation of gelation time with titania content.	51
3.3	Variation of gelation time with R ratio	52
3.4	Typical aging schedule for the preparation of titania-silica gels	53
3.5	Typical drying temperature profile for the preparation of titania-silica gels	55
3.6	Photograph of dried titania-silica gel monoliths	56
4.1	TGA for a dried 3% titania-silica gel	64
4.2	TGA of dried 5% titania-silica gel under different atmospheres	66
4.3	TGA of dried 8% titania-silica gel under different atmospheres	67

4.4 TGA for 3% titania-silica gels densified to various temperatures 68

4.5 TGA for 5% titania-silica gels densified to various temperatures 69

4.6 Derivative of TGA traces for 3% titania-silica gels densified to various temperatures 70

4.7 Derivative of TGA traces for 5% titania-silica gels densified to various temperatures 71

4.8 TGA plot for partially densified (615°C) titania-silica gel-glass under thermal cycling 73

4.9 Variation of linear dimension with temperature for a 5% titania-silica gel partially densified at 615°C 75

4.10 Variation of linear dimension with temperature for a set of 3% titania-silica gels previously densified in the range of 170°C to 850°C 77

4.11 Variation of linear dimension with temperature for a set of 5% titania-silica gels previously densified in the range of 170°C to 850°C 78

4.12 Variation of linear dimension with temperature for a set of 7% titania-silica gels previously densified in the range of 170°C to 850°C 79

4.13 Variation of linear dimension under vacuum with time for a partially densified 5% titania-silica gel-glass 82

4.14 Variation of linear dimension with time for a 5% titania-silica with respect to silica 87

4.15 Thermal hysteresis from dilatometry for pure silica gel-glass with various pore radius 89

4.16 Variation of linear dimension with temperature for a 5% titania-silica gel tested under vacuum 91

4.17 Variation of linear dimension change with temperature for 5% titania-silica gel under different atmospheres 92

4.18 Variation of linear dimension change with temperature for dried 5% titania-silica gel under various heating rates 94

4.19 Variation of linear dimension change with temperature for a partially densified 5% titania-silica gel under various heating rates . 96

4.20 Plot of Ln(shrinkage) vs. 1/T under various heating rates for 5% titania-silica gels previously densified at 615°C 99

4.21 Plot of Ln(shrinkage) vs. 1/T for 5% titania-silica gels under various heating rates 101

4.22 Plot of Ln(shrinkage) vs. Ln(heating rate) for 5% titania-silica gel. n is determined from the slope in the interval 0.5 to 3 °C/min 102

4.23 Linear thermal expansion of sol-gel derived titania-silica glasses with various titania contents 104

4.24 Coefficients of thermal expansion for titania-silica glasses with various titania contents .. 106

5.1 X-ray diffraction patterns of silica and 10% titania-silica gels 109

5.2 X-ray diffraction pattern of 10% titania-silica gel densified at 1100°C 110

5.3 X-ray diffraction of titania-silica gels 112

5.4 Variation of bulk density with titania content for dried titania-silica gels 113

5.5 Variation of bulk density with temperature for gels with various titania contents 114

5.6 Variation of true density with temperature for gels with various titania contents 116

5.7 Variation of bulk density with temperature for 3% titania-silica gel-glasses under different atmospheres 119

5.8 Variation of bulk density with temperature for 5% titania-silica gel-glasses under different atmospheres 120

5.9 BET plot for a 3% titania-silica gel monolith 122

5.10 Adsorption-desorption isotherm for a dried 3% titania-silica gel monolith 123

5.11 Pore size distribution for a dried 3% titania-silica gel monolith 124

5.12 Variation of pore radius with titania content for dried titania-silica gels 126

5.13 Variation of specific surface area with titania content for dried titania-silica gels 127

5.14 Variation of pore volume with titania content for dried titania-silica gels 128

5.15 Variation of specific surface area with R ratio for 5% titania-silica dried gels 129

5.16 Variation of pore volume with R ratio for 5% titania-silica dried gels 130

5.17 Variation of pore radius with R ratio for 5% titania-silica dried gels 131

5.18 Variation of specific surface area with temperature for 3% titania-silica gels 132

5.19 Variation of pore volume with temperature for 3% titania-silica gels 133

5.20 Variation of pore radius with temperature for 3% titania-silica gels 135

5.21 Variation of pore volume with temperature for gels with various titania contents 136

5.22 Variation of specific surface area with temperature for gels with various titania contents 137

5.23 Variation of pore radius with temperature for gels with various titania contents 138

5.24 Plot of pore volume distribution for 5% titania-silica gels densified to various temperatures 139

5.25 Plot of pore surface area distribution for 5% titania-silica gels densified to various temperatures 140

5.26 Variation of surface area with pore volume for gels with various titania contents 142

5.27 Variation of surface area with pore volume for 3% titania-silica gels densified to various temperatures 143

5.28 Variation of surface area with pore volume for 5% titania-silica gels densified to various temperature 144

5.29 Variation of volume fraction of pores with densification temperature for gels with various titania contents 147

5.30 Variation of Sv with densification temperature for gels with various titania contents 148

5.31 Plot of Sv vs. Vv for gel-glasses containing various amount of titania 150

5.32 Variation of Bv, Nv, and Gv with densification temperature for 3% titania-silica gel-glass ... 151

5.33 Variation of Bv, Nv, and Gv with densification temperature for 5% titania-silica gel-glass ... 152

5.34 Variation of Bv, Nv, and Gv with densification temperature for 8% titania-silica gel-glass ... 153

5.35 Plot of strain point, annealing point and onset temperature of pore closure for titania-silica gel-glasses 155

5.36 Plot of Log(viscosity) vs. 1/T 163

5.37 Variation of microhardness with titania content for dried gels 164

5.38 Variation of microhardness with densification temperature for gels with various titania contents 165

5.39 Effect of humidity on the microhardness for 5% titania-silica gel-glass 167

5.40 Variation of refractive index with titania content for dried gels 168

5.41 Variation of refractive index with density for 3% titania-silica gel-glass 169

5.42 Variation of refractive index with density for silica and titania-silica systems 171

5.43 XPS spectrum of 3% titania-silica gel-glass. (a) Si(2p) peak 176

5.43 XPS spectrum of 3% titania-silica gel-glass. (b) O(1s) peak 177

5.43 XPS spectrum of 3% titania-silica gel-glass. (c) Ti(2p) peak 178

5.44 FTIR spectra of dried titania-silica gels 181

5.45 Plot of peak intensity ratio (I940/I1071) as a function of titania contents for dried gels ... 183

5.46 FTIR spectra of 3% titania-silica gels densified to various temperatures 185

5.47 FTIR spectra of 15% titania-silica gels densified to various temperatures 186

5.48 FTIR of the titania-silica system. (a) alkoxide derived gel-glasses 187

5.48 FTIR of the titania-silica system. (b) Corning ULE glass 188

5.49 Comparison of FTIR spectra for pure silica and 5% titania-silica gel-glasses 190

5.50 Variation of peak position with pressure for 0% titania-silica gel-glass 192

5.51 Variation of peak position with pressure for 3% titania-silica gel-glass. (a) peak at 800 cm^{-1} 193

5.51 Variation of peak position with pressure for 3% titania-silica gel-glass. (b) peak at 940 cm^{-1} 194

5.52 Variation of peak position with pressure for 8% titania-silica gel-glass. (a) peak at 800 cm^{-1} 195

5.52 Variation of peak position with pressure for 8% titania-silica gel-glass. (b) peak at 940 cm^{-1} 196

5.53 Raman spectrum for dried 8% titania-silica gel 203

5.54 Raman spectrum for 3% titania-silica gel previously densified at 615°C 204

5.55 Raman spectrum for 8% titania-silica gel previously densified at 615°C 205

5.56 UV/VIS/NIR spectrum for a dried 5% titania-silica gel monolith 207

5.57 Variation of UV transmission with titania content for dried gels 208

5.58 Variation of UV cut-off with titania content for dried gels 211

5.59 Variation of UV/VIS/NIR spectra for a set of 5% titania-silica gels densified to various temperatures 212

5.60 Variation of UV transmission for 5% titania-silica gels densified to various temperatures . 213

6.1 2-D projection of chain structure of four silica tetrahedra 218

6.2 2-D projection of ring structure of four silica tetrahedra 219

6.3 INDO calculations 223

6.4 2-D projection of titanium doped ring structure 225

6.5 2-D projection of titanium doped ring structure with a hydrogen bonded water 231

Abstract of Dissertation Presented to the Graduate School of the University of Florida in Partial Fulfillment of the Requirements for the Degree of Doctor of Philosophy

TITANIA-SILICA GEL-GLASSES

By

Yeu-Chyi Cheng

May 1991

Chairman: Dr. Larry L. Hench
Major Department: Materials Science and Engineering

A method for producing large TiO_2-SiO_2 gel monoliths using the alkoxide sol-gel method has been developed. The gels were prepared using tetramethylorthosilicate and titanium isopropoxide as the precursors and catalyzed under acidic conditions. The sols gelled in 1 day and were dried in 4 days. The method developed does not require the addition of alcohol as solvent

Physical properties, i.e. bulk density, microhardness, specific surface area, pore volume and pore radius, of the dried gels with various titania contents (3 to 15%) are nearly identical. The refractive index, though, increases with increasing titania contents.

All the physical properties change as densification proceeds. Below 600 °C, the changes were not significant while above 600°C, these properties varied rapidly with densification temperature. X-ray diffraction indicated that for less than 10 wt% titania, the glasses obtained by heating

to 900 °C for 15 hours were not crystallized, while for the 15 wt% TiO_2 glass the crystalline phase of anatase developed.

The linear thermal expansion coefficient of the alkoxide derived TiO_2-SiO_2 glasses decreased with increasing TiO_2 content similarly to TiO_2-SiO_2 glasses prepared by the flame hydrolysis method.

Structural changes occurring during thermal treatment were monitored by FTIR Spectroscopy. The network progressively strengthened as densification proceeded. The characteristic peaks for vitreous silica, however, shift to lower wavenumbers for titania doped vitreous silica. This results from the introduction of Ti-O bonds which are of weaker character than Si-O bonds.

Variation with densification of water content in the network was monitored using UV/VIS/NIR spectroscopy. A shift of the UV cut-off to higher wavelength is observed with increasing titania content and with increasing amount of water in the network.

The binding energy for the tetrahedrally coordinated titanium is determined to be 460.6 eV using XPS. This is 1.9 eV higher than the octahedrally coordinated titanium present in TiO_2.

Quantum calculations were performed using a ring cluster of 4 tetrahedra as model structure. Results correlate well with the experimental data in terms of the shift in the UV cutoff, density of the structure, as well as structural dilation of the porous gel monolith upon water adsorption.

CHAPTER I
INTRODUCTION

In recent years, an increasing number of glasses and/or ceramics have been prepared by the sol-gel method. This method does not involve melting a mixture of crystalline raw materials. Instead, for example, mixtures of liquid solutions (alkoxides) are reacted via hydrolysis and condensation/polymerization reactions to form a solid network with liquid dispersed throughout the structure. A suitable drying treatment is then applied to expel the liquid. Subsequent dehydration and/or oxidation frees the gel of its organic constituents and hydroxyls. A final densification step is necessary to convert the gel into a solid glass devoid of residual porosity.

The development of the sol-gel process has provided a unique method for preparing TiO_2-SiO_2 glasses with various titania concentrations. This is a glass forming system which possesses unique properties. It has very low thermal expansion (in some cases negative), and at the same time, it forms some of the most refractory glasses known (more refractory than fused quartz). The system may also have an additional attraction over quartz for high

temperature applications where resistance to alkali attack is required [1].

Traditionally, glasses are made by melting. This is carried out by intimately mixing the raw materials in the solid state. The mixture is then heated above its melting temperature to yield a viscous liquid. The melt is then cooled below its glass transition temperature to form a glass. The purity of glasses thus made is adversely affected by the reaction between the melt and the refractory materials of the containers at elevated temperature.

The lowest liquidus temperature in the TiO_2-SiO_2 binary system, however, is at 1550 °C which corresponds to 10%TiO_2-90%SiO_2 [2]. There are considerable difficulties encountered during the melting and processing of this glass. The flame hydrolysis method, on the other hand, is inefficient and environmentally objectionable. As for induction melting, not only is it expensive but it generally leads to reduction of the titania, thus the glass loses its transparency.

The development of the sol-gel method provides an alternative route for preparing the TiO_2-SiO_2 glasses. It is the purpose of this work to develop a reliable method for preparing monolithic titania-silica gels via the alkoxide sol-gel route. The evolution of the structure

and physical properties of these nanometer scale alkoxide derived gel monoliths is also studied as densification proceeds. The following section gives a general overview of sol-gel processing. The processing used in this work is based upon the principles developed over many years.

1.1 Sol-Gel Processing

The history of sol-gel processing began in the 1800's with the studies by Ebelman [3,4] and Graham [5] on silica. These early investigators observed that the hydrolysis of tetraethylorthosilicate, $Si(OC_2H_5)_4$, at low pH resulted in the formation of SiO_2 as a "glass-like material" [3]. Interest in gels continued throughout the 19th century which resulted in a huge volume of descriptive literature. However, the understanding of the physical and chemical principles of the system did not increase.

The next significant development came in the 1950's and 1960's when R. Roy and co-workers recognized the potential of using the sol-gel method for achieving molecular level mixing [6-9]. They used this technique and synthesized a number of oxide composition, involving Al, Si, Ti, Zr, etc., that could not be produced by the traditional powder methods. Concurrent work of Iler [10]

and Stöber [11] in this period revealed the importance of catalysts, alkoxide type and concentration, pH and reaction temperature as processing parameters. Their work led to the commercial development of Ludox™ spheres as well as the so-called Stöber spherical silica powder.

During the past decade, an enormous growth in the interest in the sol-gel process developed. This was stimulated largely by the work of Zarzycki, Prassas and Phallipou [12,13], who demonstrated that large fully dense silica glass monoliths can be produced, using hypercritical drying, via the sol-gel method. Yoldas also showed that large monolithic pieces of alumina could be made [14]. These developments revealed practical routes for making new materials with unique properties.

Mackenzie has summarized a number of potential advantages, disadvantages and the relative economics of sol-gel methods in general [15,16]. The potential advantages of the sol-gel method include: (1) structural manipulation on an extremely fine scale, within the nanometer range and (2) much lower processing temperature, which prevents impurity pick-up. Thus, materials with higher purity and homogeneity can be obtained at a lower processing temperature compared to the traditional glass melting or ceramic powder methods.

Sol-gel derived pure silica, for example [17-19], has high homogeneity and purity, low optical loss as well as the near net shape casting capability. These features make the silica potentially applicable to a wide range of optical components, such as lenses, mirrors, waveguides and host materials for filters,lasers as well as non-linear optical elements or compounds.

In sol-gel processing, sols are dispersions of colloidal particles, i.e. solid particles with diameters ranging from 1 to 100 nm, in a liquid [20]. A gel is a interconnected, rigid, 3-dimensional network with pores of sub-micrometer dimension [21].

Generally, three approaches are used to make sol-gel monoliths: (1) gelation of a solution containing colloidal powders via evaporation or destabilization, (2) hydrolysis and polycondensation of alkoxide or nitrate precursors followed by hypercritical drying and (3) hydrolysis and polycondensation of alkoxide precursors followed by aging and drying under ambient atmosphere.

In method 1, a gel may be formed by network growth from an array of discrete colloidal particles. In this case, a suspension of colloidal particles, or sol, is formed by mechanical mixing the colloidal particles at a pH that prevents precipitation [10]. The sol is then cast into a mold and with time, the colloidal particles and

condensed silica species linked together to become a three dimensional network.

A gel can also be formed through simultaneous hydrolysis and polycondensation by mixing the precursors with water (methods 2 and 3). Here, the liquid alkoxide precursor, such as $Si(OR)_4$, where R is CH_3 or C_2H_5 is hrdrolyzed by mixing with water:

$$\text{hydrolysis: } Si(OR)_4 + 4H_2O \rightarrow Si(OH)_4 + 4ROH \qquad (2.1)$$

The condensation reaction then follows, forming ≡Si-O-Si≡ linkages:

$$\text{condensation: } \begin{array}{c} | \\ -Si-OH \\ | \end{array} + \begin{array}{c} | \\ HO-Si- \\ | \end{array} \rightarrow \begin{array}{c} | \\ -Si-O-Si- \\ | \end{array} + H_2O \qquad (2.2)$$

Linkage of the $Si(OH)_4$ tetrahedra occurs as a polycondensation reaction. When sufficient interconnected Si-O-Si bonds are formed in a region, they can respond cooperatively as colloidal particles, or as a sol. As the sol particles grow and collide, condensation takes place and macroparticles form. The sol becomes a gel when it can support a stress elastically. The H_2O and alcohol expelled from the above reactions constitute the pore-liquid.

After the gel is formed, it is maintained in liquid for a period of time. This is called aging or syneresis. During this process, the strength of the gel is increased due to the increase in interparticle necks. This results from the continuation of polycondensation as well as localized solution and reprecipitation of the gel network. Factors such as time, temperature and pH can effectively alter the aging process [10,22]. Thus, the structure of the gel formed can be further modified in this stage. A gel must develop sufficient strength in order to resist cracking during drying.

Drying is a process in which the liquid is removed from the interconnected pore network. There are two routes for removing the pore liquid: (1) via hypercritical drying and (2) via thermal evaporation. In hypercritical drying, the liquid is removed as a gas phase at a condition above its critical point. The network thus formed, which is called an *aerogel*, does not collapse and has a low density. When the pore liquid is removed at or near ambient pressure by thermal evaporation, the network collapses and shrinkage of the gel occurs. The monolith thus formed is called an *xerogel*. From a practical point of view, the *xerogel* route is more attractive as it avoids the high temperatures and pressures involved in producing *aerogel*.

There are three stages of drying as described by Sherwood [23-25]:

Stage 1 (or the constant rate period) [26-30]: During this stage, the volume of the pore liquid lost by evaporation is equal to the reduction in volume of the gel and the meniscus remains at the surface. The large capillary forces generated within the pores collapse the structure and the gel undergoes considerable shrinkage. This behavior is applicable to base catalyzed alkoxide gels with average pore diameters > 20 nm as well as gels made by colloidal precipitation.

Stage 2 (or the first falling rate period) [26-31]: The second stage of drying begins when the strength of the network has increased sufficiently to resist further shrinkage. This starts at the critical point. The meniscus now is drawn below the surface and pores begin to empty. The remaining liquid is transported through small saturated pores and through continuous films on the pore surface to the surface of the body where it evaporates.

Stage 3 (or the second falling rate period) [25]: The third stage of drying begins when the pores have substantially emptied and the surface films along the pore can no longer be sustained. The remaining liquid can then escape only by evaporation from within the pores and diffusion of vapor to the surface. There are no further

dimensional changes in this stage. Rather, this is a slow progressive loss of weight until equilibrium, determined by the ambient temperature and partial pressure of water, is reached.

A gel is termed "dried" when all of its physically adsorbed water is completely evacuated. This usually occurs between 100 °C and 180 °C [32].

In order to be used in an ambient environment, a gel needs to be thermally and chemically stabilized [32]. This is due to the fact that there is a large concentration of silanol groups on the surface of the pores. Thermal stabilization involves reducing the surface area sufficiently to enable the material to be used at a given temperature without reversible structural changes. Chemical stabilization involves removing the concentration of surface silanols below a critical level so that the surface does not rehydroxylate in use. The mechanisms of these two are interrelated due to the effects that surface silanols and chemisorbed water have on structural changes.

The final step of processing a gel is densification. By heating the porous gel at high temperature, the pores are eliminated via (1) capillary contraction; (2) condensation; (3)structural relaxation; (4) viscous sintering [33], leading to increase of the bulk density.

The temperature of the beginning of densification depends on the amount of water present in the gel as well as the dimension of the pore network. The more the water, the lower the viscosity [34,35], thus lowering the densification temperature. Figure 1.1 is a schematic illustration which summarizes the seven processing steps in the sol-gel method described above.

1.2 Objectives of This Study

The purpose of this work is to develop a reliable method for preparing monolithic titania-silica gels via the alkoxide sol-gel route. The evolution of the structure and physical properties of these nanometer scale alkoxide derived gel monoliths is also studied as densification proceeds. Quantum calculations are also performed in order to evaluate the effect of titanium ions on the silica and their results are correlated with the experimental data of titania-silica gels.

A general overview of the sol-gel method concerning the seven processing steps has been described in the previous section. Chapter II reviews the literature which concerns the preparation and properties of the sol-gel derived titania-silica gels and gel-glasses. The majority of the samples in these studies are powders and in best

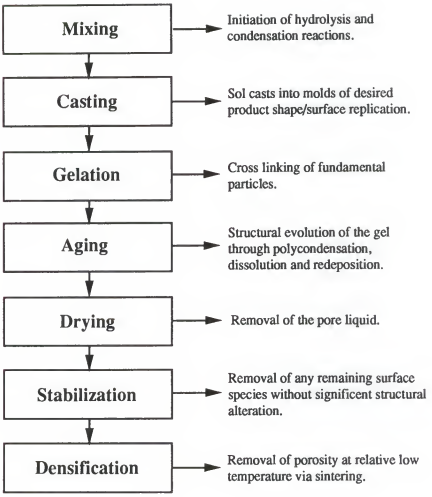
Mixing
Initiation of hydrolysis and condensation reactions.
Casting
Sol casts into molds of desired product shape/surface replication.
Gelation
Cross linking of fundamental particles.
Aging
Structural evolution of the gel through polycondensation, dissolution and redeposition.
Drying
Removal of the pore liquid.
Stabilization
Removal of any remaining surface species without significent structural alteration.
Densification
Removal of porosity at relative low temperature via sintering.

Figure 1.1 Schematic illustration of sol-gel processing.

cases cracked pieces. The method employed in this study for the preparation of the titania-silica gels and the experimental techniques used for characterization are described in Chapter III. The process developed yields large monolithic samples with high yield. Data on thermal characterization with emphasis on dilatometry are reported in Chapter IV. In Chapter V, data on the evolution of physical and chemical properties with densification are presented. Results of quantum calculations and their correlation with the experimental data are presented in Chapter VI. The general conclusions of this study are given in Chapter VII.

CHAPTER II
LITERATURE REVIEW

2.1 Introduction

Vitreous silica glasses containing titanium have received considerable interest in the past due to their unusual thermal expansion behavior. It is well known that a low concentration of TiO_2 decreases the thermal expansion of vitreous silica. Therefore, with certain amounts of TiO_2, it is possible to obtain a glass with zero thermal expansion.

Probably the first report of TiO_2-SiO_2 glasses having an expansion coefficient lower than vitreous silica was the patent by Norberg [36]. He reported a series of binary silicate glasses having decreased thermal expansion coefficients as the TiO_2 content increased in the 5-11wt% range. Dietzel [37] attributed this unusual behavior to the direct replacement of silicon cations by titanium cations in the glass network. However, only a very brief explanation of the phenomena was given.

Later in 1966, Corning introduced on the market a zero expansion glass under code number 7971. This is a binary

titanium silicate glass having an expansion coefficient of essentially zero in the 5-35°C range.

Conventionally, the titania doped silica glasses are produced either by batch melting or by flame hydrolysis. In the flame hydrolysis process, vapor of $TiCl_4$ and $SiCl_4$ are oxidized in a two-burner furnace to produce a glassy particulate (spheres ~ 100 to 1000Å in diameter) which are ejected from a flame and deposited on a refractory cup at ~1750°C. This amorphous soot immediately sinters together under the heat from the flame to produce a vitreous mass [38]. Although this method can produce clear glasses containing more than 10wt% titania, the deposition rate is relatively slow and complex shapes must be machined from the bulk glasses.

In recent years, the sol-gel technique has been successfully applied to prepare silica [17-19,39] and silicate glasses [40-44] at a relatively lower temperature. This method has the advantages of better homogeneity, better purity, lower processing temperature and even the possibility of preparing glasses which otherwise have a strong tendency to crystallize upon cooling [15,16]. The sol-gel method also has the important advantage of producing near net shape optical components without excessive grinding or polishing [17-19]. The following

section summarizes the sol-gel route in the literature for making TiO_2-SiO_2 glasses.

2.2 Sol-Gel Procedure for Making Titania-Silica Glasses

The sol-gel route for making binary titania-silica system has been attempted by many workers [45-60]. The alkoxide precursors used for silica are mostly silicon tetramethoxide (TMOS) or silicon tetraethoxide (TEOS). On the other hand, titanium ethoxide (TET), titanium isopropoxide (TIP) and titanium butoxide (TB) are most commonly used as precursors for titania. The procedures for preparing gels of TiO_2-SiO_2 can be categorized as co-hydrolysis, pre-hydrolysis and colloidal sol-gel route as described below. Usually, lengthy drying schedules (up to two months) are needed for obtaining samples, when reported by other investigators.

2.2.1 Co-Hydrolysis

The co-hydrolysis method is extensively used by Japanese researchers [46-50,52,53]. Generally speaking, this method involves, first, mixing precursors in an anhydrous alcohol and then very slowly adding a mixture of water, catalyst and alcohol under vigorous stirring. Thus, Kamiya and Sakka [46-49], using TEOS and TIP as

precursors, were able to prepare transparent TiO_2-SiO_2 glass with up to 7.7 mole% TiO_2. The alkoxide mixtures were first diluted with ethanol. A mixture of water, glacial acetic acid and ethanol was then added to the alkoxide mixture for hydrolysis. The molar ratios of water and glacial acetic acid to alkoxide were 50 and 0.01 respectively. The clear solution was kept at 40°C and gelation occurred in 5 days. The gels were then heated slowly to 90°C, kept there for 1 days, and then heated at 6°C/hr up to 900°C to remove organic matters and water.

Hayashi et al. [50] , using hydrochloric acid as the acid catalyst, also obtained non-crystalline glasses when the gels were heated to 1000°C or higher if the TiO_2 content was less than 10.4 wt%. TEOS and TIP were also used as the alkoxide precursors and were mixed with ethanol. The mixture containing water, hydrochloric acid and ethanol was added very slowly to the alkoxide mixture for hydrolysis. The molar ratio of water and hydrochloric acid to alkoxides was 2:50 and 0.01:0.5, respectively. Gelation occurred in 1 to 10 days depending on the hydrolysis conditions and bulk glasses were obtained by slowly heating the samples to 100°C, holding there for 1 day and then heating to 800°C using 10°C/hr.

According to the authors, the size of the dried gels thus obtained is greatly affected by amount of water

added. When the amount of water added was less, the gels cracked extensively into small particles 2 to 5 mm in diameter. However, if the H_2O/alkoxide molar ratio was 16, the gels cracked into large pieces (~ 50 mm).

TiO_2-SiO_2 gel glasses have also been prepared by co-hydrolysis, using titanium butoxide and silicon tetraethoxide as precursors as in Emili et al.[51] The sol was prepared by dissolving titanium butoxide and silicon tetraethoxide in a mixture of ethanol and butanol with a small amount of acetylacetone and refluxing at 80°C. Heat treatment was performed using a heating rate of 60°C/hr with a hold at 430°C for 40 hr to remove the solvent and organic radicals. However, the materials thus obtained were white powders, not monoliths.

Titanium ter-amyloxide was used as the titania source in Yamane et al. [52] This was mechanically mixed with methanol, ter-amylalcohol and silicon methoxide. Ammonia water of pH=11.2~11.3 dissolved in methanol was added dropwise into this mixture at 5°C under vigorous stirring. Gelation occurred in several minutes after the addition of ammonia water. If the mixture was hydrolyzed with ammonia water of pH<11.0, white powder formed instead of a clear solution. This was explained in terms of the decrease in the rate of hydrolysis of titanium ter-amyloxide. In other words, the rate of hydrolysis of titanium ter-

amyloxide approaches that of TMOS if ammonia water of pH=11.2~11.3 is used.

$Si(OC_2H_5)_4$ and $Ti(OC_4H_9)_4$ were used as the raw materials for gel preparation by Morikawa et al. [53]. The chemical compositions of the gels studied were 10 and 20 wt% TiO_2. The pre-determined amounts of alkoxide precursors were first mixed together. The alkoxide solution was diluted drop by drop with a mixture of ethanol, water and glacial acetic acid. Additional water was added to complete the hydrolysis of the alkoxides. Samples were cast in glass containers for gelation and aging. No information was reported regarding aging, drying, or the sample appearance.

2.2.2 Pre-Hydrolysis

The most important consideration in the preparation of a homogeneous gel for a multicomponent system using metal alkoxides is the reaction kinetics. Gels with high homogeneity can only be obtained readily if alkoxides having similar rates of hydrolysis are used. However, in practice, the rates of hydrolysis of metal alkoxides differ widely. The hydrolysis rate of silicon alkoxides, for example, is very low compared to that of titanium alkoxides. This means that precipitation will occur during

hydrolysis if a solution of titanium and other alkoxides is prepared by physical mixing. The situation can be circumvented by generating a soluble polymerizable intermediate from the slow hydrolyzed precursor which is capable of reacting preferentially with the fast hydrolyzed precursor or by slowing down the fast hydrolyzer to match the hydrolysis rate of the slow hydrolyzer. In terms of the reaction kinetics, the former method is a common approach for organic systems. Therefore, Yoldas [45] partially hydrolyzed silicon ethoxide first with limited amounts of water, followed by the addition of fast hydrolyzed titanium ethoxide:

$$Si(OEt)_4 + H_2O \rightarrow Si(OH)(OEt)_3 + EtOH \qquad (2.1)$$

$$Ti(OEt)_4 + Si(OH)(OEt)_3 \rightarrow (EtO)_3Ti\text{-}O\text{-}Si(OEt)_3 + EtOH \qquad (2.2)$$

The product of the equation (2.2) remains liquid due to insufficient water to cause complete polymerization. Further addition of water is necessary to remove the remaining "OR" groups and to promote polymerization and cross-linking to form a 3-dimensional network.

The titania precursors in Gonalez-Oliver et al. [54] were titanium isopropoxide (TIP), alkanolamine chelated isopropoxide (TB) and chelated glycol ester (TC). The source of silica was tetraethylorthosilicate (TEOS). This

was dissolved in a mixture of ethanol and methanol together with small amounts of acetylacetone. The TIP hydrolyzes much faster than TEOS and white precipitates formed upon addition of water. This did not happen to mixtures containing compounds TB and TC. Water was added to the TEOS mixture for pre-hydrolysis before the titanium compounds (TB and TC) were added. Gelation time varies with the amount of water and the content and source of titania. The gelation time was not significantly affected by the presence of acetyl acetone. Drying of the samples was carried out in a ventilated oven at 50-60°C for 3-4 weeks. The heat treatments were carried out in a slow stream of air using a heating rate of 2°C/min. No large densified monoliths were obtained.

Yuan and Yao [55] used $Si(OC_2H_5)_4$ and $Ti(OC_4H_9)_4$ as precursors and prepared gels with no less than 20 mol% TiO_2. The TEOS was pre-hydrolyzed at 75°C for 2 hours using hydrochloric acid as the catalyst (molar ratio of H_2O to HCl was 50:0.01). The mixture containing $Ti(OC_4H_9)_4$ and ethanol was then added drop by drop into the partially hydrolyzed TEOS solution. Further addition of H_2O and HCl was necessary to complete the reaction. A transparent bulk gel was obtained after 3 months drying. Cheng and Wang [56] also used $Si(OC_2H_5)_4$ and $Ti(OC_4H_9)_4$ as precursors and studied the gel formation in the (100-

x)TiO_2.xSiO_2 (where x=0-10 mole%) system. TEOS was pre-hydrolyzed in ethanol solution with a minimum amount of water. However, no detailed preparation procedures or description of the final product were given.

2.2.3 Colloidal Sol-Gel Process

A novel process for making TiO_2-SiO_2 glasses was developed by Scherer and Pantano.[57] This involves gelling a colloidal fume silica in an aqueous solution containing polymeric titanium/glycol complex. The tetraisopropyltitanate was first mixed with ethylene glycol and anhydrous citric acid was then added. This mixture was heated at 120°C for 2 hours during which the propanol was driven off and the solution became clear. This procedure stabilized the titanium complex so that the solution could be mixed with water and then used as the medium for dispersion of colloidal silica. The sol was made by mixing the titanium/glycol solution with water (1:1 ratio), then adding the colloidal silica powder and homogenizing in a conventional blender. Samples were cast in borosilicate tubes and held at 40°C for the evolution of bubbles created during blending. Gelation was carried out at 60-65°C. Gels could be dried crack-free within 24-36 hr at room temperature. The gels were then heated from

400°C to 1000°C at 100°C/hr in an oxygen atmosphere to initiate densification. Final densification was carried out by further heating to 1230°C in air. This method is less expensive, more expedient and has the potential of making large monolithic pieces. However, the glasses are translucent and TEM examination [57] reveals that this is due to the presence of uniformly distributed microcrystallites (~150Å) of crystalline TiO_2 (anatase). Thus, it is necessary to obtain a very uniform dispersion of fumed silica to avoid the problem of segregation. Suitable titanium precursors must be used or titania hydrate will precipitate out and poor gelling behavior will occur. In addition, carbonization of the residual glycoxides is difficult which leads to crystallization during sintering.

A similar approach was taken by Deng et al. [58] The clear stable titania solution was prepared by first mixing titanium isopropoxide with acetic acid, and then adding water. The solution became clear after stirring for 30-60 minutes and was stable at room temperature for 2-3 days. The colloidal silica was dispersed in the titania solution using a conventional blender. The gelation occurred within four days at 25°C. These gels were dried at 25 °C for 1 week and then heat-treated in air at 500°C for 30 minutes for organic burn out and water removal. Sintering

was accomplished by rapid heating (20-50°C/min) with plateaus at 1200-1250°C and 1450-1500°C. The clarity of the glass is drastically improved if the gels are sintered to 1200°C in helium, and then to 1450-1500°C in air. However, the gels heated to 1200°C in helium are distinctly blue-purple. Thus, final heat treatment at 1500°C is necessary for the gels to become fully dense and clear and to reduce the tendency toward bloating at higher temperature.

Minehan et al. [59] also reported the preparation of titania-silica glasses by sintering alkoxide synthesized colloidal powders. The colloidal titania-silica powders were derived by mixing a 1:1 molar ratio of TEOS and deionized water in ethanol. Hydrochloric acid was used as the acid catalyst. The mixture was refluxed at 50°C for 90 minutes and titanium isopropoxide was then added. The TiO_2-SiO_2 solution was further refluxed at 50°C for 5 hours before an NH_4OH solution of 0.69 M was added. Powder dispersion resembling milk was formed spontaneously. The solvent was then evaporated slowly below the boiling point until the dispersion showed a tendency toward gelation. The colloidal powder compacts were dried in air at 25°C for less than one week and then dried at 70°C for an hour. The samples were heated to 600°C in 10 hr. From 600°C to 1200°C, the samples were

sintered in helium at 10°C/min and held for 1 hr. Final densification was carried out by reheating these samples in air at 1440 °C for 1 minute to reoxidize the titania and to remove residual porosity.

2.3 Characterization of Sol-Gel Derived TiO_2-SiO_2 Glass

2.3.1. Chemical Analysis

Yamane et al. [52] discussed the conditions for the preparation of gels in order to obtain oxide glasses of high homogeneity by the sol-gel method with reference to the system titania-silica. Three kinds of titanium alkoxides (ethoxide, isopropoxide and ter-amyloxide) were mixed with silicon methoxide or ethoxide by various methods and were hydrolyzed to form gels. Since there is no appropriate method to determine the uniformity of composition in the gel directly, the homogeneity of the gels prepared was determined indirectly on the glasses. This was achieved by measuring the homogeneity of the glasses obtained by melting the mixtures of gels and sodium nitrate for a very short time (at 1300°C for 5 to 20 minutes), i.e., until immediately after the melt became batch free. This treatment was enough to keep the mutual diffusion of Ti^{4+} and Si^{4+} ions minimal, but long enough

for Na^+ ions to spread uniformly in the melt. The homogeneity of the glass thus formed would not be very different from the homogeneity of the original gel. The glass was then annealed at 560°C for 8 hours followed by testing using Shelyubskii method for transmission [52]. The authors concluded that a gel of fairly high homogeneity is obtained once one succeeds in obtaining a clear solution, regardless of the preparation methods.

2.3.2 Thermal Characterization

A dried gel contains a large amount of hydroxyls as well as organic residues on the surface of the pores. Upon thermal treatment, the gels lose water and organic species and begin to change their structure. Organic residues which are not lost by volatilization can be removed by oxidation. Many of these changes can be monitored by differential thermal analysis (DTA), thermal gravimetric (TGA) and thermal mechanical (TMA) analysis.

An endothermic peak was observed around 150°C by Hayashi et al. [50] which was attributed to the evaporation of the adsorbed water and solvent. Weight loss was observed from room temperature to 700°C which was attributed to the evaporation of the water liberated by the polycondensation of surface silanol groups. For gels

prepared with low water content (H_2O/alkoxides of 16/1 molar ratio), the shrinkage occurred until about 700°C. When the amount of water added was large, the gels continued to shrink until about 1000°C. This difference was attributed to the different gel structure obtained under different hydrolysis condition.

Gonzalez-Oliver et al. [54] carried out DTA and TGA runs in a flowing O_2/N_2 gas mixture and studied the effect of changing the composition of this gas mixture. An endothermic peak was observed at about 130°C, presumably due to physical desorption of water and alcohol from the surface of the gel. This is in accordance with a report by Emili et al. [51] The position of this peak is irrespective of whether the experiments were carried out in nitrogen or oxygen. Also, the magnitude and position of this peak is independent of the oxygen content of the atmosphere. Well defined exothermic peaks were observed in the range of 260°C-280°C for runs carried out in O_2, which was attributed to the combustion of carbonaceous materials. The runs carried out in a N_2 atmosphere showed no departure from the base line in this temperature range, but a small endothermic peak was observed at about 560°C. The peak position in the range of 260°C-280°C is affected by the composition of the atmosphere. As the oxygen content decreased, the peak broadened considerably, but

the area under the peak remained about the same. In addition, a ~40°C decrease in the position of the exothermic peak due to oxidation was reported when the content of TiO_2 was increased from 5 to 30wt%. The total weight loss for a series of TiO_2-SiO_2 gels heated in O_2 increases with increasing TiO_2 content.

The thermal expansion of the metal alkoxide derived TiO_2-SiO_2 glasses has been determined in the temperature range 25°C to 700°C [46-48]. As shown in Table 2.1, the values of the linear thermal expansion coefficient (α) were as low as those reported for flame-hydrolysis [38,61] or melt derived [38] glasses of similar compositions.

It is noted that the thermal expansion coefficient of the TiO_2-SiO_2 glasses decreased as TiO_2 content increased. The systematic decrease in the thermal expansion coefficient of TiO_2-SiO_2 glasses can be considered from two fundamental aspects: (a) the increased mass of the Ti^{4+} ions, which should decrease the average cation root mean square displacement that occurs with an increase in temperature, and (b) the increased volume per mole of oxygen created by the TiO_2 solution. As Evans [62] has stated:

> The larger volume, that is dynamically available to the oxygens as temperature is raised, means that larger r.m.s. displacements from their mean positions can occur for the same $\Delta L/L$ change. In other words, a

Table 2.1 Thermal Expansion of Titania-Silica

From Metal Alkoxide [46-48]		From Melting [38,61]	
Titania (wt%)	Alpha (x10^-7)	Titania (wt%)	Alpha (x10^-7)
3.0	1.3	3.42	2.312
5.0	-1.6	6.00	0.133
7.9	-0.7	7.40	-0.326
10.0	-4.3	8.36	-1.156
		9.45	-1.926

larger ΔT for the same $\Delta L/L$ is expected as available volume increases.

The average linear coefficients of thermal expansion (CTE) were determined using a differential dilatometer for colloidal sol/gel derived TiO_2-SiO_2 glass by Deng et al. [58]. The data, as shown in Figure 2.1(a), were also consistent with those reported for glasses prepared by the flame hydrolysis method [38], as shown in Figure 2.1(b). In addition, the expansion curves for these sol/gel derived glasses appear to be more linear than those reported for glasses prepared by flame hydrolysis which is consistent with Hench et al. [63] on alkoxide derived pure SiO_2 glasses.

2.3.3 Structural Characterization

The density of the sol-gel derived TiO_2-SiO_2 glasses has been reported by Kamiya and Sakka [46-48]. The data were measured by Archimedes' method at 19°C using water as the replacing liquid. As shown in Table 2.2, the densities of the sol-gel derived titania-silica glasses are slightly lower than those prepared by the flame hydrolysis method [38]. These difference were attributed to the inclusion of small closed pores which gave a "foggy" appearance to the sample.

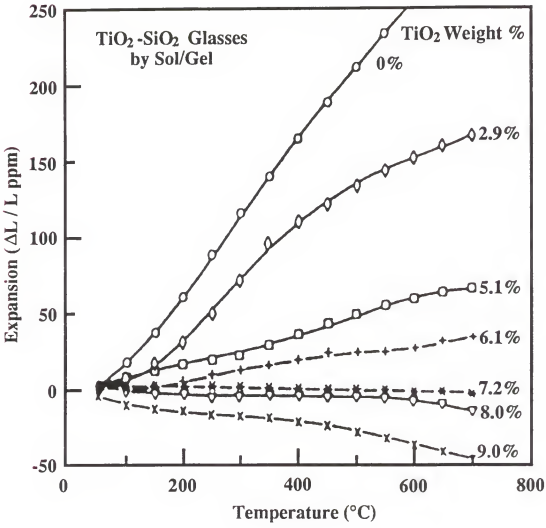

Figure 2.1(a) Thermal expansion of titania-silica glasses (a) prepared by colloidal sol-gel method [58].

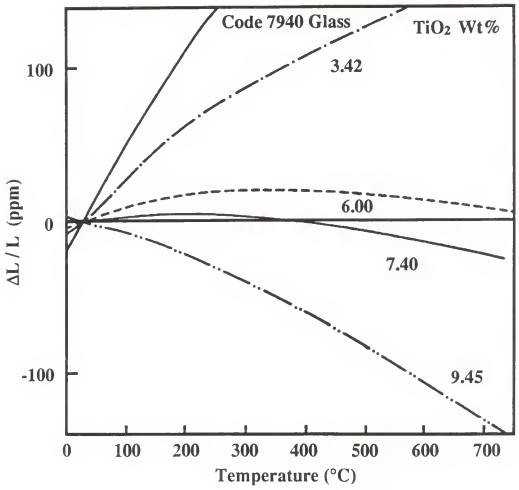

Figure 2.1(b) Thermal expansion of titania-silica glasses (b) prepared by flame hydrolysis method [38].

Table 2.2 Density of Titania-Silica Glass

From Metal Alkoxides [46-48]		From Melting [38]	
Titania (wt%)	Density (g/cc)	Titania (wt%)	Density (g/cc)
3.0	2.197	3.42	2.201
5.0	2.157	6.00	2.199
7.9	2.166	7.20	2.200
		7.40	2.199

The constant density of TiO_2-SiO_2 glasses with low TiO_2 concentration has been interpreted by Shelby in terms of molar volume [64]. As TiO_2 replaces SiO_2 in the glass network, the average R-O-R' bond length increases since size of Ti^{4+} ions is larger than that of Si^{4+}. Also, the average energy needed to deform the bond decreases since the field strength of Ti^{4+} is smaller relative to that of Si^{4+}. These changes result in an increase in molar volume. Thus, the increase in molar volume compensates for the increase in mass by Ti and a constant density is observed.

Sakka and Kamiya [48] studied the crystallization tendency of the TiO_2-SiO_2 glasses by heating in air at 1450°C for 2 hours. It was found that only tetragonal, α-cristobalite type SiO_2 crystals precipitated in the TiO_2-SiO_2 glasses system containing up to 6.2 mole% TiO_2. If the TiO_2 content exceeded 7.7 mole%, a small amount of anatase precipitated along with the α-cristobalite crystals. The lattice constants a_o and c_o of the α-cristobalite type crystals were determined as a function of TiO_2 content. The results indicated that there is a linear relationship between the lattice constants and the TiO_2 content, suggesting that Ti^{4+} ions substituted for the Si^{4+} ions of the cristobalite crystals. That is, Ti^{4+}

ions are four-fold coordinated with oxygen up to a titania content of 6.6 mole%.

This is similar to the results by Evans [62] on flame-hydrolysis derived TiO_2-SiO_2 glasses. Similar results have been reported by Hayashi et al. [50]. By heating the glass at 1450°C for 1 hour, they found that complete solid solution of TiO_2 in SiO_2 can be obtained in the range of less than 7.4 wt% TiO_2, while in the more than 10 wt% TiO_2 range, anatase and rutile are precipitated. The precipitation of anatase is assumed to be associated with the presence of the six-fold coordinated titanium ions, which is formed in the hydrolysis and gelation processes of the metal alkoxides.

On the other hand, Emili et al. [51] reported the observation of crystallinity in 10 wt% TiO_2 glass when the gel powders were treated at 1000°C for 3 hours. The crystallization temperature decreased as the TiO_2 content increased. The crystallites were determined to be anatase, even though some other XRD peaks not attributed to anatase were also observed, suggesting the existence of another unidentifiable crystalline phase containing titanium ions. The crystallite size distribution was obtained by plotting the second derivative of the Fourier coefficients as a function of distance. The mean values of the anatase crystallite size are 5.0±1.0 nm and

10.0±2.0 nm for samples containing 19 wt% TiO_2 partially crystallized at 1000°C and 1200°C, respectively. Since the crystallite size increased with increasing temperature, it was suggested that "diffusion controlled growth and probably precipitation coarsening effects were occurring".[51]

The crystallite size in the colloidal sol-gel derived glasses containing 10 wt% TiO_2 is ~13 nm as determined by transmission electron microscopy when the sample was sintered at 1230°C [57]. These glasses appeared to be translucent. The TiO_2 was in the form of rutile microcrystals of the order 1-5 nm in size in the dried gel stage by Deng et al. [58] After sintering to 1200-1250°C, the rutile crystallites were transformed into TiO_2 anatase crystallites which were of the order of 5-10 nm in size and were uniformly distributed in the amorphous silica matrix. After final densification at 1450-1500°C, the presence of the crystals could no longer be observed. This indicated that the titania crystals dissolved at 1450-1500°C, at which temperature the mobility of the Ti ions is sufficient to create a homogeneous amorphous structure.

Emili et al. [51] determined the Ti-O bond distances from the EXAFS spectra. For low TiO_2 concentration, the Ti-O bond distance is reported to range from 1.80 Å to

1.86 Å. These values are too short for an octahedral coordination of Ti-sites, whereas they are in good agreement with the Ti-O bond distances in Ba_2TiO_4 which is the only known crystalline Ti compound which exhibits a tetrahedral coordination of oxygen ions around Ti^{4+} ions [65]. When a sample containing 19 wt% TiO_2 was heated at 1200°C for 3 hours, small anatase crystallites with sizes in the range of 5.0-10.0 nm appeared. The Ti-O bond distances found in this sample range from 1.93 Å to 1.95 Å which corresponds to a six-fold coordination.

When the SiO_2-TiO_2 glass was prepared by the flame hydrolysis method, the results were somewhat different. Greegor et al. [66] reported that at concentrations below approximately 0.05 wt% TiO_2, Ti^{4+} occupies an rutile-like octahedral site in the SiO_2 glass. The site is probably formed as a result of breaking the oxygen bridging bond of the SiO_2 matrix. With increase in the titania content, a two-site model applies. For up to approximately 9 wt% TiO_2, the Ti^{4+} predominantly substitutes for Si in its tetrahedrally coordinated site, while maintaining a small fraction in the octahedral coordination (less than 5%). This is consistent with a previous study by Sandrom et al. [67] which also concluded a two-site model for the coordination of Ti in TiO_2-SiO_2 glasses. Above 9 wt% TiO_2, the octahedral/tetrahedral ratio increases

appreciably and eventually at ~15 wt% TiO_2, a second phase is formed with a crystal structure identical to that of rutile or anatase. The Ti-O-Si bond angle was calculated to be 159° which is slightly greater than the most probable value for the Si-O-Si bond angle of 152°.

2.3.4 Physical Properties

The change of micro-Vicker's hardness values of TiO_2-SiO_2 glasses as a function of temperature was reported by Hayashi et al. [50]. As shown in Figure 2.2, the hardness of the gels increased gradually with temperature up to 500°C and then increased dramatically between 500°C to 700°C. The hardness of the glasses heated to 700°C decreased as the amount of water added for hydrolysis increased. This was attributed to the presence of micropores which still exist at 700°C.

Refractive indices of the titania-silica glasses obtained from alkoxides by heat treatment up to 800°C have been reported by Hayashi et al. [50]. Figure 2.3 compares the refractive indices and densities of sol-gel derived titania-silica glasses with those derived from melting. The data points are for sol-gel derived while the dash lines are for melt derived titania-silica glasses. As shown in Figure 2.3, the refractive indices for gels

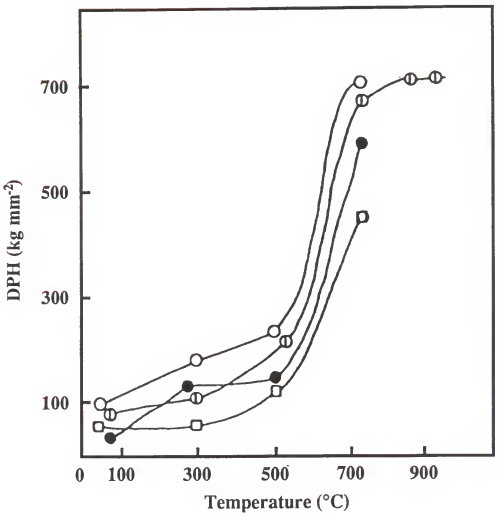

Figure 2.2 Vicker hardness of titania-silica gels as a function of temperature [50].
○ 12.9 wt%, no addition of water.
◍ 12.9 wt%, water/alkoxides= 2 molar ratio.
● 12.9 wt%, water/alkoxides=16 molar ratio.
□ 7.4 wt%, water/alkoxides=16 molar ratio.

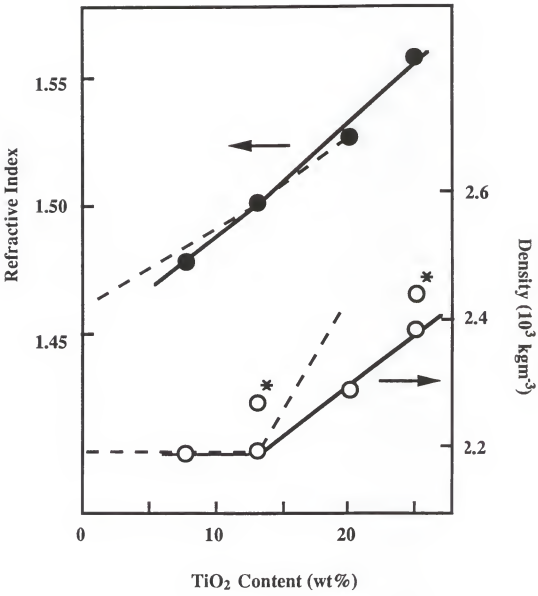

Figure 2.3 Refractive index and density for gel-glasses with various titania contents [50]. Dotted lines:data obtained by flame hydrolysis method [61].

prepared with more than 13 wt% TiO_2 are comparable with those obtained by the flame hydrolysis method. Below 13 wt% TiO_2, the refractive indices are somewhat lower than that prepared by flame hydrolysis method. This is due to the presence of pores in the bulk glasses, as indicated by the density curve in Figure 2.3. Density value increases if anatase crystals precipitate out in the glass matrix.

2.3.5 Spectroscopy

Vibrational spectroscopy provides one of the most direct structural probes for investigating glass structure. Using KBr pellets of the TiO_2-SiO_2 glasses, Sakka and Kamiya [48] measured the infrared spectra, as shown in Figure 2.4. The TiO_2-containing SiO_2 glasses showed an additional absorption peak around 950 cm^{-1}. When anatase crystals coexisted in the SiO_2 glass containing 7.7 mole% TiO_2, a broad absorption band around 650 cm^{-1} appeared. Gonzalez-Oliver et al. [54] reported a slight shift of the absorption band around 1100 cm^{-1}, which was attributed to Si-O vibrations in the SiO_4 tetrahedra, when the gels were heated to around 300°C. When the temperature was further raised to above 400°C, the absorption band shifted to higher frequencies,

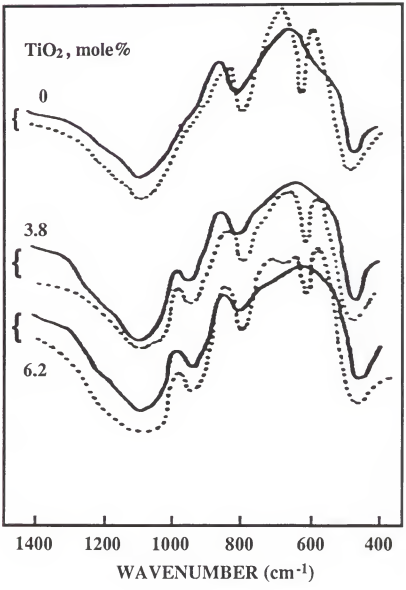

Figure 2.4 Infrared spectra of the glasses (——) and precipitated crystals of the titania-silica system [50].

suggesting that the Si-O bonds in the tetrahedra were strengthened.

When the gels were prepared using the colloidal sol-gel route, only the silicon-oxygen vibrations associated with the amorphous silica fume could be observed in the dried gel [58]. The titanium-oxygen vibrations in the gels could not be seen due to their six-fold coordinations at this stage. After the gels were sintered at 1450-1550°C, a new band appeared at 945 cm^{-1}. This band, which is also observed in Corning 7971 glass, has been attributed to the vibration of titanium ions in four-fold coordination with oxygen. Therefore, the authors stated that the titania, which originally was dispersed between the silica particles, had dissolved in the silica to create an amorphous solid solution.

One thing which is noteworthy in the colloidal sol-gel route is that the 945 cm^{-1} band begins to appear even after the gels were heat treated at 1200-1250°C [58]. However, anatase crystals form when the gel-glass is cooled, as indicated by X-ray diffraction. Thus, the titania only dissolved in the silica matrix at 1450-1500°C for glass prepared through the colloidal sol-gel route.

One problem of using infrared spectroscopy to investigate these glasses is that the normal infrared spectra of the bulk silica matrix overshadows the spectra

of the vibrational bands for the titania portion. Smith et al. [68] overcame this problem by using a difference infrared (DIR) spectral technique that involves placing extremely thin plates (down to 8μm thickness) of Corning 7971 and high purity silica in the sample and reference beams respectively. No bands were observed in the 500 to 600 cm-1 region of the DIR spectra which are associated with the Ti-O stretching modes for octahedrally structured titanium-containing groups. However, a band was observed at 735 cm^{-1} which is assigned as the asymmetric Ti-O stretching modes for a tetrahedrally structured titanium-containing group. Hayashi et al. [50] used a similar approach to diminish the overlapping of the absorption peaks of Si-O and Ti-O bonds. The difference spectra were obtained by placing the titanium containing silica gel-glass in the sample beam and vitreous silica in the reference beam. A band was observed at about 735 cm^{-1} (in stead of 950 cm^{-1}), which is reported to be the asymmetric Ti-O stretching mode for a tetrahedrally structured titanium containing group as in Smith et al. [68].

2.4 Summary

Sol-gel research has grown rapidly in recent years due to potentially unique applications for this new class of materials. Vitreous silica containing titanium is a glass which has received considerable attention due to its important and anomalous thermal expansion behavior. Many researchers have attempted to produce monolithic titania-silica glasses through the sol-gel route. Most of the products, however, are either powders or cracked pieces not monoliths. Thus, the majority of the data reported are for these powders or cracked pieces. In addition, lengthy drying schedules (weeks to months) are needed which is undesirable. A reliable process to make as-cast monolithic titania-silica glasses by the sol-gel processing has yet to be established. The work described in this dissertation describes such a process for the first time, albeit limited to optically transparent porous matrices.

The recent development of the sol-gel process has also lead to the manufacture of a new type of silica: Type VI, which is a porous silica monolith [17-19]. This porous gel has enough strength to withstand further treatments, such as impregnation with solutions of inorganic or

organic materials, which can potentially lead to new developments in optics and optoelectronics.

The porous Type VI silica is optically transparent since its pore size is smaller than that which scatters visible light. They are formed by applying a stabilization treatment to a dried gel up to a point before pore closure occurs. With sufficient control of the kinetics and ultrastructure, an optical element of substantial quantities of interconnected porosity can be produced. The amount and size distribution of the porosity can be tailored for specific applications during the stabilization treatment [17].

The Type VI gel-silica is suitable for: (1) lightweight optical components, (2) thermally cooled optics due to the interconnected porosity, (3) substrates for producing graded refractive index optics, (4) substrates for silica waveguides [69] or (5) matrices for fluors, non-linear optical compounds, wavelength shifters [70] and laser dyes.

The process developed for making the porous Type VI silica via the sol-gel route should also apply to the preparation of monolithic porous titania-silica, although the densification temperature may vary due to the presence of the titanium ions. This arises from the decrease in viscosity as titania is added to vitreous silica [61].

The physical properties of the titania-silica glasses are similar to that of pure amorphous silica [1]. They also are isotropic, have high chemical and thermal stability, have excellent optical transmission from visible to NIR wavelengths, and have mechanical properties comparable to that of vitreous silica. Above all, they have a coefficient of thermal expansion (CTE) lower than that of the pure vitreous silica (see Figure 2.1). Thus, titania-silica gel-glasses are an excellent candidate as optical components for which dimensional stability with respect to temperature is of concern, e.g. lens and laser cavities. In addition, they can also be used as substrates for waveguides and graded refractive index optics since their refractive indices are higher than that for vitreous silica. This type of monolithic, porous optically transparent titania-silica can not be obtained through the colloidal sol-gel route, as presence of the colloidal particles will scatter light. Thus, a colloidal based titania-silica material has insufficient transparency to be used for optical components. However, as shown in this work titania-silica gel-glasses made by the alkoxide based sol-gel route have the required transparency in the visible, and even into ultraviolet, which make them excellent candidates for optical applications.

CHAPTER III
EXPERIMENTAL PROCEDURES

3.1 Sol Preparation

The titania-silica sols investigated in this study were prepared under acidic condition using a pre-hydrolysis method. The approach involves the addition of a limited amount of water directly to the silicon alkoxide for pre-hydrolysis without relying on air humidity. A flow chart showing the sol-gel processing steps for the preparation of titania-silica monoliths used in this work is illustrated in Figure 3.1. The alkoxide precursors used for the titania and silica were titanium isopropoxide (TIP) and tetramethylorthosilicate (TMOS) respectively. Nitric acid with concentrations of $2x10^{-3}$ to 1.1N was used as the catalyst. Since TIP hydrolyzes much faster than that of TMOS, rapid addition of water to a mixture containing these two will cause preferential hydrolysis of the titanium isopropoxide and the solution becomes cloudy. In this work, clear sols were obtained by first adding one-fourth of the stoichiometric amount of water for hydrolysis into the desired amount of TMOS, followed by slow addition of titanium isopropoxide under vigorous

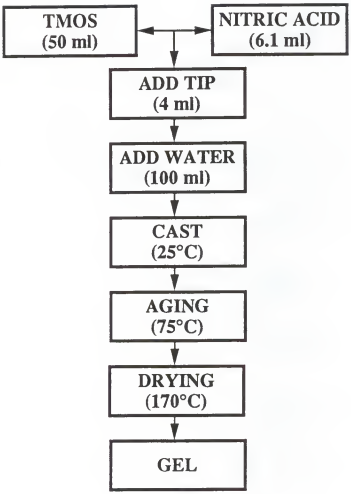

Figure 3.1 Schematic illustration of the sol-gel processing of 5% titania-silica gel monoliths.

stirring. The partially hydrolyzed $Si(OR)_{4-x}(OH)_x$ species thus reacts with $Ti(OR)_4$ to form the Ti-O-Si bonds which then react as a unit. No alcohol is used as the solvent since its addition will lead to a larger volume shrinkage upon drying causing the samples to crack. After sufficient mixing, additional water was added to complete the reaction. All of the above procedures were carried out in Teflon® containers. The resulting clear solution was then transferred to polyethylene or polystyrene containers, covered with lids and sealed with tapes to minimize evaporation.

3.2 Gelation and Aging

The gelation point is characterized by a sharp increase in viscosity.[32,33] This occurs as a result of the condensation reaction such that the polymeric species link together to become a three-dimensional network. At gelation, a solid object forms which takes the shape and the surface finish of the mold.

The gelation time varies with a number of variables, such as the amount of water added, the temperature at which gelation occurs, the pH of the mixture solution and the concentration of titania. The gelation of samples prepared in this study was achieved by leaving the cast

solution at room temperature until gel formation. This usually occurs in one to two days at room temperature after casting. As shown in Figure 3.2, the gelation time (which is defined by no observable surface movement upon tilting the container) increases as the titania content decreases. It also increases as the amount of the added water increases, as illustrated in Figure 3.3. It was observed that the smaller the amount of water added, the greater the tendency of the gel to crack while drying. Also, the gelation time when the reaction was carried out at 45°C was nearly half that carried out at room temperature. However, the tendency of bubble formation is much greater when gelation was carried out at higher temperature. Thus, all the reactions were carried out at room temperature with an R ratio of 16 for all the gels characterized in this study.

After gelation, the cast samples, while remaining in the same container used for casting, were transferred to an oven for aging. During aging, the condensation reaction continues as well as localized dissolution and reprecipitation which increases the thickness of interparticle necks and decreases the porosity. This is an important step to increase the strength of the gel. A typical aging temperature profile used is shown in Figure 3.4.

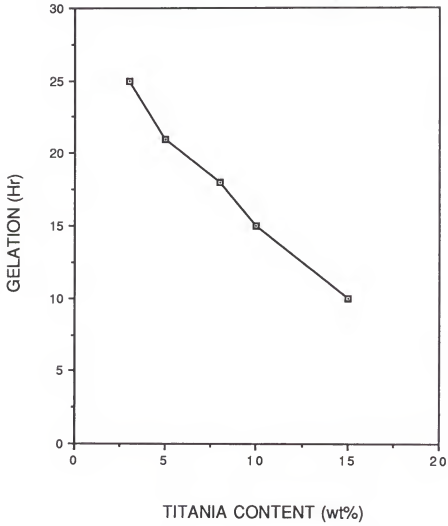

Figure 3.2 Variation of gelation time with titania content.

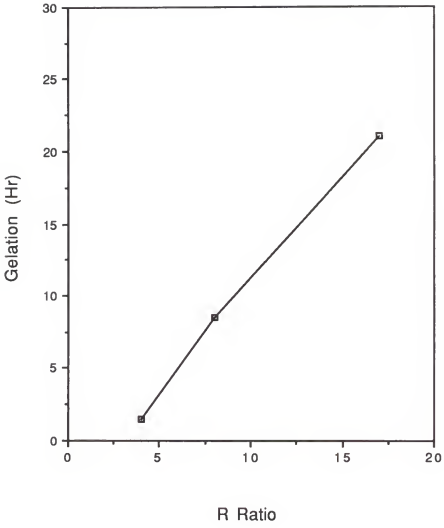

Figure 3.3 Variation of gelation time with R ratio.

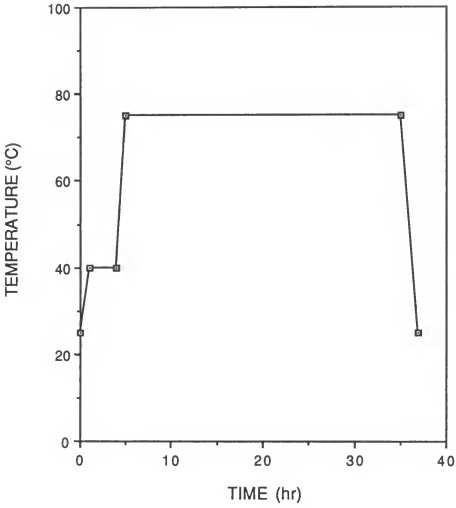

Figure 3.4 Typical aging schedule for the preparation of titania-silica gels.

3.3 Drying

Drying is a stage during which liquid is removed from the interconnected pore channels.[33] An aged gel must develop sufficient strength in order to resist the stress during drying. Drying of the samples prepared in this work was carried out by taking them out of the casting containers and transferring them carefully to the drying oven. These gels were then dried by slowly heating from room temperature to 170°C in four days. A typical drying temperature profile is shown in Figure 3.5.

Figure 3.6 is a photograph of the optically transparent dried 3% titania-silica gel monoliths prepared in this work using nitric acid as the catalyst. Rods of 2cm x 9cm and discs of 3cm x 1cm are routinely prepared using this method.

3.4 Characterization Techniques

3.4.1 Thermal Analysis

The thermogravimetric analysis (TGA) of the samples was performed using a Thermogravimetric Analyzer (Dupont 1090 thermal analysis system, Model 951). Monolithic titania-silica gels densified from 170°C to 1000°C were

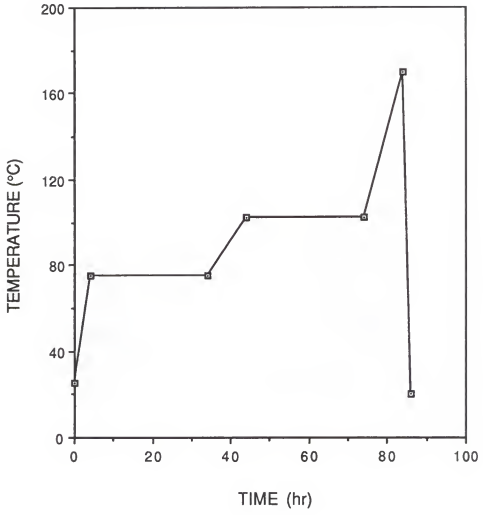

Figure 3.5 Typical drying temperature profile for the preparation of titania-silica gels.

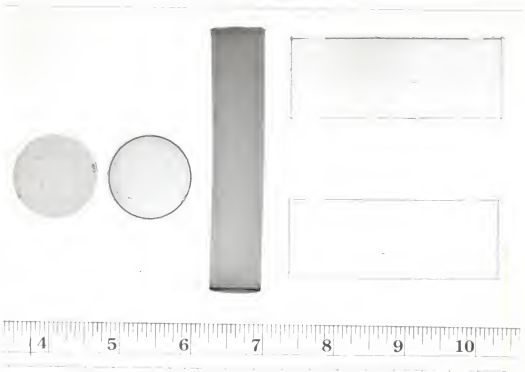

Figure 3.6 Photograph of dried titania-silica gel monoliths.

ground into fine powder for the analysis. Before each analysis, samples were outgassed overnight in a vacuum oven at 150°C in order to desorb the physisorbed water. Approximately 25mg of sample was used for each measurement.

The thermomechanical change of the sample as a function of testing temperature was determined using an automatic recording differential dual push-rod dilatometer (Theta industries, Dilatronic II-R). Basically, the machine measures the difference in linear dimension of the sample and reference material as a function of temperature through the relative displacement of its dual pushrods. Since the value of thermal expansion for NIST* silica is known, the value of the sample material can be calculated. From this aspect, this is an absolute not relative method for determining the thermal expansion of materials. A typical sample and reference materials used for the analysis were small rods of 10mm in length. Samples were cut using a low speed diamond saw and polished to ±0.5mm within the specified length. The samples were then stored in an oven at 170°C overnight before testing. Unless otherwise stated, NIST* vitreous silica was used as the reference material in all the measurements.

---

* National Institutes of Standards and Technology.

3.4.2 Structural Analysis

The structure of the titania-silica gel-glasses was determined using X-ray diffraction (Philips, Model APD 3520). The dried gels were crushed into fine powder and heated in air using a rate of 60°C/hr from room temperature to 600°C. After holding at 600°C for 10 hours, the sample was further heated at 30°C/hr and held at the temperature desired for 15 hours before cooling and submitting for X-ray analysis. Samples were scanned at two-theta angles from 5° to 80°.

The specific gravity (or structural density) of the samples was evaluated using a helium gas micropycnometer (Quantachrome, Inc. Model MPY-1). The machine operates by measuring the change in pressure in a cell with and without sample with a fixed amount of helium. Using the ideal gas law, the volume of the sample in the cell is determined and the density can then be calculated.

The specific surface area, pore volume and pore radius of the samples were determined using an automatic gas adsorption instrument (Quantachrome, Inc. Model Autosorb-6). This machine operates with nitrogen gas as adsorbate. It degases the sample and measures the volume of nitrogen adsorbed onto (V_{ads}) or desorbed from (V_{des}) the adsorbent surface as a function of relative pressure P/P_o. The

monolithic gel samples were ground into fine powder and outgassed in the testing cell at 170°C overnight before the measurement. Using the multipoint BET method, the specific surface area was deduced from the raw volume vs. relative pressure data. The pore volume is calculated from V_{ads} at a pressure close to $P/P_o=1$. The measurement usually takes 20 hours.

3.4.3 Physical Property Characterization

The Vicker microhardness (also called diamond pyramid hardness) of the gel-glass samples was determined using a semiautomatic Leco DM-400F Hardness Tester which incorporates an ACP-94 computing printer (Leco, Inc.). The Vicker hardness number (VHN) is defined as the load divided by the surface area of the indentation. Monolithic samples were heated to the designated temperature and cooled to room temperature before being placed under the indenter. Indentations were made using a 136° diamond pyramid indenter with a load of 100g and a loading time of 12 seconds. Both diagonals of the indentation were measured and the average value was used to calculate the diamond pyramid hardness.

The refractive index for the gel-glasses is determined using a reflectance method. This is carried out by

measuring the photoelectronic current reflected from the sample as well as that from a reference, i.e. silicon carbide, at a wavelength of 632.8 nm. The reflectance of the sample (R) is thus the current ratio multiplies the reflectance of silicon carbide. The refractive index (n) is then calculated using the following formula:

$$n = (1+\sqrt{R})/(1-\sqrt{R}) \qquad (3.1)$$

3.4.4 Chemical Analysis

The chemical composition of the gels prepared in this work were analyzed using Neutron Activation Analysis (NAA) at the University of Florida, Department of Nuclear and Engineering Sciences. Monolithic samples were ground into fine powder before submitting for analysis.

3.4.5 Spectroscopy Characterization

The infrared spectra of the TiO_2-SiO_2 gel-glasses were recorded on a Nicolet FTIR spectrometer (Nicolet, Model MX-1) using the reflectance stage. Monolithic samples with flat surfaces were outgassed at 170°C overnight before taking the spectra. Spectra were collected in the range of 400 cm^{-1} to 4000 cm^{-1}. Accumulation of 32 scans

were used which gave good resolution. This is a relatively easy method which gives qualitative information regarding the structure and composition of the gel-glass system.

The high pressure IR study was carried out using the facility at Department of Chemistry, University of Illinois at Urbana-Champaign. Monolithic samples densified at high temperature were ground into fine powders. The powdered sample was loaded into a diamond anvil cell which was linked to a Nicolet FT-IR spectrometer.

The ultraviolet-visible-near infrared spectra were obtained using a Perkin-Elmer UV/VIS/NIR spectrophotometer (Model Lambda 9). Samples densified to different temperatures were transferred immediately to the spectrophotometer after they are cooled to ambient temperature. Spectra were collected over the range of 185 nm to 3200 nm.

The XPS data were collected using a Perkin-Elmer model 5100 spectrometer with Mg Kα radiation from a source operated at 300W. A take-off angle of 45° was used. Monolithic samples in the shape of plane-parallel plates, (10x10x1) mm^3, were mounted on the sample holder. The samples were vacuumed overnight before spectra collection. All the measurements were carried out at room temperature.

The high instrument sensitivity of the XPS allowed small quantities of carbon to be detected in each sample. This carbon was used as a charge reference. No other impurities were detected.

The Raman spectra of the gels prepared in this work were collected, in collaboration with Dr. Martin Vala, at the University of Florida, Department of Chemistry. Monolithic samples were ground into fine powder before submitting for the analysis.

CHAPTER IV
THERMAL CHARACTERIZATION

The surface of a dried gel contains a large amount of hydroxyls as well as organic residues [71]. On gentle heating, evaporation, oxidation and condensation reactions occur leaving a porous oxide network. On further heating, this porous structure gradually collapses to form a dense amorphous or crystalline material depending on the material composition, the atmosphere and the maximum temperature of processing. Thermal analysis provides a mean of monitoring these changes as a function of temperature as well as characterizing gels with various degree of densification.

In this chapter, results from thermogravimetric analysis as well as thermomechanical analysis (i.e. dilatometry) are presented.

4.1 Thermogravimetric Analysis

Figure 4.1 shows a typical thermogravimetric plot for a dried 3% titania-silica gel. As shown in the figure, the sample loses weight continuously as it is heated. It

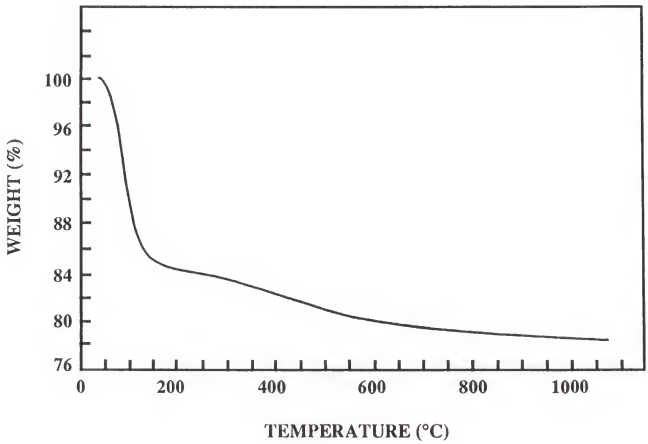

Figure 4.1 Thermogravimetric analysis for a dried 3% titania -silica gel.

is noted that the rate of weight loss is larger with temperatures below about 200°C. The weight loss that occurs below 200°C is due to the evaporation of the adsorbed water from the surface of the sample. Above 200°C, the weight loss is usually associated with the pyrolysis of organic species. In addition, evaporation of water molecules which are liberated from the polycondensation of silanol groups also contributes to weight loss at higher temperatures.

Figure 4.2 shows the TGA traces for a dried 5% titania-silica gel heated under two different atmospheres. Again, a sharp decrease in the sample weight is observed as the sample is heated from room temperature to 200°C, regardless of the atmosphere. A similar plot for a dried 8% titania-silica gel is shown in Figure 4.3. This indicates that a dried air atmosphere is more effective in dehydrating the sample.

The variation of TGA traces for a set of 3% titania-silica samples densified to different temperatures is shown in Figure 4.4. This figure shows that as the densification temperature increases the weight loss of the sample decreases. A similar trend is observed for a set of 5% titania-silica gels, as shown in Figure 4.5.

When one plots the derivative of TGA traces as a function of temperature, Figure 4.6 and 4.7 are obtained.

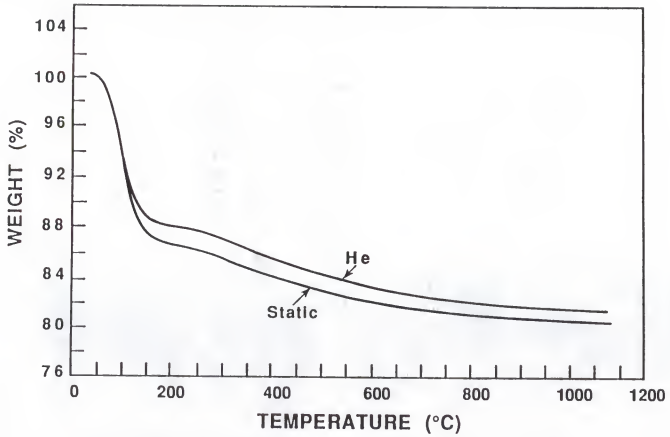

Figure 4.2 TGA of dried 5% titania-silica gel under different atmospheres.

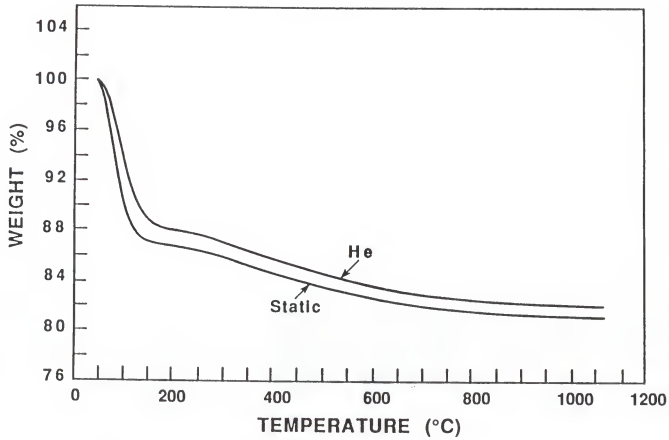

Figure 4.3 TGA of dried 8% titania-silica gel under different atmospheres.

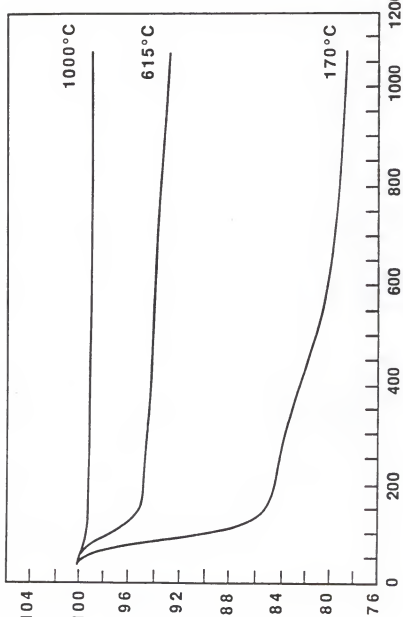

Figure 4.4 TGA for 3% titania-silica gels densified to various temperature.

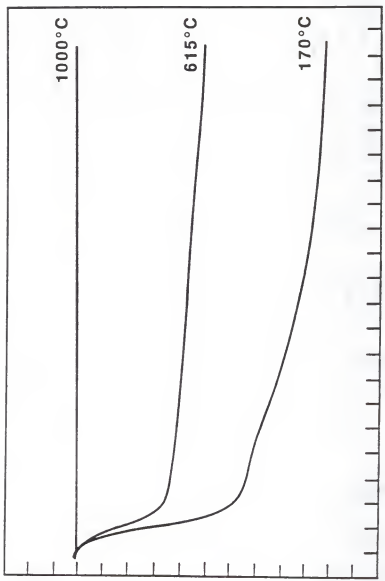

Figure 4.5 TGA for 5% titania-silica gels densified to various temperature.

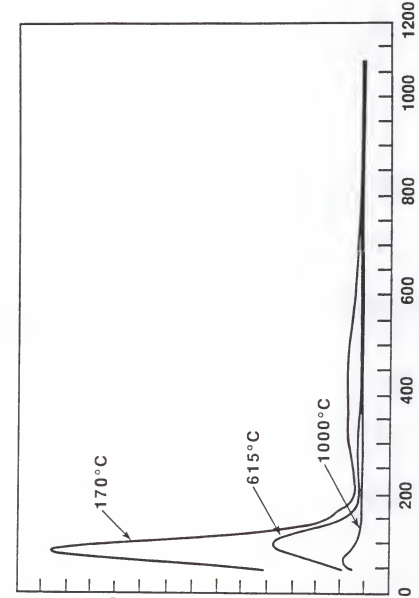

Figure 4.6 Derivative of TGA traces for 3% titania-silica gels densified to various temperature.

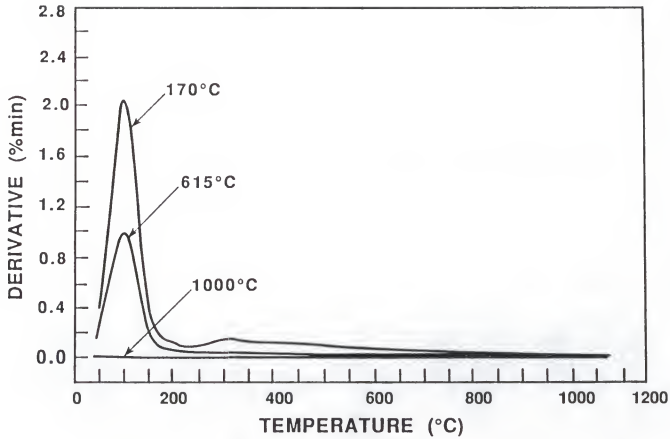

Figure 4.7 Derivative of TGA traces for 5% titania-silica gels densified to various temperature.

From these figures it is observed that as the densification temperature increases the amount of physisorbed water molecules decreases as indicated by the decrease in the area associated with the peak around 100°C. For a gel dried at 170°C, there is a second peak which spreads from 200°C to above 700°C. When the sample is densified at 615°C, this peak skews toward a lower temperature and the area associated with this peak decreases. The peak disappears when the sample is densified at 1000°C.

The appearance of the second peak in the derivative of the TGA trace of the dried gel is due to the evaporation of organic species and/or water from polycondensation of surface silanols as well as the liberation of bound water molecules. After the sample is densified at 615°C, evaporation of the organic species is completed with some water being liberated as a result of a polycondensation reaction. Thus, the peak area decreases with its shape skewing toward lower temperature. However, this partially densified gel-glass (615°C) is very hydroscopic due to its high surface area and small pore radius. Water molecules from the ambient atmosphere can adsorb rapidly back onto the surface of the gel. This is shown in Figure 4.8 with both the temperature profile and weight loss plotted as a function of time for a 5% titania-silica gel densified at

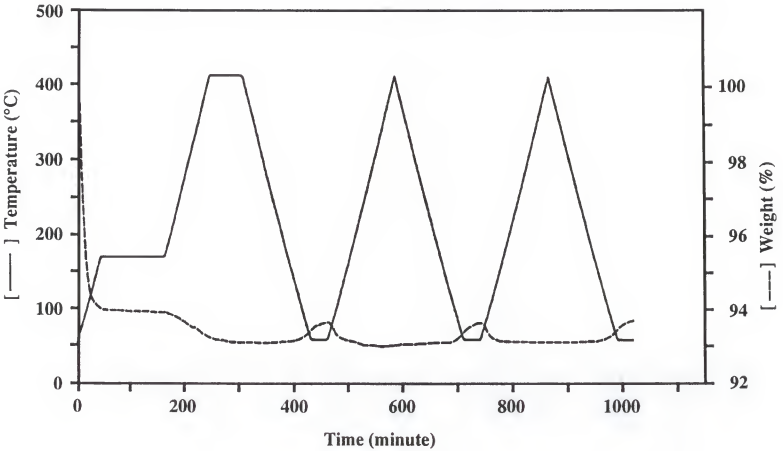

Figure 4.8 TGA plot for partially densified (615 °C) titania-silica gel-glass under thermal cycling.

615°C. It is noted that the sample begins to gain weight when it is cooled below ~180°C. This phenomena is reproducible as shown in the figure. Within the time frame of this experiment, the adsorbed water molecules desorb from the surface of the gel upon heating. It is possible that with prolonged holding at room temperature, these adsorbed water molecules can hydrate the surface of the gel by forming silanol groups. For this reason, all the gels studied in this work were stored in a vacuum desiccator after the desired thermal treatment.

4.2. Dilatometry

Figure 4.9 is a typical curve of dimensional change as a function of temperature for a partially densified gel when tested under dry air. As shown in this figure, as the sample is heated from room temperature (30°C) at a rate of 3 °C/min, it begins to expand up to a maximum value before shrinkage commences. The sample continues to shrink until the maximum testing temperature is reached. When cooling starts, the sample still shrinks a certain amount, but below a certain temperature, the dimension of the sample begins to increase. The hysteresis in this curve indicates that the shrinkage is irreversible for this particular sample.

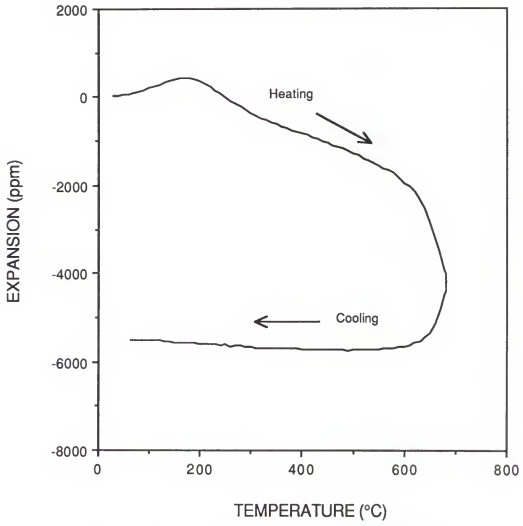

Figure 4.9 Variation of linear dimension with temperature for a 5% titania-silica gel partially densified at 615°C.

4.2.1 Effect of Thermal Treatment

Figure 4.10 shows the variation of linear dimensional change as a function of temperature for a set of 3% titania-silica gels densified to different temperatures. A heating rate of 3°C/min was used for this set of data and the reference point was chosen as 30°C. Similar plots for 5% and 7% titania-silica are shown in Figure 4.11 and Figure 4.12. As illustrated in these figures, the dried gel shrinks the most upon heating and the amount of total shrinkage decreases as the densification temperature increases. In addition, if the gel has been pre-densified at a certain temperature (e.g. 400°C), the amount of shrinkage before the sample reaches that temperature is much less compared to that after this temperature.

4.2.2 Effect of Adsorbed Water

It is interesting to note that all the porous gels show a certain magnitude of initial dimensional increase before shrinkage commences under the testing condition. The amount of this initial expansion decreases as the densification temperature increases. Similar results were reported for monolithic silica gel by Kawaguchi et al. [28] and Vasconcelos [72]. It has been suggested that this

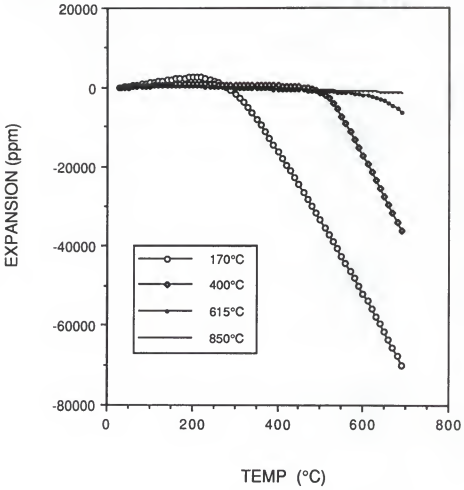

Figure 4.10 Variation of linear dimension with temperature for a set of 3% titania-silica gels previously densified in the range of 170°C to 850°C.

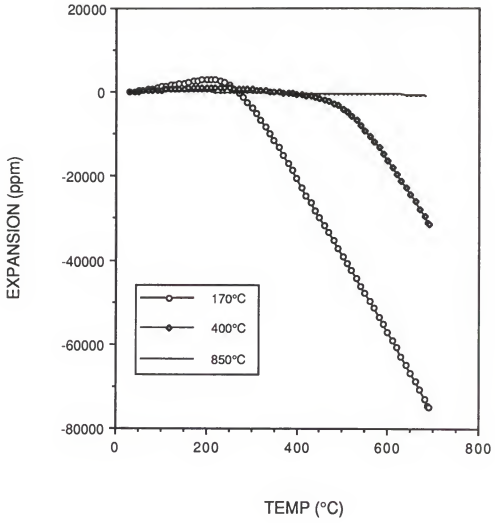

Figure 4.11 Variation of linear dimension with temperature for a set of 5% titania-silica gels previously densified in the range of 170°C to 850°C.

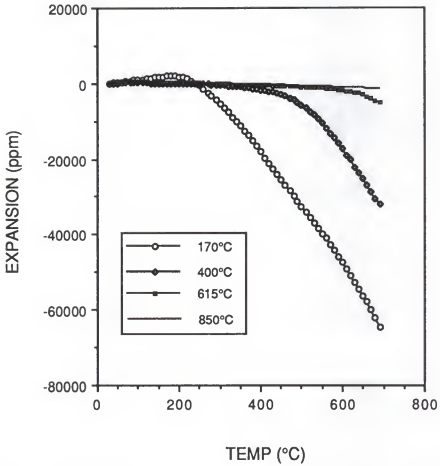

Figure 4.12 Variation of linear dimension with temperature for a set of 7% titania-silica gels previously densified in the range of 170°C to 850°C.

initial expansion for samples densified at lower temperature is associated with the presence of water in the sample [32,73,74]. This is very likely since a pore with 2 nm diameter can host only a few water molecules in its cross-section (diameter of H_2O is 0.31 nm). This allows little freedom for structural rearrangement to occur. Indeed, Lakhanpal and Puri [75] showed that the boiling point elevation of water condensed in pores of radii less than 1060, 102, 30, 15.5 and 9Å were 2.4, 4.9, 12.6, 21.2 and 34.1 °C respectively. Their results also showed that, for a given capillary radius, the boiling point elevation is about the same, irrespective of the nature of the adsorbent (silica gel, charcoal, bentonite and clay loam) or the amount of the liquid contained in it. Similar trends in melting point elevation was recently reported by Wallace and Hench [76] for monolithic silica gels. All of this suggests that the adsorbed water molecules are very much confined (or entrapped) in the small pore channels. As the testing temperature of the sample increases, the sample expands as if it were composed of the porous gel skeleton and the "frozen" water phase. The observed expansion is a result of this two phase "composite". After the sample has been densified at higher temperature, its capacity of adsorbing water decreases as shown in the TGA trace in Figure 4.4. Thus,

the volume fraction of the "frozen" water phase is less for the densified gel leading to a lower value of expansion. As the pore radius increases, this phenomena is less pronounced since the adsorbed water molecules will be less constrained in the pore channels, as reported by Elias [77] for monolithic silica gels.

Figure 4.13 shows the linear dimensional change at constant temperature under vacuum for a porous 5% titania-silica gel, with different amounts of adsorbed water. The sample was first held under vacuum at 180°C for 24 hours before it was cooled to room temperature (in vacuum). The weight was quickly determined once it was in air. The sample was then transfered to a water chamber for a certain period of time and its weight redetermined. The amount of weight gain, i.e. the amount of water adsorbed, was represented in terms of percentage in Figure 4.13. The sample was then quickly transfered to the dilatometer and its dimensional change was recorded at 30°C under vacuum. After the first test, the same sample was again outgassed under vacuum at 180°C for 24 hours and the whole process was repeated. As shown in Figure 4.13, there is linear shrinkage when the adsorbed water leaves the sample. The more the amount of adsorbed water, the more the amount of shrinkage when the sample is subjected to vacuum. In other words, the gel structure dilates upon

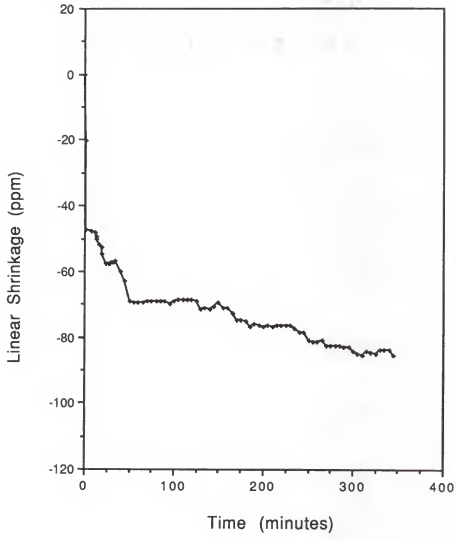

Figure 4.13 Variation of linear dimension under vacuum with time for a partially densified 5% titania-silica gel-glass. (a) with 0.6 wt% of adsorbed water.

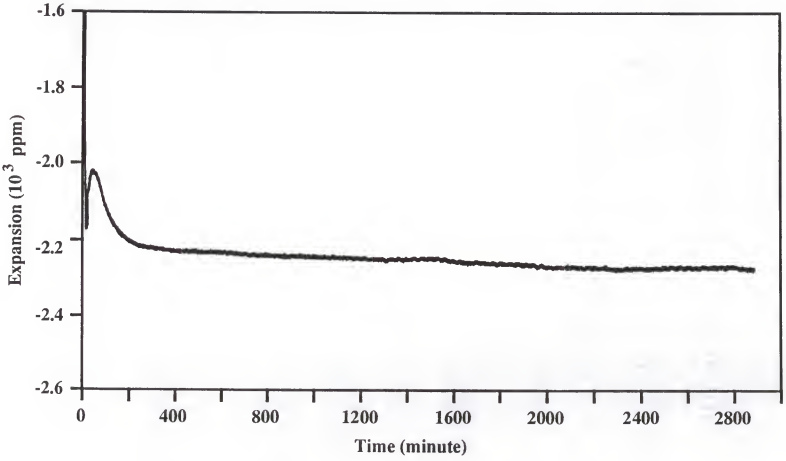

Figure 4.13(b) Variation of linear dimension under vaccum as a function of time for a partially densified 5% titania-silica gel-glass (b) with 21 wt% of adsorbed water.

water adsorption. Note that not all of the adsorbed water molecules are desorbed from the surface of the gel within the time frame of this experiment. This is indicated by the small but continuous shrinkage for the curves in Figure 4.13. This infers that the actual structural dilation should be larger than the results shown in Figure 4.13.

Similar results of structural dilation upon water adsorption has been reported in a pure silica gel system. Demediuk and Cole [78] used silicon tetrachloride as a precursor and fired the resulting gel from 800°C to 1100°C. The samples were then subjected to an autoclave at 200°C for 24 hours. They reported that there was a small expansion for all the silica gels. In addition, there is a progressive decrease in the amount of expansion with increasing firing temperature. Recently, Hench and West [32] reported that the dimensions of a porous silica gel monolith will increase with time when exposed to a moist ambient atmosphere, presumably due to structural dilation upon the adsorption of water molecules.

The structural dilation of a porous gel monolith upon water adsorption can be realized from the point of surface energy. The specific surface energy (γ) of a solid body should change upon the adsorption of a vapor or immersion in a liquid. If the specific surface energy of the solid

increases upon adsorption, the solid will deform in order to reduce its surface area. On the other hand, if γ decreases, there should be a consequent dilation of the body as if the solid behaves elastically. This deformation which is structural dependent would require mechanical work, and the elastic energy thus needed is provided by the change in surface energy.

Considering that the surface energy of hydroxylated silica to be 170 erg/cm^2 and that of liquid water to be 118 erg/cm^2 [10, p464], a decrease in γ of 52 erg/cm^2 is calculated as water is adsorbed onto the silica surface. Thus, the structure of the porous gel monolith should expand as water adsorbs onto its surface.

In order to compare the relative amount of structural dilation upon water adsorption, a pure silica monolith and a 5% titania silica gel monolith were used. The specific surface areas and pore radii were 453 m^2/g, 12.2 Å and 465 m^2/g, 11.5 Å respectively for the silica and titania-silica gel monoliths. The samples were both loaded into the dilatometer with the silica at the reference side and titania-silica at the sample side. The gel monoliths were then slowly heated to 600 °C in dry air in the dilatometer, held for 4 hours before cooling to room temperature. The gels were then exposed to ambient atmosphere at room temperature and their relative

dimensional change was monitored as a function of time. Figure 4.14 shows the dimensional change as a function of time of the 5% titania-silica with respect to the silica. The titania-silica gel monolith shrinks compared to the silica gel. Since both samples expand upon water adsorption, this figure illustrates that the amount of structural dilation is smaller for a titania-silica gel than that for a silica gel monolith, assuming same amount of water adsorbed. Change in slope as observed in this figure probably arises from rehydroxylation of the sample surface. As the Ti-O bond is of weaker character than the Si-O bond, rehydroxylation of the titania-silica gel is probably faster than that of a pure silica gel, which contributes to structural dilation.

The above discussion outlines the characteristic changes in linear dimension that one observes when a porous gel monolith is subjected to a temperature profile. Since the sample has a high affinity toward water which depends strongly on its degree of densification, its dimension has already expanded a certain amount before the thermal testing starts. This amount of structural dilation depends on the amount of adsorbed water which varies from sample to sample due to its different length of contact with the ambient atmosphere. As the thermal testing starts, the entrapped water molecules will expand

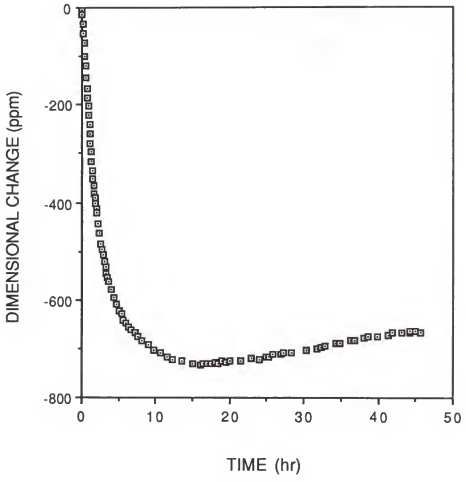

Figure 4.14 Variation of linear dimension with time for a 5% titania-silica with respect to silica.

in the pore channels leading to expansion of the sample while departure of the water molecules from the surface will lead to shrinkage of the sample. The observed dimensional change is composed of these two opposite contributions.

For a sample with small pore size, the initial expansion resulting from "frozen" water outweighs the structural shrinkage upon water desorption. Thus, an expansion is observed before shrinkage commences. As the pore size increases, this positive contribution gradually diminishes since water molecules are less constrained in the pore channels. In any case, the transition in the dominant mechanism should be reflected as a change in the slope in the dimensional change curve as shown in Figure 4.15. When the pore channels are large enough so that water molecules can leave freely, no expansion contribution will be present and the dimension of the sample will decrease continuously without a change in the slope. This is illustrated in Figure 4.15 for a series of porous silica gel monoliths with varying pore size [77]. Note that the temperature at which the slope changes decreases as the pore size increases. This indicates a smaller temperature regime at which the "frozen" water phase will dominate.

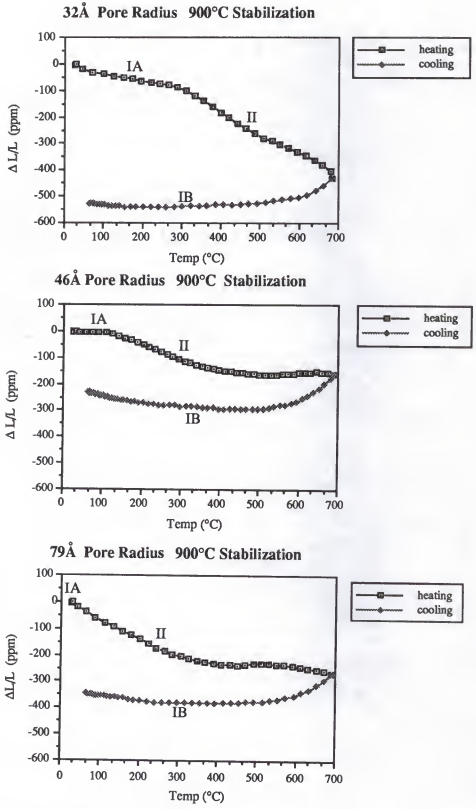

Figure 4.15 Thermal hysteresis from dilatometry for pure silica gel-glass with various pore radius [77].

It is of interest to find out at what temperature these adsorbed water molecules can be thermally driven away. Figure 4.16 shows the linear dimensional change as a function of temperature for a 5% titania-silica gel tested under vacuum . The curve was recorded after the sample was first thermally cycled twice under vacuum and then purged with dry air (<3 ppm of H_2O) for 10 minutes. Again, the initial shrinkage is a result of the departure of the adsorbed water. However, the sample exhibits normal expansion behavior upon heating above 400°C. This suggests that the physisorbed water molecules can only be thermally driven off at a temperature above 400°C. This high temperature probably is a result of the porous nature of the material as well as the small pore radius which holds the surface hydroxyls much more closer. The fact that a partially densified sample (e.g. 850°C) shows continuous shrinkage above 450°C infers that the sample surface was already rehydrated by the adsorbed water molecules and any further shrinkage is observed due to condensation of the hydroxyls [73,77].

4.2.3 Effect of Atmosphere

Figure 4.17 shows the change in linear dimension as a function of temperature for a 5% titania-silica gel under

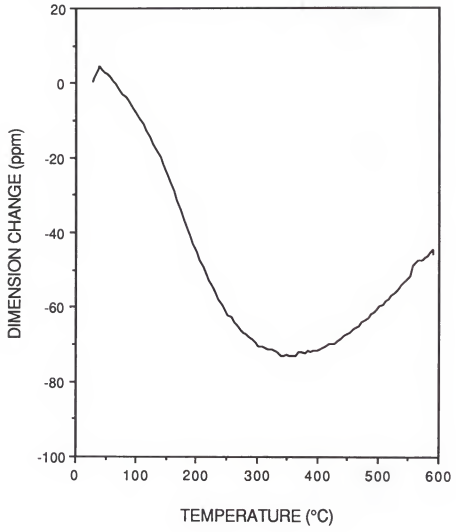

Figure 4.16 Variation of linear dimension with temperature for a 5% titania-silica gel tested under vacuum.

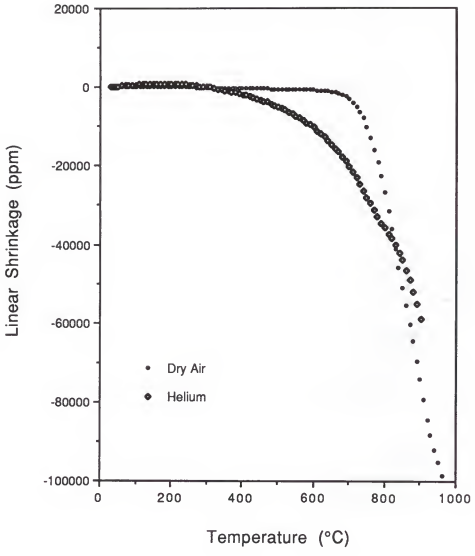

Figure 4.17 Variation of linear dimensional change with temperature for a 5% titania-silica gel under different atmospheres.

different atmospheres. Since a dried gel contains organic species which can be burned out at a temperature above 500°C, the sample shown in this figure was thermally treated at 615°C before the thermal test. As shown in this figure, the sample shrinks differently under different atmospheres. In a helium atmosphere, the onset of shrinkage commenced at a lower temperature than that in a dried air atmosphere. From this point of view, it is better to use a dried air atmosphere at a lower temperature for densification since the sample can be dehydrated without the accompanying shrinkage which may lead to pore closure and foaming of the sample at a later stage.

4.2.4 Effect of Heating Rate

The linear dimensional change as a function of temperature for a dried 5% titania-silica gel tested under various heating rates is plotted in Figure 4.18. It is noted that there is no heating rate dependence of dimensional change below 200°C. As the temperature is raised above 200°C, shrinkage commences for samples with the lowest heating rate. There is about a 1.5% difference in linear shrinkage at ca. 400°C as the heating rate changes from 1.5°C/min to 10°C/min. This can be explained

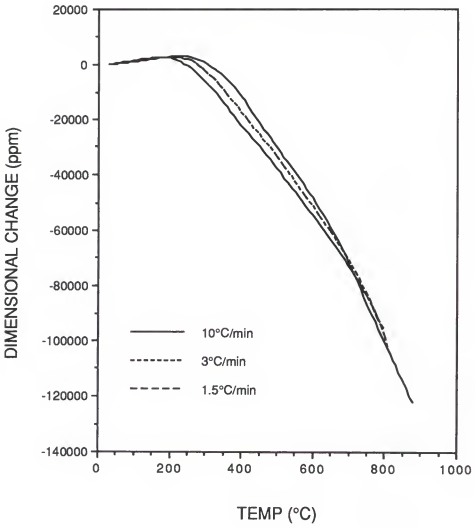

Figure 4.18 Variation of linear dimensional change with temperature for dried 5% titania-silica gel under various heating rates.

in terms of the reduction in the time spent for the same amount of temperature increment. At the same temperature, the amount of adsorbed water evolved from the surface is larger for a sample with lower heating rate than that with a faster rate (due to longer time spent before reaching that temperature). This gives a smaller temperature regime at which the adsorbed water will contribute to the positive dimensional change. Thus, shrinkage commences at a lower temperature for samples with a lower heating rate. It is interesting to note that above 700°C, there is again no heating rate dependence on the shrinkage behavior. This is unexpected since one would expect densification to be structurally dependent. At a particular temperature, the degree of polymerization (crosslinking) and/or structural relaxation should differ for samples tested under different heating rates. This difference should lead to a difference in viscosity of the sample which would result in a difference in the kinetics of viscous sintering. The fact that the shrinkage behavior does not appear to be heating rate dependent above 700°C for a dried gel probably results from the different temperature regime of positive water contribution which obscure the shrinkage behavior.

Figure 4.19 plots the linear dimensional change as a function of temperature under various heating rates for 5%

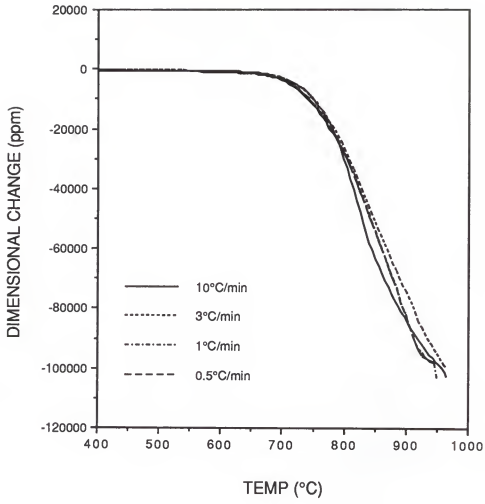

Figure 4.19 Variation of linear dimensional change with temperature for a partially densified 5% titania-silica gel under various heating rates.

titania-silica gel pre-treated at 615°C for 15 hours. As a result of this pre-treatment, the samples behave identically at temperature below 600°C. Above 600°C, one does observe a heating rate dependence on the shrinkage behavior.

Constant heating rate (CHR) shrinkage equations are appealing to apply to the gel shrinkage data [79-82]. Woolfrey and Bannister [79] had developed general CHR equations which made no assumptions regarding the geometry or densification mechanisms, except that only one rate-controlling mechanism predominates. The basic assumption is that at any combination of shrinkage and temperature, the isothermal and nonisothermal shrinkage rates are equal. Thus

$$\frac{d}{dt}\left(\frac{\Delta l}{l_o}\right) = \frac{K_o \exp(-Q/RT)}{(\Delta l/l_o)^n} \qquad (4.5)$$

The activation energy, Q and n, a geometric factor, are characteristic of the rate-controlling mechanism. For viscous sintering, K_o is a constant and n normally equals 0. If Q, n and the heating rate, **a**, remain constant, the above equation may be integrated and approximated (since Q>>RT) by

$$(\Delta l/l_o)^{n+1} = [K_o RT^2 (n+1)/aQ]\exp(-Q/RT) \qquad (4.6)$$

In a constant heating rate experiment (dT/dt=a), the sample temperature is increased at a constant rate, a, and the linear shrinkage or shrinkage rate is recorded as a function of temperature. From the above equation, it is noted that a plot of $\ln(\Delta l/l_o)$ versus (1/T) gives a straight line of slope $-Q/(n+1)R$. The parameter n can be determined when one performs a set of CHR experiments with different heating rate. By plotting $\ln(\Delta l/l_o)$ versus $\ln(a)$ at a specific temperature, a line with slope of $-1/(n+1)$ will result.

In some cases, the plot of $\ln(\Delta l/l_o)$ versus (1/T) may consist not of a single straight line but of two or more straight lines separated by curved transition regions. This change of slope could be caused by a change in the mass transport mechanism (assuming different activation energies) or by a change in the relative importance of competing mechanisms. Thus, by using the CHR method, it may be possible to obtain mechanistic information for the gel-glass conversion.

A plot of $\ln(\Delta l/l_o)$ versus (1/T) with various heating rates is shown in Figure 4.20 for a series of 5% titania-silica gel-glasses pre-treated at 615°C. This plot is obtained using the values of total shrinkage from the

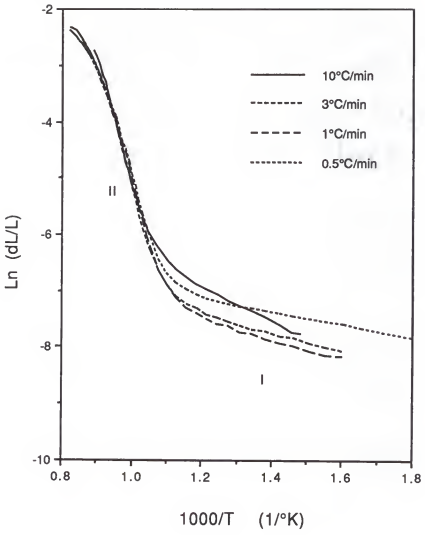

Figure 4.20 Plot of Ln(shrinkage) vs. 1/T under various heating rates for 5% titania-silica gels previously densified at 615°C.

dilatometer. It is observed that there are two straight lines separated by a curved transition region. The slope of this plot is predicted to be proportional to an activation energy. This figure suggests that one shrinkage mechanism predominates below 700°C and a different shrinkage mechanism (i.e. one with a different activation energy) predominates above 700°C. Since the samples have been thermally stabilized at 615°C before the testing, shrinkage in the lower temperature regime (Region I) should result from the desorption of adsorbed water molecules. For the higher temperature regime (above 700°C), the sample shrinks sharply where viscous sintering is the predominant mechanism (Region II).

Equation (4.6) describes the initial stage sintering and predicts that the slope in Region II (Fig 4.20) equals $-Q/(n+1)R$, where for a viscous sintering mechanism, Q is the activation energy for viscous flow and n equals zero. A plot of $\ln(\Delta l/l_o)$ versus $(1/T)$ for Region II only is shown in Figure 4.21. Values for the slope, $-Q/(n+1)R$, are in the range of 22321 to 24304. The value of n is derived from the plot of $\ln(\Delta l/l_o)$ versus $\ln(a)$, as shown in Figure 4.22, which ranges from 5.8 to 6.1. Similar high values of n in the CHR experiments for initial stage sintering has been reported by Brinker et al. [83] for the multicomponent silicate gel of 66 $SiO_2 \cdot 18\ B_2O_3 \cdot 7\ Al_2O_3 \cdot 3$

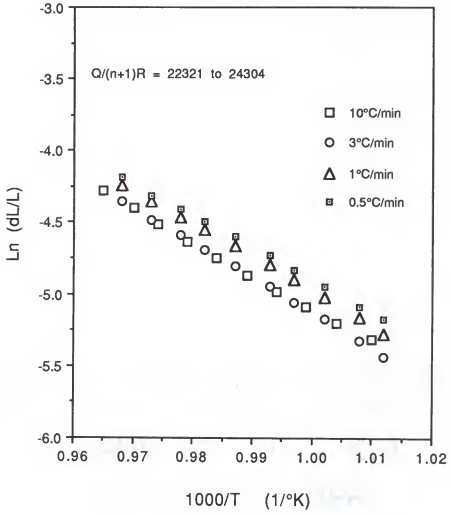

Figure 4.21 Plot of Ln(shrinkage) vs. 1/T for 5% titania-silica gels under various heating rates.

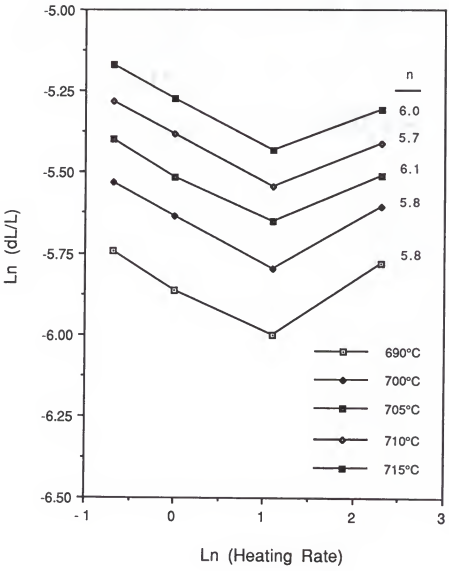

Figure 4.22 Plot of Ln(shrinkage) vs Ln(heating rate) for 5% titania-silica gel. n is determined from the slope in the interval 0.5 to 3°C/min.

BaO. They reported a value of n ranging from 7.9 to 13.1. As mentioned above, in viscous sintering, Q is the activation energy for viscous flow and n equals zero. Thus a high value of n will result in a low value of the activation energy, Q.

In the CHR model, the viscosity is assumed to be a single-valued function of temperature. In a gel-glass system, however, η is also time dependent [84,85]. This arises from the fact that several mechanisms, e.g. condensation polymerization, structural relaxation and viscous sintering, can be operative over the same temperature regime [33,86,87]. Therefore, η is not only temperature but also time dependent. Experimentally, shrinkage is thus not strongly dependent upon heating rate leading to a high value of n.

4.2.5 Effect of Titania Content

Figure 4.23 plots the thermal expansion curves for 3% and 5% titania-silica gel-glass densified at 950 °C. Compared with that of vitreous silica (NIST* standard, also plotted in Figure 4.23) , this set of curves show that the thermal expansion of the gel-glass decreases as the titania content increases.

---

* National Institutes of Standards and Technology.

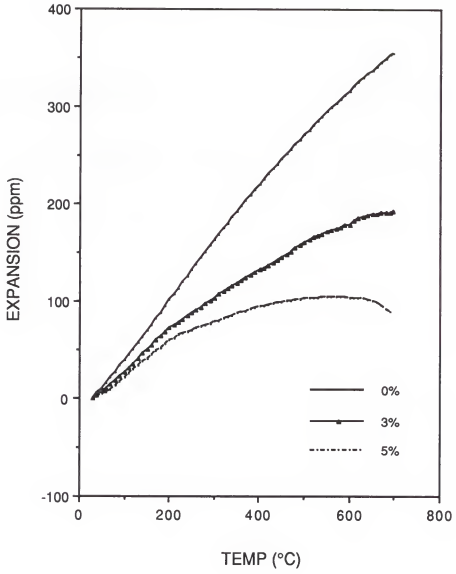

Figure 4.23 Linear thermal expansion of sol-gel derived titania-silica glasses with various titania contents.

The corresponding average linear thermal expansion (CTE) values were determined for the 3% and 5% titania-silica gel-glasses between the temperature range of 30 °C to 700 °C, as plotted in Figure 4.24. The CTE for 3wt% and 5wt% titania-silica gel-glasses is 0.298 ppm/°C and 0.16 ppm/°C respectively. The CTE between the temperature range of 25 °C to 700 °C for flame hydrolysis derived 3.42wt% and 6wt% titania-silica glass is 0.231 ppm/°C and 0.013 ppm/°C respectively [38]. It is evident that the CTE decreases as titania content increases in the gel-glasses, as is known for melt-derived [38] or flame hydrolysis derived titania-silica glasses [38,61]. In addition, it is also evident that the expansion values and their dependence upon composition for sol-gel derived titania-silica glasses are consistent with the data reported for glasses prepared by melting method [38].

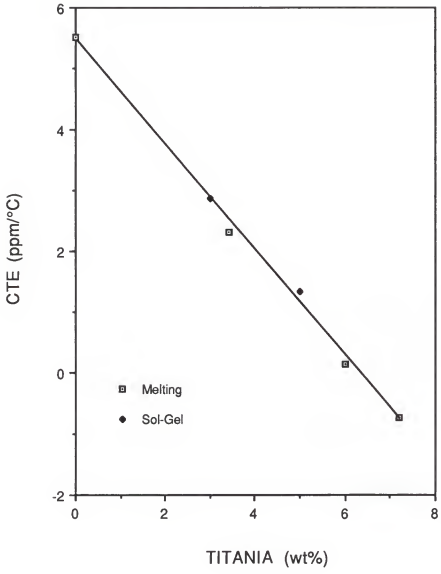

Figure 4.24 Coefficients of thermal expansion for titania-silica glasses with various titania contents.

CHAPTER V
PHYSICAL AND CHEMICAL CHARACTERIZATION

5.1 Structural Analysis

Densification is the increase in bulk density that occurs in a material as a result of the decrease in the the volume fraction of pores [32,33]. Thus, structural evolution during sintering can be characterized following the change in density as well as the change in the volume fraction of pores.

Gas adsorption techniques have been extensively applied to the study of the texture of sol-gel derived silica [38,88-90]. Using the BET theory, one can monitor the change in surface area of the gel as densification proceeds. Information regarding changes in the pore volume, average pore radius, as well as the pore size distribution can also be obtained. These offer a means for following the structural evolution during the gel to glass conversion.

Recently, Vasconselos [72] and Vasconcelos, DeHoff and Hench [91] have attempted to understand the structural evolution of silica gel monolith using topological

concepts. This approach provides complementary information about the sintering process which is also of value in the characterization of the interconnected pore structures present in the gels.

5.1.1 X-Ray Diffraction

Figure 5.1 shows the X-ray diffraction pattern of a dried silica gel and a 10 wt% TiO_2-SiO_2 gel monolith. The scattering patterns are nearly identical. It is observed there is a broad band centered at $2\theta=22°$. This is characteristic for vitreous silica. However, the silica diffraction features are slightly smeared and skewed as titania is added to the silica matrix. This is to be expected since the Ti^{4+} ions are larger than that of Si^{4+}. As the Ti^{4+} replaces Si^{4+}, there will be an increase in the spread of cation-oxygen bond lengths as well as oxygen-oxygen separation [62].

The XRD patterns for a 10 wt% titania-silica gel densified to high temperature are shown in Figure 5.2. As shown in the figure, the broadening of the gel diffraction peak decreases with increasing temperature, indicating an increase in the ordering of the gel network. A similar observation has been reported for the monolithic silica gel system [39]. When the sample is heat treated above

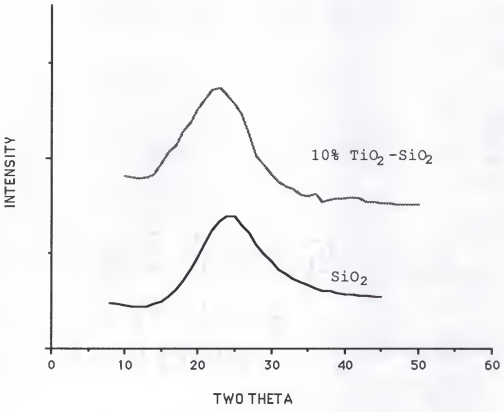

Figure 5.1 X-ray diffraction patterns of silica and 10% titania-silica gels.

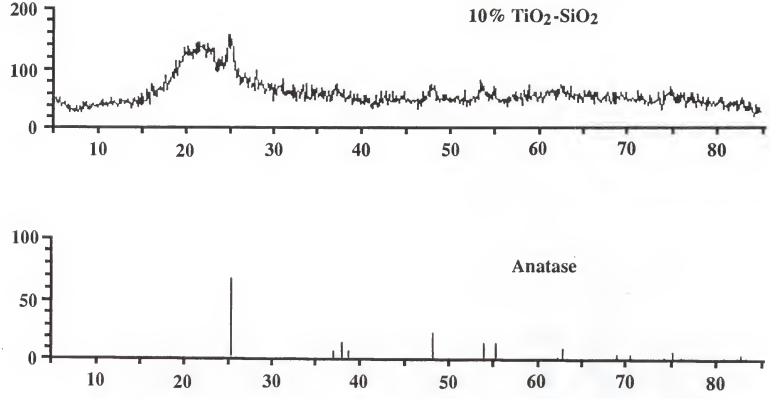

Figure 5.2 X-ray diffraction pattern of 10% titania-silica gel densified at 1100 °C.

1100°C, characteristic peaks for the crystal phase of anatase appear, as shown in Figure 5.2. Emili et al. [51] also reported the observation of anatase crystals in 10wt% titania-silica gel-glass when the sample was treated at 1000°C for 3 hours. Figure 5.3 plots the boundary of the amorphous regime for various titania content in the titania-silica gels. For less than 10 wt% TiO_2, the samples heated at 950°C for 15 hours in air are still amorphous. The temperature at which the anatase precipitates out decreases as the TiO_2 content increases. This is similar to the results by Hayashi et al. [50] and Sakka and Kamiya [48].

5.1.2 Density

5.1.2.1 Effect of titania content

The bulk densities for various dried titania-silica gels are plotted in Figure 5.4. The bulk densities are essentially constant irrespective of the titania content. As densification proceeds in a dried air atmosphere, the bulk density increases as the temperature increases, as shown in Figure 5.5. The rate of increase is relatively slow at temperature below 600°C, while above 800°C, the rate of increase is much sharper. The increase of density

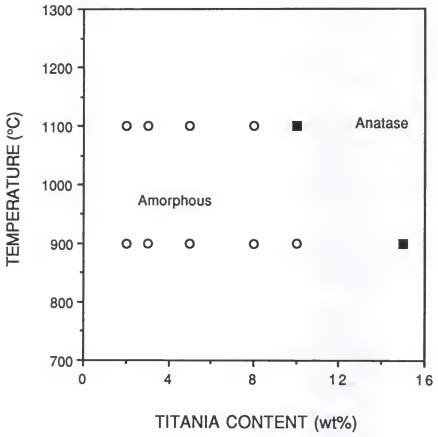

Figure 5.3 X-ray diffration of titania-silica gels.

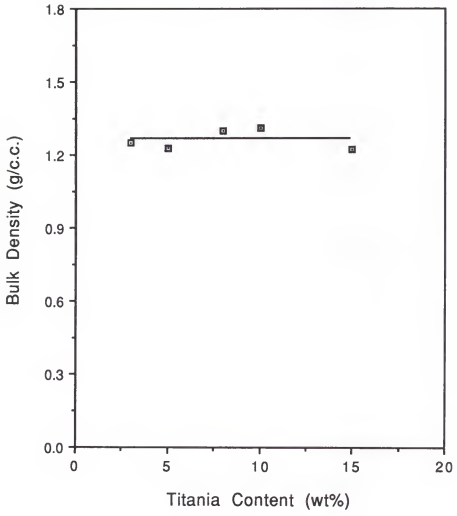

Figure 5.4 Variation of bulk density with titania content for dried titania-silica gels.

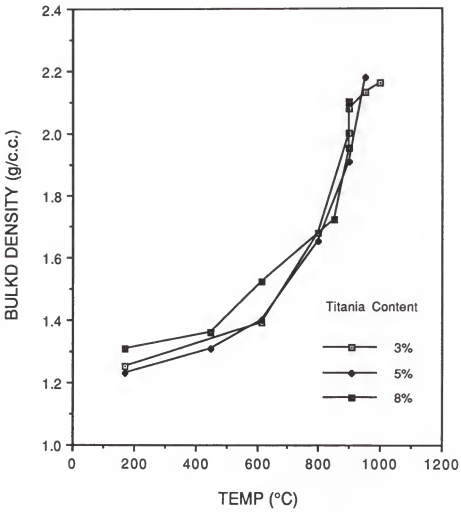

Figure 5.5 Variation of bulk density with temperature for gels with various titania contents.

with temperature is nearly identical for the 3%, 5% and 8% titania-silica gels.

The true densities of the titania-silica gels were evaluated using helium pycnometry. The variation of the structural density with densification temperature for 3%, 5%, 8% and 15% titania-silica gels is shown in Figure 5.6. For low concentration of titania, the structural density of the dried gels is around 2.1 g/cm^3 irrespective of the titania content. As the densification proceeds, it is observed that the structural densities of the titania-silica gels increase. The skeletal densities for gels densified above 950 °C are comparable to that reported in literature [38]. The anomalous increase in density for 15 wt% TiO_2-SiO_2 glasses at 950°C is attributed to the precipitation of anatase crystals, as illustrated in Figure 5.3. One notes that the true densities for the 3%, 5% and 8% TiO_2-SiO_2 glass are nearly identical at higher temperature. This can be considered as a result of a balance between the increase in molar volume and the mass increase as the Ti ions enter the structure of the gel network.

In the case of pure silica gel, the dried gel monolith is reported to have a structural (true) density similar to that of the titania-silica [72]. It is also reported that the structural density increases as densification proceeds

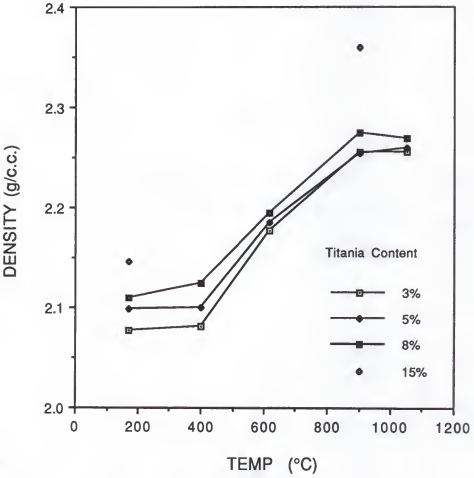

Figure 5.6 Variation of true density with temperature for gels with various titania contents.

irrespective of the pore dimension [70,92]. However, a maximum in structural density of ca. 2.30 g/cm^3 is reported in silica gel at around 900°C before equilibrating at full densification at about 2.22 g/cm^3 [92]. This maximum in structural density at an intermediate temperature is not observed in the titania-silica system. One possible explanation for this phenomenon is the formation and elimination as a function of temperature of the strained defects (D1 and D2 ring structure) in the silica gel. Peak intensities associated with these defect structure have been reported to decrease with the addition of titania [93]. This implies the opening up of the strained defects to accommodate the larger titanium ions, i.e., elimination of the defect structure formation. Thus, a maximum in structural density at an intermediate temperature is not observed in the titania-silica system (see Section 5.3.4).

5.1.2.2 Effect of sintering atmosphere

The effect of humidity on the sintering behavior of the titania-silica gels was evaluated using a humid ambient atmosphere furnace. The variation of bulk densities as a function of densification temperature for the 3% and 5% TiO_2-SiO_2 gel monoliths are shown in Figures

5.7 and 5.8, respectively. Below 600°C, the bulk density increases gradually as temperature increases regardless of the sintering atmosphere. Above this temperature, the density increases sharply. In both cases, samples sintered in the static ambient furnace all foamed when densification was carried out at 850°C. This is not the case when sintering is conducted under a dried air atmosphere. The fact that samples densified in humid air will bloat or foam easier (i.e. at lower temperature) is associated with the entrapment of water molecules inside the closed pores. The rate of densification for a glass increases as the viscosity of the glass decreases. As the OH content of the glass increases, densification increases [94] leading to pore closure before water can be thermally desorbed, as in the case of static ambient atmosphere sintering.

5.1.3 Characterization of Texture

5.1.3.1 Gas adsorption analysis

5.1.3.1.1 Characterization of dried gels

The gas adsorption analysis of the titania-silica gel-glasses densified to different temperatures was carried out using the automatic Autosorb-6 sorption instrument

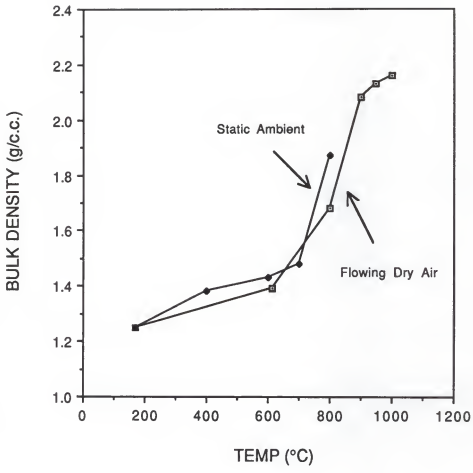

Figure 5.7 Variation of bulk density with temperature for 3% titania-silica gel-glasses under different atmospheres.

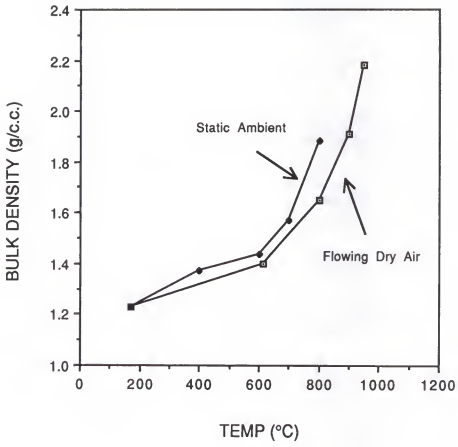

Figure 5.8 Variation of bulk density with temperature for 5% titania-silica gel-glasses under different atmospheres.

(Quantachrome, Inc.). Figure 5.9 shows the BET plots for a dried 3% titania-silica monolith. Little deviation from linearity is observed in this plot. This is typical for all the dried titania-silica gels characterized in this work. Figure 5.10 shows the adsorption-desorption isotherms for a dried 3 wt% titania-silica gel. Isotherms for other weight percentages of dried TiO2-SiO2 gels are similar to that shown in Figure 5.10. There is little hysteresis between the adsorption and the desorption isotherm. Similar results have been reported for nitric acid derived silica gel with an average pore radius of 12Å.[72].

There are 5 possible types of "Adsorption Isotherms" when gas is adsorbed on solid surfaces at a fixed temperature [95]. The type I isotherm, as that shown in Figure 5.10, occurs when adsorption is limited to, at most, only a few molecular layers. This type of isotherm indicates that all the surface sites are occupied for values of P/P_0 approaching unity, 1.0. In the case of physical adsorption (as in nitrogen gas adsorption analysis), this isotherm is encountered for microporous systems where the pore size is defined to be less than 15 Å [95].

Figure 5.11 shows the pore size distribution for a dried 3 wt% titania-silica gel. The pore size

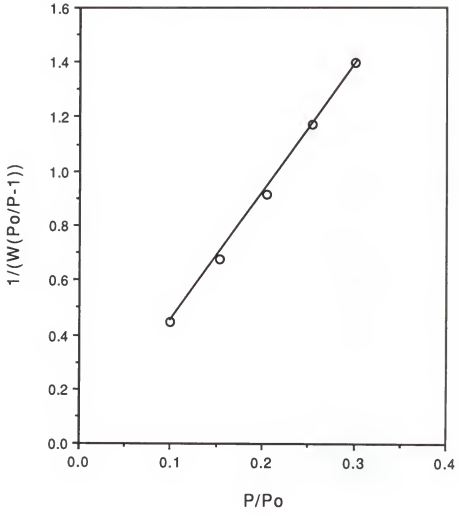

Figure 5.9 BET plot for a 3% titania-silica gel monolith.

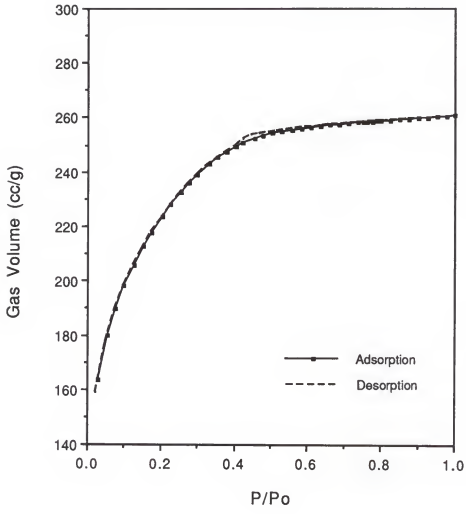

Figure 5.10 Adsorption-desorption isotherm for a dried 3% titania-silica gel monolith.

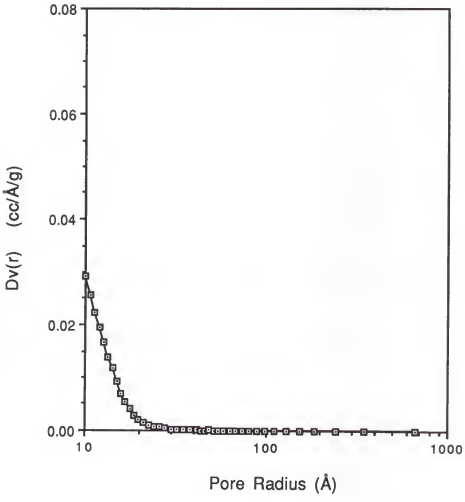

Figure 5.11 Pore size distribution for a dried 3% titania-silica gel monolith.

distribution plots for other weight percent titania-silica gels are similar to that shown in Figure 5.11. The average pore radius for this sample is 11.5Å. The cutoff in the distribution at around 3.5Å represents the smallest possible resolution available in the nitrogen gas absorption analysis.

For the dried titania-silica gel monoliths prepared using nitric acid as the catalyst, the average pore radius, specific surface area and pore volume appeared to be constant regardless of the titania content, as shown in Figures 5.12, 5.13 and 5.14.

As the R ratio increases, both the specific surface area and the pore volume of the dried gel increase, as shown in Figure 5.15 and Figure 5.16 for a 5 wt% titania-silica gel. However, the pore radius, calculated using a cylindrical pore geometry, remains essentially constant as shown in Figure 5.17.

5.1.3.1.2 Densification

As the densification temperature increases, the surface area and volume of pores decreases, as shown in Figures 5.18 and 5.19 for a set of 3% titania-silica gel monoliths densified in a dried air atmosphere. Again, as the total volume of pores decreases, the average pore

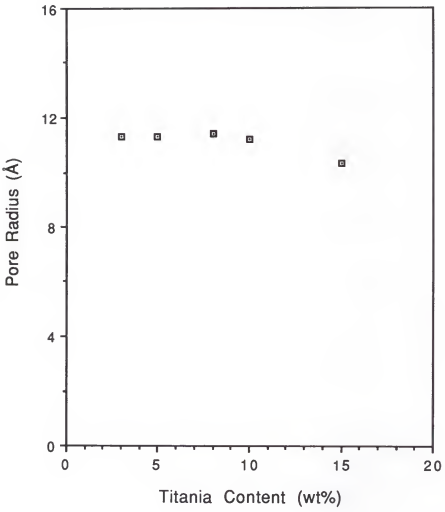

Figure 5.12 Variation of pore radius with titania content for dried titania-silica gels.

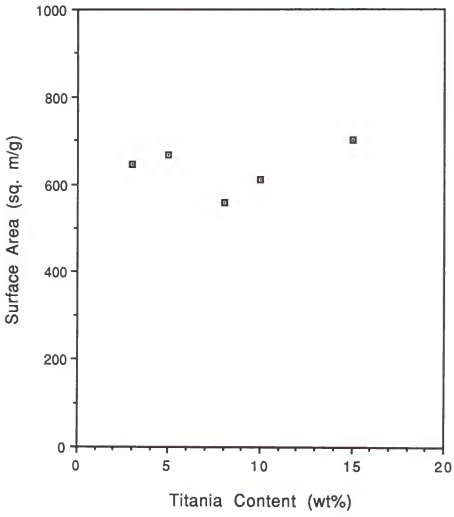

Figure 5.13 Variation of specific surface area with titania content for dried titania-silica gels.

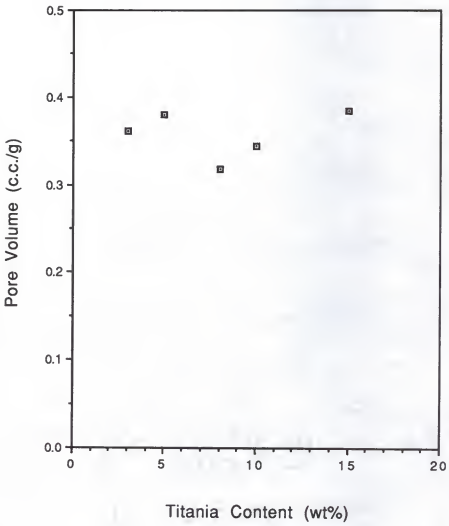

Figure 5.14 Variation of pore volume with titania content for dried titania-silica gels.

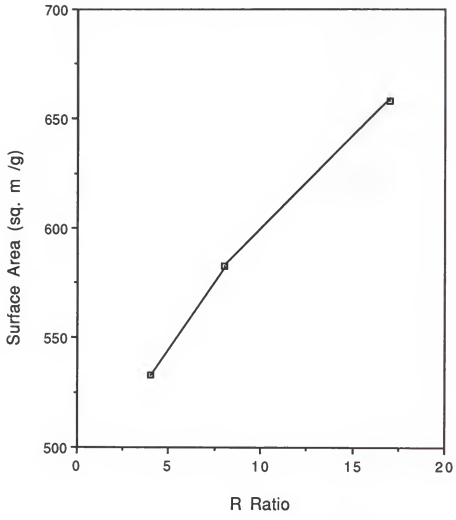

Figure 5.15 Variation of specific surface area with R ratio for dried 5% titania-silica gels.

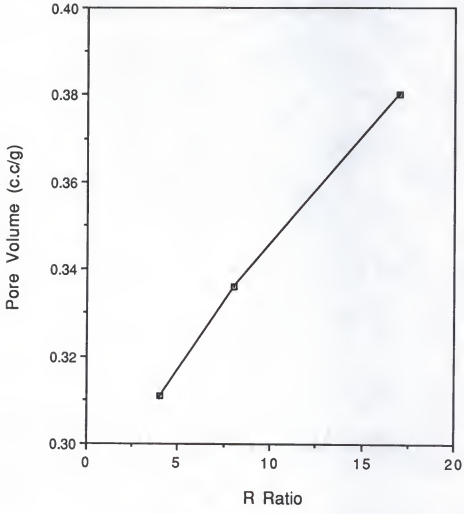

Figure 5.16 Variation of pore volume with R Ratio for dried 5% titania-silica gels.

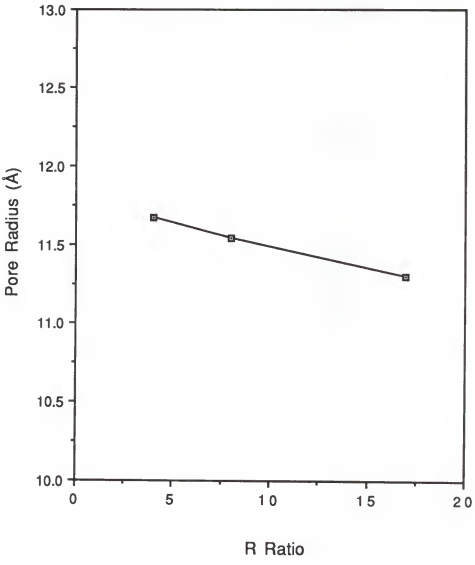

Figure 5.17 Variation of pore radius with R Ratio for 5% titania-silica dried gels.

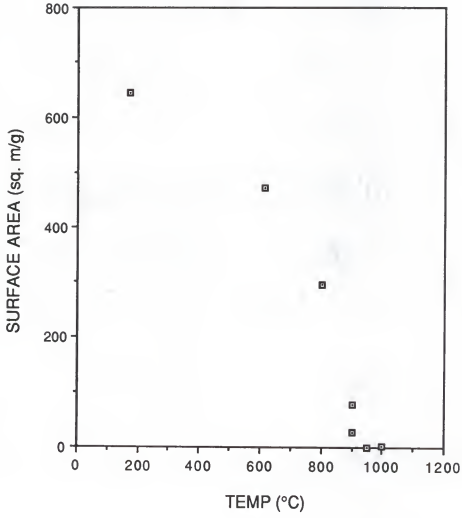

Figure 5.18 Variation of specific surface area with temperature for 3% titania-silica gels.

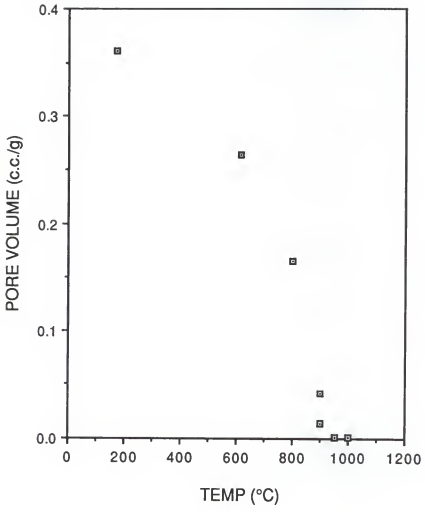

Figure 5.19 Variation of pore volume with temperature for 3% titania-silica gels.

radius remains unchanged, as shown in Figure 5.20. Plot of pore volume vs. densification temperature for 5%, 7% and 8% titania-silica gel monoliths is shown in Figure 5.21. For all the compositions, a similar trend of decrease in pore volume as densification temperature increases is observed. Plot of surface area as a function of densification temperature for 5%, 7% and 8% TiO_2-SiO_2 gel-glass is shown in Figure 5.22. Similar to 3% TiO_2-SiO_2 (Figure 5.18), the surface area decreases as the densification temperature increases. The plot of pore radius as function of densification temperature for 5%, 7% and 8% titania-silica gel monoliths is shown in Figure 5.23. The average pore radius remains unchanged as the densification proceeds.

Figure 5.24 and 5.25 shows the pore volume and surface area distribution, respectively, from the adsorption curves for a set of 5% titania-silica gels densified at different temperatures. As shown in Figure 5.25, most of the surface area is contributed by the smallest pores. During densification, elinimation of those pores produce a rapid loss of surface area. However, as indicated in Figure 5.24, no pores grow as densification proceeds.

When the surface area is plotted as a function of pore volume for gels with various titania content, all the data fall on a straight line regardless of the titania content,

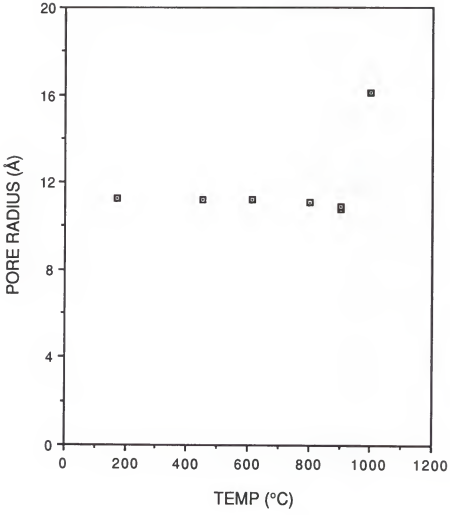

Figure 5.20 Variation of pore radius with temperature for 3% titania-silica gels.

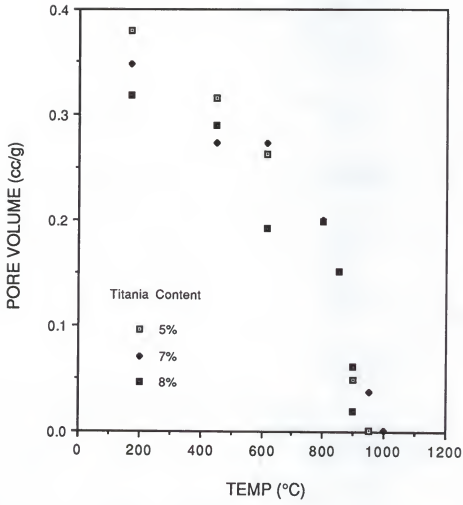

Figure 5.21 Variation of pore volume with temperature for gels with various titania contents.

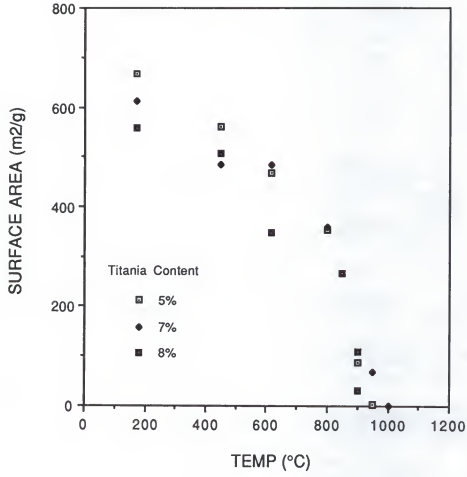

Figure 5.22 Variation of specific surface area with temperature for gels with various titania contents.

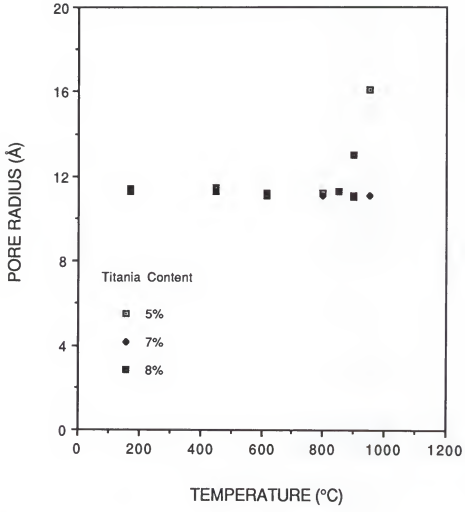

Figure 5.23 Variation of pore radius with temperature for gels with various titania contents.

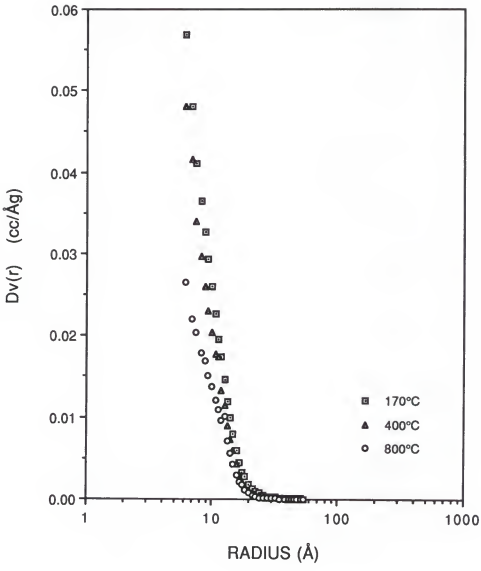

Figure 5.24 Plot of pore volume distribution for 5% titania-silica gels densified to various temperatures.

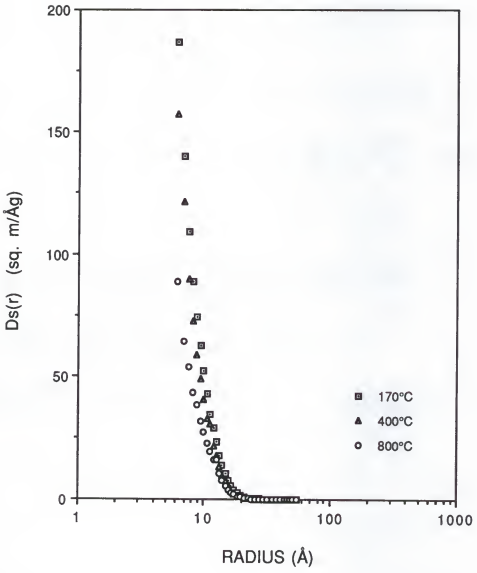

Figure 5.25 Plot of pore surface area distribution for 5% titania-silica gels densified to various temperatures.

as shown in Figure 5.26. In addition, when densification is carried out in a humid atmosphere, this linear relationship remains, as shown in Figures 5.27 and 5.28 for 3% and 5% TiO_2-SiO_2 gel-glass respectively. This infers that the densification proceeds with a similar path irrespective of the titania content and/or water content in the atmosphere.

5.1.3.2 Topological analysis

Densification, as defined by Rhines [96] is a geometric change in which a mass of separate particles becomes a coherent body, motivated by a decrease in surface free energy. One of the most important concepts of topology is the genus (G), or connectivity, which can be described as:

$$G = B - N + 1$$

where B is the number of interparticle contacts or branches and N is the number of particles or nodes. Based on this concept, the densification process can be divided into three stages, according to the genus of the material or system [96]:

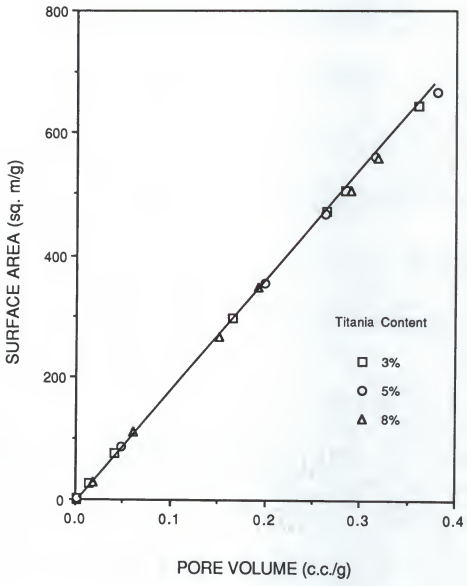

Figure 5.26 Variation of surface area with pore volume for gels with various titania contents.

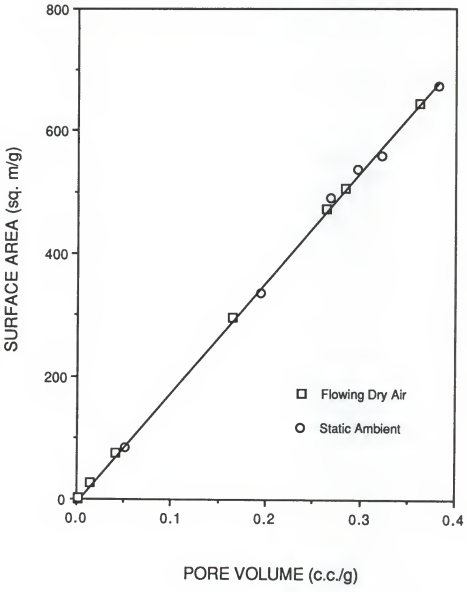

Figure 5.27 Variation of surface area with pore volume for 3% titania-silica gels densified to various temperatures.

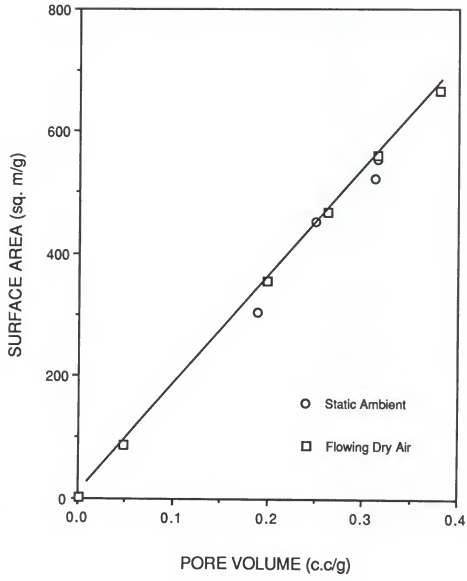

Figure 5.28 Variation of surface area with pore volume for 5% titania-silica gels densified to various temperatures.

First stage; growth of the weld necks while genus remains constant.

Second stage: the genus decreases towards zero while the pores becomes isolated.

Third stage: the genus is constant at zero as the pores disappear.

Vasconcelos [72] has used the topological concept to understand the structural evolution of the gel-glass transition in pure silica gel. Due to the impracticability of applying a serial sectioning technique to a structure with a nanometer scale, one has to assume certain models to carry out a topological evaluation of the structural changes which occur during sintering. In his cylindrical model, it is assumed that all the pore volume and all the surface area is associated with the cylindrical branches of the pore structure. The point at which the branches meet constitutes a node which has no volume associated with it.

Therefore, if one assumes, see Vasconcelos [72], that D is the average diameter of the pore and L is the average length of a cylindrical branch:

$$Vv = \pi \; Bv \; D^2 \; L \; / \; 4 \quad ; \quad Sv = \pi \; Bv \; D \; L \qquad (5.2)$$

where Vv is the volume fraction of pores, Sv is the surface area per unit volume and Bv is the number of branches per unit volume. Taking the ratio of the above two equations, one can see that

$$D = 4\ Vv\ /\ Sv \qquad (5.3)$$

which is a fixed number. In order to solve for Bv, one needs to assume a value for the parameter L. By assuming L=4(1-Vv)/Sv, one can then solve for Bv:

$$Bv = 4\ Vv\ /\pi\ D^2\ L = 4\ Sv\ /\ \pi\ D\ L \qquad (5.4)$$

Figure 5.29 illustrates the variation of volume fraction of pores (Vv) as a function of densification temperature for gel-glass monoliths with various titania contents. It is observed that as the densification proceeds there is a continuous decrease in the volume fraction of pores. The decrease is slow when the temperature is below 600°C. Above 800°C, the decrease is much more pronounced. A similar trend is also observed when the metric property Sv, surface area per unit volume, is plotted as a function of temperature for different weight percentages of titania in the silica matrix, as shown in Figure 5.30. This behavior is similar to that

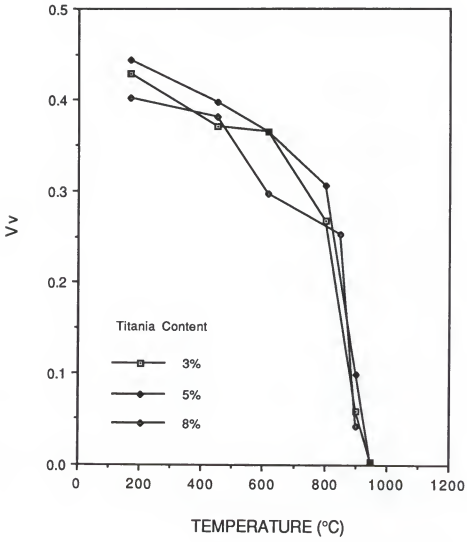

Figure 5.29 Variation of volume fraction of pores with densification temperature for gels with various titania contents.

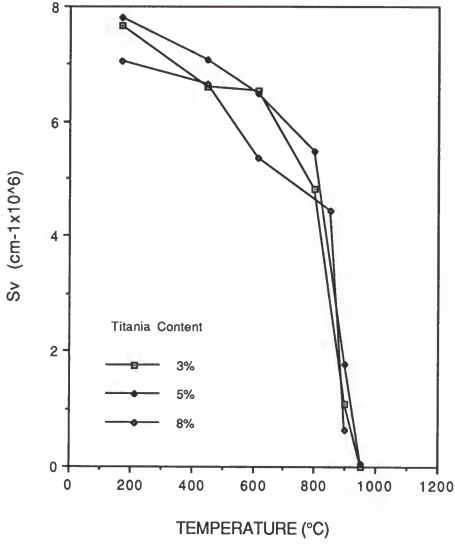

Figure 5.30 Variation of Sv with densification temperature for gels with various titania contents.

reported in the pure silica gel system [39,72]. It is noted that as the titania content increases, the rate of decrease in the metric properties increases to a small extent.

When the surface area per unit volume, Sv, is plotted against the volume fraction of pores, Vv, a linear relationship, as shown in Figure 5.31, is obtained regardless of the titania content. This suggests that there is a similar path of densification for the various titania-silica gels. It also indicates that the pore radius remains constant as densification proceeds.

The dried gel usually corresponds to a state of maximum number of branches, nodes and genus, which, in the topological point of view, corresponds to the first stage of densification. The average coordination number of pores for the dried gels is assumed by Vasconcelos [72] to be 4 in the above model. The choice of this initial pore coordination number does not affect the value of Bv as shown by Vasconcelos [72] in the pure silica gel system. In Figures 5.32-5.34, Bv, Nv and Gv are plotted as a function of the densification temperature for 3%, 5% and 8% titania in the silica matrix, i.e. the temperature dependence of the structural evolution. As the densification temperature increases (second stage of densification), both the number of branches (Bv) and the

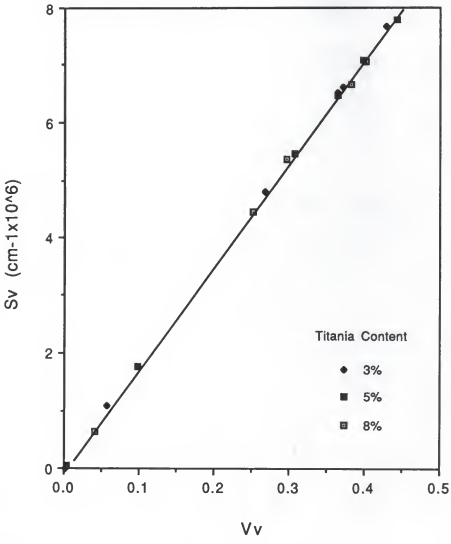

Figure 5.31 Plot of Sv vs. Vv for gel-glasses containing various amount of titania.

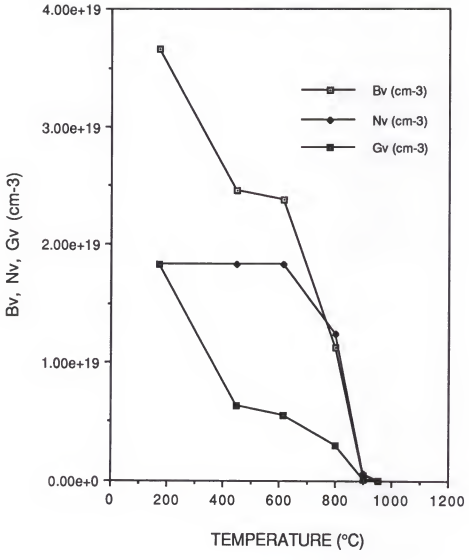

Figure 5.32 Variation of Bv, Nv, and Gv with densification temperature for 3% titania-silica gels-glass.

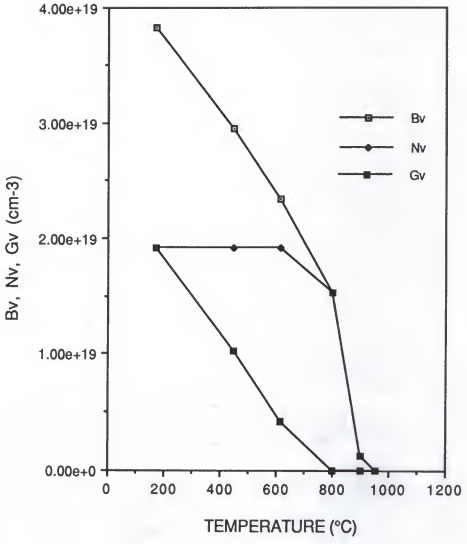

Figure 5.33 Variation of Bv, Nv, and Gv with densification temperature for 5% titania-silica gel-glass.

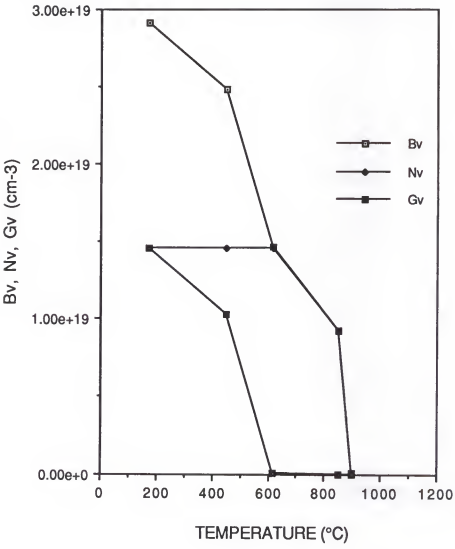

Figure 5.34 Variation of Bv, Nv, and Gv with densification temperature for 8% titania-silica gel-glass.

genus (Gv) decrease, while the number of nodes (Nv) remains constant as the number in the dried stage. When the pore coordination number decreases to 2 (i.e. when Bv reaches the value of Nv^o), the genus goes to zero. This occurs at above 800°C for 3% titania while for 8% titania, it occurs below 700°C. The exact location of this temperature (T_{pc}, which corresponds to the onset of pore closure) is , of course, processing dependent. This results from the fact that viscosity of a glass decreases as the amount of water increases. Therefore, the Tpc for a pure silica gel processed using a similar thermal treatment is around 860°C [39] while Vasconcelos [72], using a much slower thermal schedule, reported a T_{pc} at ca. 960°C. Thus, the higher the titania content in the silica matrix, the lower is the temperature at which the third stage of densification commences (onset of pore closure). Figure 5.35 plots the strain point (log η=14.6 P), annealing point (log η=13.2 P) [38] and onset temperature of pore closure for flame hydrolysis glass and gel-glass with various titania contents. It is seen that these three curves have a similar trend of decrease in value as titania content increases. This leads to the experimental observation that gel samples with higher titania content are much more difficult to sinter without pore closure prior to desorption of water from the pores.

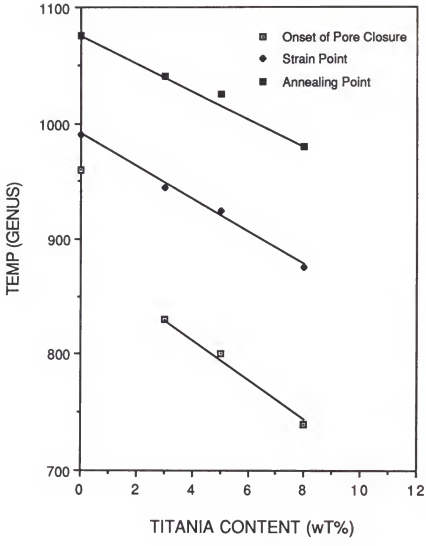

Figure 5.35 Plot of strain point, annealing point and onset temperature of pore closure for titania-silica gel-glasses.

The difficulties in sintering gels with higher titania content lies in their lower viscosity values [61]. It has been shown that for addition of up to 10 wt% titania, there is very little change in density but the viscosity decreases, which leads to the lower densification temperature. The change in viscosity as the titania content increases will be analyzed in the following section.

5.1.3.3 Calculation of viscosity of titania-silica glasses

There are a number of viscosity models in the literature which describe the temperature dependence of the flow behavior of molten glasses [97-103]. Most of these models are phenomenological and different models have been applied to different glass forming systems. In all the models, the relationship

$$\eta = G \tau \tag{5.5}$$

is true. Here, η is the shear viscosity, G is the shear modulus and τ is the relaxation time. In the derivations of viscosity models, one considers a suitable mechanism for the molecules to move. This probability of jumping gives the temperature dependence of the diffusion

coefficient. Since the diffusion coefficient is related to the viscosity through the Stökes-Einstein Equation,

$$D = k\,T\,/\,3\,\pi\,a\,\eta \tag{5.6}$$

where D is the diffusion coefficient and a is the molecular diameter, the temperature dependence of diffusion coefficient is reduced to the temperature dependence of the viscosity.

A. Arrhenius Model

In this model, a molecular jump is possible if the molecule obtains enough energy to break its bonds. A general form of the equation is given as

$$\eta = \eta_o \exp(\Delta E/kT) \tag{5.7}$$

where ΔE is the activation energy, k is the Boltzman constant and T is the absolute temperature.

B. The Free-Volume Approach

According to this model, the critical step for flow is by opening a void of some critical size to permit the movement of molecules [98,100]. The voids are formed by the redistribution of the free volume (V_f) in the system, which is defined as

$$V_f = V - V_o \tag{5.8}$$

where V is the molecular volume in the liquid and V_o is the van der Waals volume of the molecule. This excess free volume is redistributed through thermal fluctuations and costs no additional energy. The viscosity-temperature equation has the form

$$\log \eta = A + B/(V-V_o) \tag{5.9}$$

where A and B are constants. This equation is identical to the Fulcher equation if one assumes a constant expansion coefficient, i.e. the free volume term $(V-V_o)$ is then proportional to $(T-T_o)$ [98].

C. Hybrid Equation

The shortcoming of the above two models is that they completely neglect each other. A hybrid equation is thus yielded by considering the critical aspects of those two models. In the hybrid model developed by Macedo and Litovitz [97], a molecule is pictured as vibrating about an equilibrium position until the combination of the following two events occurs:(1) the molecule attains sufficient energy to break away the attractive forces holding it to its neighbors, and (2) an empty site is available into which the molecule can jump. Thus the

probability of a jump (P_j) from one site to another is given by

$$P_j = P_E \times P_v \tag{5.10}$$

where P_E is the probability of attaining sufficient energy to break bonds and P_v is the probability that there is sufficient local free volume for a jump to occur. The equation has the form of

$$\eta = A_o \exp(\Delta E/RT + \gamma v_o/v_f) \tag{5.11}$$

where γ is a numerical constant needed to correct for the overlap of free volume and lies between 0.5 and 1.

For those liquids where $\Delta E/RT << v_o/v_f$, the above equation becomes identical to the free volume equation. On the other hand, it is possible for the free volume to play a significant role and yet the liquid still behaves in an Arrhenius manner. This occurs in liquids with the coefficient of thermal expansion either zero or very small ($\sim 10^{-5}$). Thus, v_f is effectively independent of the temperature and the hybrid equation becomes

$$\eta = A'_o \exp(\Delta E/RT) \tag{5.12}$$

where

$$A'_o = A_o \exp(\gamma V_o/V-V_o) \qquad (5.13)$$

Therefore, the free volume plays no role in the temperature dependence of η but it affects the absolute value of η through the pre-exponential term.

Bacon et al. [104] has shown that in vitreous SiO_2 the viscosity over a range from 10^4 to 10^{13} poise is very close to having an Arrhenius behavior. The relationship between the viscosity and temperature for pure vitreous silica can be written as

$$\log \eta = 3.05x10^4/T - 7.7415 \qquad (5.14)$$

This is because the density for amorphous SiO_2 over the temperature range 1300°C to 2300°C does not change appreciably, as shown by Douglas and Isard [105] and Bacon et al. [104] Thus, amorphous SiO_2 has a very small coefficient of thermal expansion and the free volume does not change. That is, vitreous silica is an example of the limiting case of the hybrid model where the free volume effects contribute only to the magnitude of the viscosity but not to the temperature dependence.

To estimate the viscosity of the titania-silica gel-glass, one must start by assuming that the titania-silica gel-glass is iso-structure to that of the silica. Thus,

the flow behavior is also Arrhenius. However, the activation energy for flow should be less for titania-silica due to the presence of the weaker Ti-O bond. The bond length of the Ti-O and Si-O bonds in the titania-silica glass has been reported by Greegor et al. to be 1.83 Å and 1.62 Å, respectively [66]. With the activation energy of 142 Kcal/mole for silica [34], the activation energy for titania-silica is estimated to be 142x1.62/1.83=125 Kcal/mole. This value should not change with an increase in titania content since flow should initiate from the weaker Ti-O bonds as long as the titanium ions replace silicon ions iso-structurally in the system.

To estimate the role of the free volume in SiO_2, Macedo and Litovitz [97] reported a value of $V_f/V \sim 0.16$ using the pressure densification data of Mackenzie [106]. This is done by assuming that most of the change in volume with pressure is due to squeezing out of the free volume. Following a similar approach, the free volume for a 10% titania-silica glass is estimated to be 0.17 [107]. Thus, the viscosity-temperature relationship for titania-silica glass can be written as

$$\eta = 9.053 \times 10^{-9} \exp(125000/RT) \qquad (5.15)$$

Figure 5.36 compares the results from the above equation with the data of Pavlova and Amatuni [108]. As the available pressure densification data is for 10wt% titania-silica and the data of viscosity is for 8% titania-silica, the above equation should predict a lower value of viscosity than the experimental data. This is observed in Figure 5.36.

5.2 Physical Properties

The Vickers hardness number (VHN) of the samples was obtained using a load of 0.1 Kg and a loading time of 12 seconds. Figure 5.37 shows the variation of VHN as a function of titania content for a set of dried gels. It can be seen from the figure that there is no difference in the hardness between gels with different titania contents. The VHN for the dried TiO_2-SiO_2 gels has a value of ca. 50 Kg/mm^2 which is of the same magnitude for nitric acid derived 12 Å silica gels [72]. The variation of VHN with densification temperature for gels with different titania contents is shown in Figure 5.38. For all the samples, the Vickers hardness number increases with increasing sintering temperature. In general, the rate of increase is slow below 600°C while above 800°C it is much sharper.

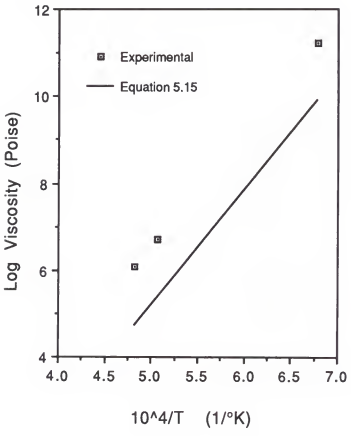

Figure 5.36 Plot of Log(viscosity) vs. 1/T.

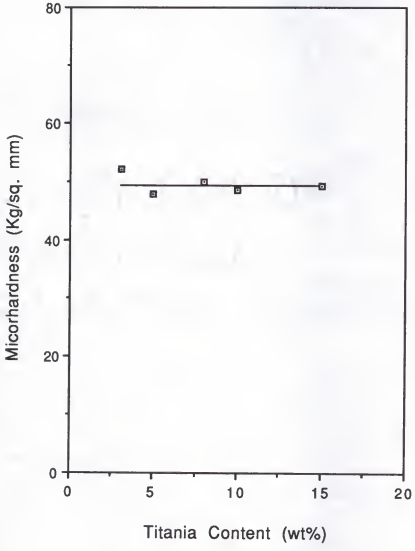

Figure 5.37 Variation of microhardness with titania content for dried gels.

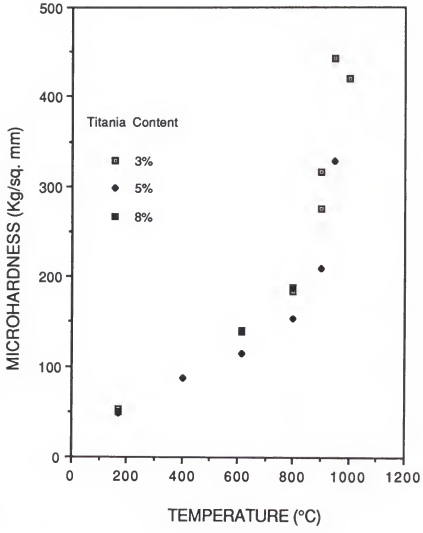

Figure 5.38 Variation of microhardness with densification temperature for gels with various titania contents.

Figure 5.39 shows the effect of humidity on the VHN for a set of 5% TiO_2-SiO_2 gels. Again, as densification temperature increases, the VHN increases. The rate of increase is sharper when densification is carried out in a humid environment. This is to be expected since the presence of water will lower the viscosity of glass which leads to a higher densification rate (i.e. densification will commence at a lower temperature). Thus, fewer pores will be present in the area of the sample directly supporting the applied load leading to a higher value of VHN.

The index of refraction for a set of dried TiO_2-SiO_2 gels is plotted as a function of titania content in Figure 5.40. The index of refraction increases as the titania content in the dried gels increases, as expected because of the higher electronic polarization of the titanium ions. Figure 5.41 plots the change of refractive index as a function of density for a set of 3% titania-silica gel-glasses when heat treated to different temperatures. As the density increases, the index of refraction increases. A similar trend was observed in the pure silica gel system [39]. This illustrates the possibility of monitoring the index of refraction of the porous gels through density control when proper processing steps are undertaken.

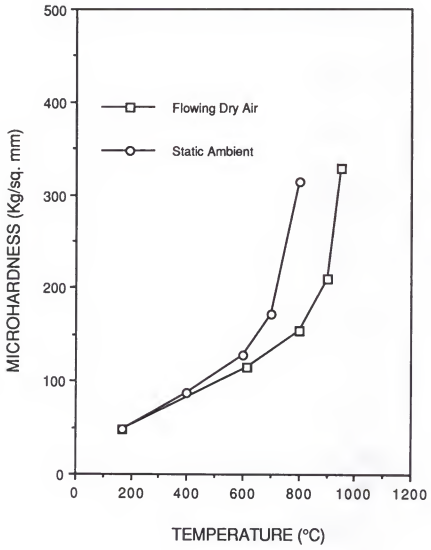

Figure 5.39 Effect of humidity on the microhardness for 5% titania-silica gel-glass.

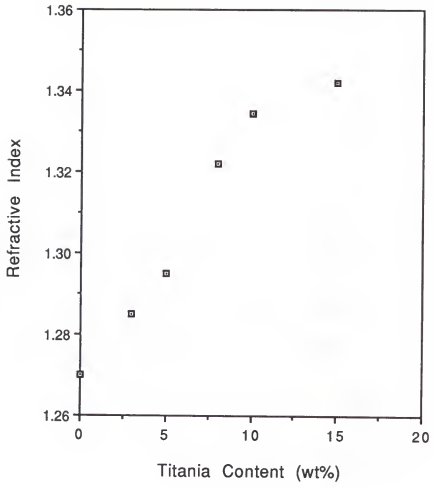

Figure 5.40 Variation of refractive index with titania content for dried gels.

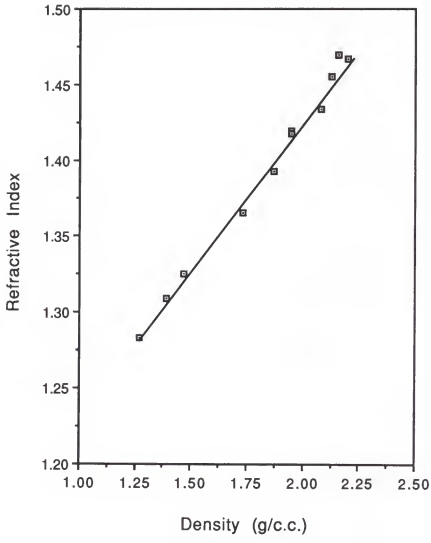

Figure 5.41 Variation of refractive index with density for 3% titania-silica gel-glass.

As light waves (electromagnetic radiation) pass through a material, the waves are retarded due to its interaction with the electronic system of the atoms. The electron cloud around the atomic nucleus will be displaced giving rise to dipole moment and electronic polarization. The index of refraction of a material is related to the number and size of these dipoles per unit volume [109,110]. Thus, there are two conditions which will contribute to higher indices of refraction: (1) presence of atoms with higher atomic number, i.e. more electrons per atom, as in the case of Figure 5.40 and (2) higher density, i.e. more dipoles per unit volume, as in the case of Figure 5.41.

Figure 5.42 compares the refractive index-density relationship for SiO_2 [39] and 3% TiO_2-SiO_2 gel-glass system. Data for 4.7 % TiO_2-SiO_2 glasses densified under static pressure is also included [107]. It is observed that within each isochemical series, the linear relationship between refractive index and density holds.

5.3 Composition and Spectroscopy Characterization

The surface of a gel is covered with a large amount of water as well as hydroxyl groups. The removal of these surface silanol bonds from the pore network results in a

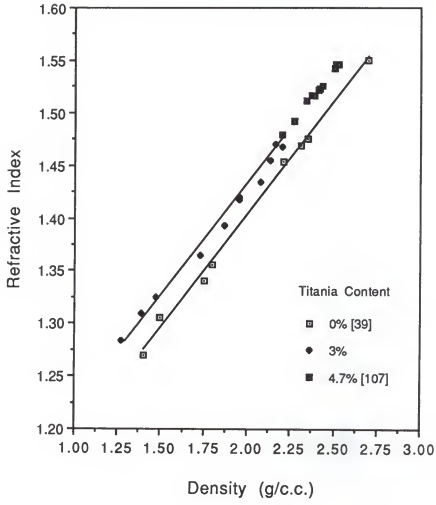

Figure 5.42 Variation of refractive index with density for silica and titania-silica systems.

chemically stable solid. It is recognized that "water" in the porous network is present in two forms: free water within the porous gel structure (i.e. physisorbed water) and hydroxyl groups associated with the gel surface (i.e. chemisorbed water) [111]. The hydration/dehydration behavior of the silica gel/water system has been extensively studied [112-114], as summarized below:

(1) The physisorbed water can be eliminated and condensation of the surface silanol groups starts at ca. 170 °C. The concentration of hydroxyls is estimated to be 4 to 5 SiOH groups per square nanometer at this stage.

(2) Between 170 °C and 400 °C, dehyration of the surface is completely reversible. This occurs via the elimination of surface water and the formation of both single and adjacent surface hydroxyl groups. At 400 °C, most of the remaining surface hydroxyls are adjacent to each other. Thus, they act as the preferential sites for water adsorption.

(3) Above 400 °C, the dehydration process causes an irreversible elimination of adjacent hydroxyl group, decreasing the concentration of SiOH to about 2 SiOH/nm^2 and leaving siloxane groups (Si-O-Si) on the surface.

(4) At ca. 800 °C, only single hydroxyl groups remain on the surface with a concentration of ca. 1.2 SiOH/nm^2.

Further heating causes the departure of these single hydroxyls, leading to densification of the gels.

Spectroscopic methods offer a mean of characterizing, as a function of temperature, the structural evolution of the network as well as the changes described above. Results from various spectroscopic methods will presented in this chapter.

5.3.1 Composition of Gel-Glasses

The compositions of the gel-glass prepared in this work were determined using neutron activation analysis. The results are shown in Table 5.1. It can be seen that the titania concentration is within 5% of the nominal value. This suggests that there is no differential loss of the titanium atoms during the processing.

5.3.2 X-Ray Photoelectron Spectroscopy

X-ray photoelectron spectroscopy is a useful method for probing the bonding states of various elements in solids. The value of the binding energy of photoelectrons is affected by any changes in the distribution of electron density in the given atom and in its environment caused by a change in the oxidation degree of the atom, number and type of ligands and their spatial configuration. These

Table 5.1 Neutron activation analysis of titania-silica gels.

Ti Content (%) (nominal)	Ti Content (ppm) (determined)
3%	3.273 x E4
3%	3.316 x E4
5%	5.398 x E4
8%	8.020 x E4
10%	1.022 x E5
15%	1.517 x E5

changes can bring about a "chemical shift" of the corresponding bands in the XPS spectrum [115].

Figure 5.43 shows the O(1S), Si(2P) and Ti(2P) XPS signals for a monolithic 3% TiO_2-SiO_2 gel-glass densified to 1000 °C. Table 5.2 shows the binding energies for these signals in the present study as well as some values from the literature. The values for the binding energy in the present work are in good agreement with Anpo et al. [116] in which the sample was prepared by coprecipitation of mixed solution of $Si(OC_2H_5)_4$ and $TiCl_4$ with addition of dilute aqueous solution of ammonia [117]. The binding energy for the Ti(2p) in the 3% titania-silica gel-glass is determined to be 460.6 eV. Compared to that of pure TiO_2 powder, a chemical shift of 1.9 ev is observed for the Ti(2P).

The silica gel in Laczka et al.[118] was prepared using TEOS as the precursor and hydrochloric acid as the catalyst. The sample was heat treated up to 1000°C at a rate of 1°C/min. The Si(2P) and O(1S) XPS signals in the Laczka et al. [118] are reported to be doublets. This indicates that the silica gel-glass samples examined in their study are not homogeneous, but are made up of two regions differing in their physico-chemical properties. According to these authors, these might be for domains differing in their degree of ordering. This is not

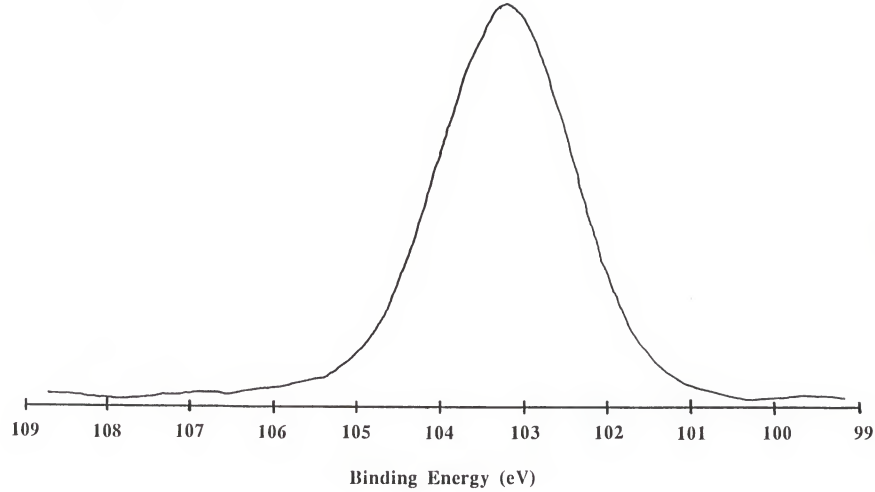

Figure 5.43 XPS spectrum of 3% titania-silica gel-glass.
(a) Si(2p) peak.

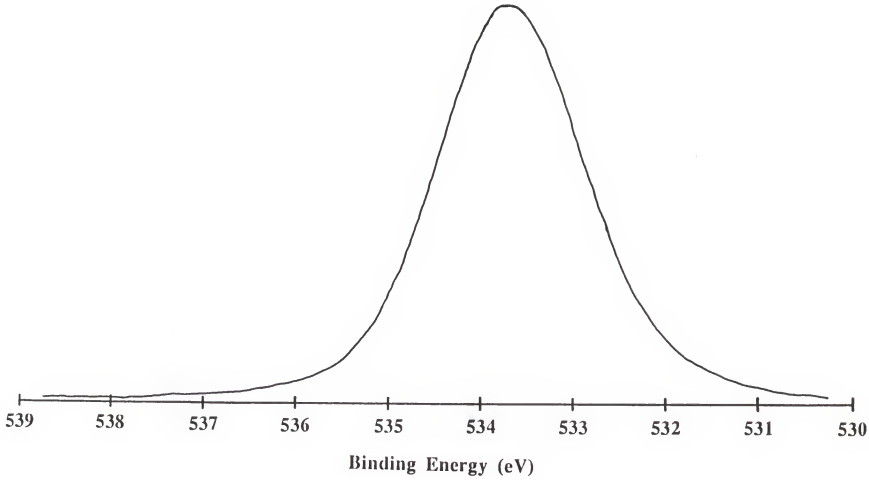

Figure 5.43 XPS spectrum of 3% titania-silica gel-glass.
(b) O(1s) peak.

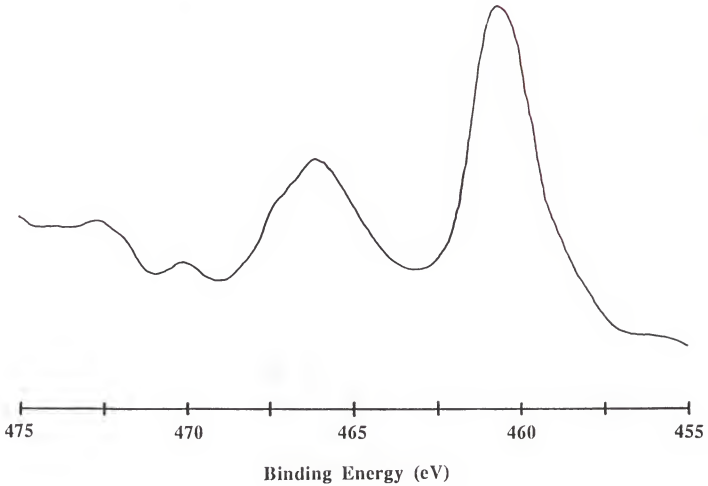

Figure 5.43 XPS spectrum of 3% titania-silica gel-glass.
(c) Ti(2p) peak.

TABLE 5.2 Results of XPS Investigations

Sample	Binding Energy (eV)		
	Si (2p)	O (1s)	Ti (2p)
3 wt% TiO_2-SiO_2	103.1	533.5	460.6
3 mole% TiO_2-SiO_2 [116]	103.0	N/A	460.5
Quartz [118]	103.5	533.4	---
SiO_2 Gel-Glass [116]	102.9	N/A	---
SiO_2 Gel-Glass [118]	102.9	533.4	---
SiO_2 Melted [118]	102.6	532.9	---
TiO_2 [116]	---	---	458.7

observed in the present study indicating that the titania-silica gel-glass in the present study is more homogeneous than the Laczka material. This demonstrates the importance of controlling reactions at molecular level, which affects the properties of the glass formed and even the local distribution of cations.

5.3.3 Fourier Transform Infrared Spectroscopy

The FTIR absorbance spectra of the dried TiO_2-SiO_2 gels as a function of titania content is shown in Figure 5.44. Characteristic peaks are observed at 1070, 940, 790 and 445 cm^{-1}. These vibration bands in the sample should originate from two structural units, the SiO_4 and TiO_4 tetrahedra.

The basic structure of vitreous silica is SiO_4 tetrahedra in which each silicon atom is tetrahedrally bonded to four oxygen atoms, each being commonly shared by two tetrahedra. In vitreous silica, the arrangement of the individual SiO_4 tetrahedra is repeated in a random fashion. The infrared spectra of silica glass have been characterized by three main absorption bands at ca. 1100, 800 and 460 cm^{-1}, which correspond to the vibrations of SiO_4 groups. These vibration bands have been assigned by Lippicott et al. [119]:

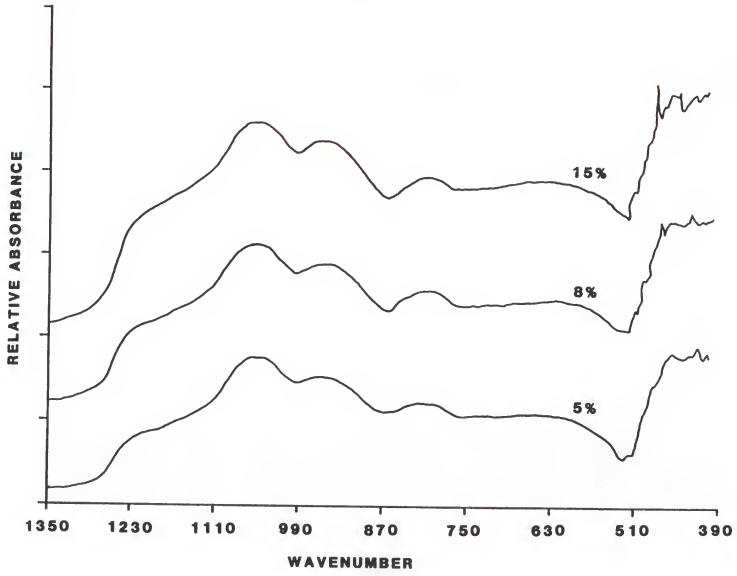

Figure 5.44 FTIR spectra of dried titania-silica gels.

1) High frequency absorption, ~1100 cm^{-1} , is assigned to the Si-O stretching mode corresponding to the motion of silicon and oxygen atoms in opposite directions within the tetrahedra. (i.e. ← SiO →← Si).

2) Intermediate frequency absorption, ~800 cm^{-1} , is assigned to the Si stretching mode in which the Si stretched between the tetrahedra. (i.e. ← Si-O-Si→).

3) Low frequency absorption, ~460 cm^{-1} , is assigned to the bending vibration which involves a combination of the O-Si-O bending mode within the tetrahedra and the Si-O-Si bending mode between the tetrahedra. This absorption usually appears as a broad band in the spectra.

Thus, the characteristic peaks observed at 1070 cm^{-1}, 790 cm^{-1} and 455 cm^{-1} in Figure 5.44 are associated with the structural unit, SiO_4 tetrahedra, in the TiO_2-SiO_2 gel. The vibration band occurred at 940 cm^{-1} has been assigned previously [48] to be associated with the TiO_4 tetrahedra in the gel.

By plotting the ratio of peak intensity at 1070 cm^{-1} to that of 940 cm^{-1}, as shown in Figure 5.45, it is determined that the intensity ratio increases as TiO_2 content increases, suggesting that Ti ions substitute into

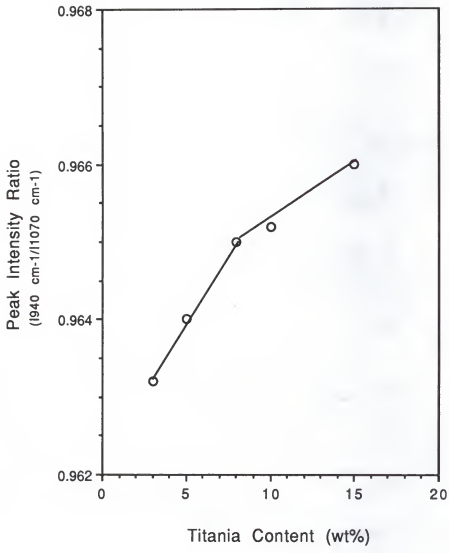

Figure 5.45 Plot of peak intensity ratio (I940/I1070) as a function of titania content for dried gels.

the position of Si ions. It is noted that the curve does not follow a linear relationship. Rather, it levels off at higher titania content. This infers that even though some of the titanium ions substitute in the position of the silicon ions as network formers, there are titanium ions which have six-fold coordination with oxygen ions, which can precipitate out later at a higher temperature as the anatase crystals, as indicated by the X-ray diffraction results (Figure 5.3).

The FTIR spectra for 3% and 15% TiO_2-SiO_2 gel-glasses as a function of densification temperature are shown in Figures 5.46 and 5.47, respectively. As the gels are subjected to higher thermal treatments, the intensities for all the peaks increase. While the peak at 940 cm^{-1} shifted slightly toward lower wavenumber, all the other bands shift toward higher wavenumbers, suggesting a higher force constant for the vibration. This infers that the Si-O-Si network structure is strengthened as densification proceeds. This result is similar to the increase in structural density of the network as processing temperature increases (See Figure 5.6)

Figure 5.48 compares the FTIR spectra of Coring ULE glass (code 7971, containing ~7.4 wt% TiO_2) with the sol-gel derived titania-silica glass in this work. The spectra for the sol-gel derived 5% titania-silica is

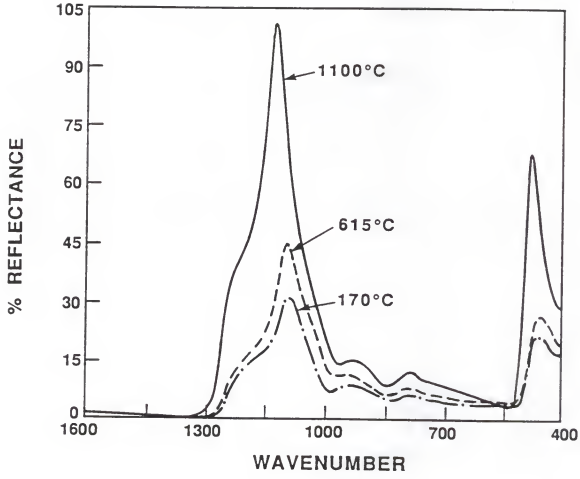

Figure 5.46 FTIR spectra of 3% titania-silica gels densified to various temperature.

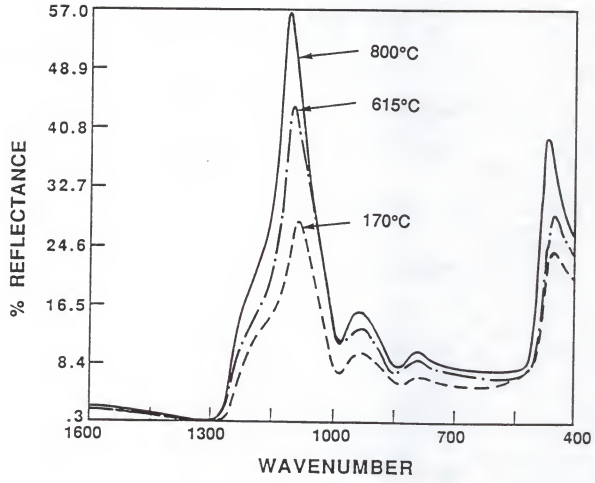

Figure 5.47 FTIR spectra of 15% titania-silica densified to various temperatures.

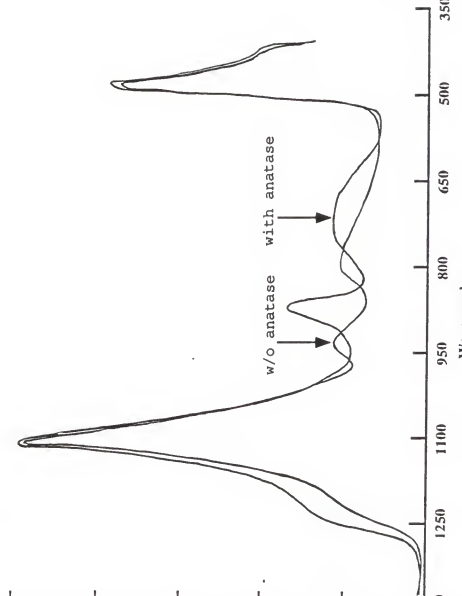

Figure 5.48 FTIR of the titania-silica system (a) alkoxide derived gel-glasses.

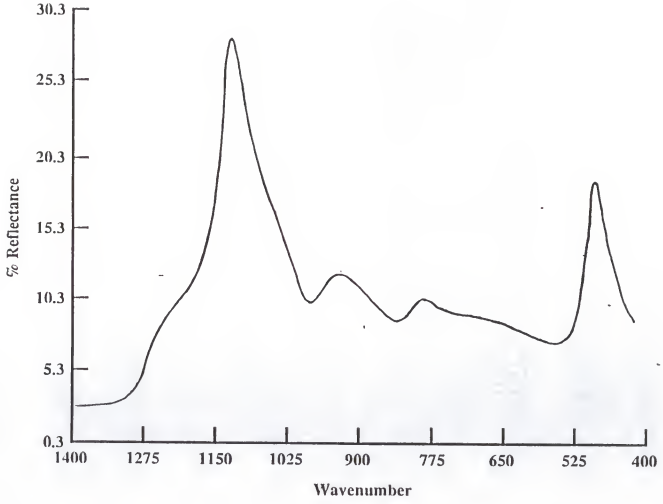

Figure 5.48 FTIR of the titania-silica system
(b) Corning ULE glass.

nearly identical to that of the ULE glass. When anatase crystals precipitate in the gel-glass sample, however, the characteristic peak associated with the TiO_4 tetrahedra disappears (at ca. 940 cm^{-1}). Instead, a broad new band appears at ca. 700 cm^{-1} which arises from vibration in the TiO_6 tetrahedra [48].

Figure 5.49 compares the spectra of a 5% TiO_2-SiO_2 gel-glass with that of a pure vitreous silica sample [120], both densified to 900 °C. Again, the spectra of vitreous silica containing TiO_2 are remarkably similar to those of pure vitreous silica. There is an additional band at ca. 935 cm^{-1} arising from vibrations of TiO_4 tetrahedra, as mentioned previously, which is relatively sharp. It is interesting to note that while the peak at ca. 790 cm^{-1} remains nearly unchanged with the presence of TiO_2, peaks at ca. 470 cm^{-1} and 1100 cm^{-1} shift to lower wave numbers when TiO_2 is doped into vitreous silica. The amounts of decrease in wavenumber are 8 cm^{-1} and 14 cm^{-1} for peaks at ca. 1100 cm^{-1} and 470 cm^{-1} respectively. With the introduction of Ti-O bonds which are of weaker character than the Si-O bonds, the strength of bonds between the connected tetrahedra will be altered. Therefore, vibrations associated with the SiO_4 tetrahedra should experience less resistance leading to a lower force

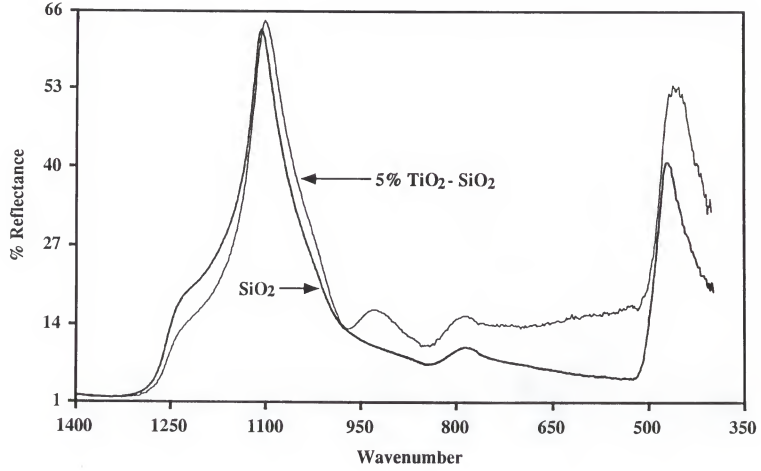

Figure 5.49 Comparison of FTIR spectra for pure silica and 5% titania-silica gel-glasses.

constant. Thus, the wave number shifts to lower values for titanium doped vitreous silica.

The pressure infrared spectra of the titania-silica gel-glass are nearly identical to that taken at ambient temperature and pressure, with characteristic peaks occurring at ~ 1100 cm^{-1}, 940 cm^{-1}, 800 cm^{-1} and 470 cm^{-1}. With increase in pressure, though, the peaks become broader and in some cases, shifts in the peak position are observed. Figures 5.50, 5.51 and 5.52 plot the peak position as a function of pressure for a 0%, 3% and 8% TiO_2-SiO_2 gel-glass, respectively. Data from different runs are represented using open and closed circles in these figures. It is observed that the peaks at 800 cm^{-1} and 940 cm^{-1} shift to higher wavenumbers as pressure increases. In all cases, the peak at ~1100 cm^{-1}, which is not included in these figures, remains unchanged as pressure increases. The peak at 470 cm^{-1}, also excluded from these figures, becomes too broad and noisy as pressure increases, which makes it difficult to identify the peak position.

The infrared pressure study by Ferraro et al. [121] has shown that while the stretching mode at 815 cm^{-1} in fused silica increases with increase in pressure, the stretching mode at 1100 cm^{-1} remains unchanged. This is in agreement with the present results for the 0% TiO_2-SiO_2

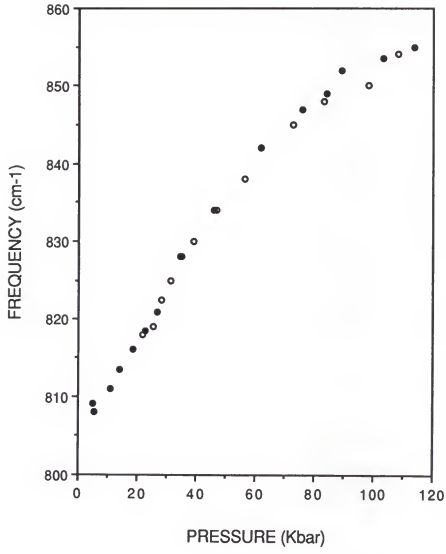

Figure 5.50 Variation of peak position with pressure for 0% titania-silica gel-glass.

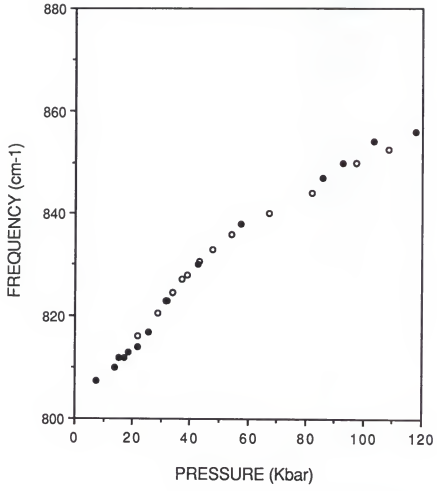

Figure 5.51 Variation of peak position with pressure for 3% titania-silica gel-glass. (a) peak at 800 cm-1.

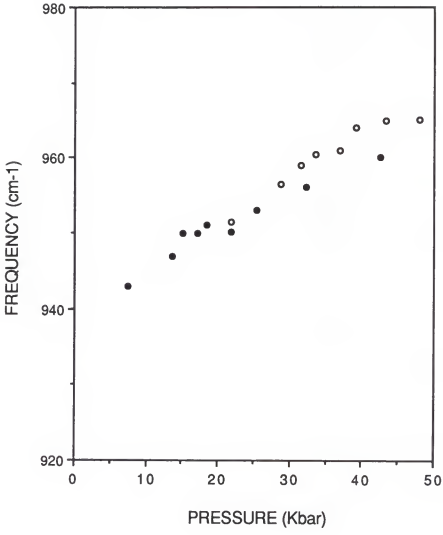

Figure 5.51 Variation of peak position with pressure for 3% titania-silica gel-glass. (b) peak at 940 cm-1.

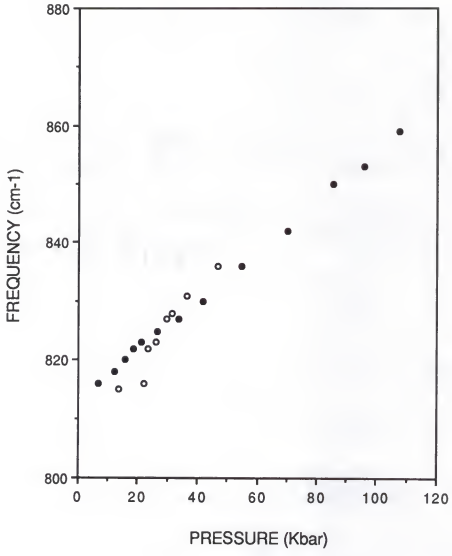

Figure 5.52 Variation of peak position with pressure for 8% titania-silica gel-glass. (a) peak at 800 cm-1.

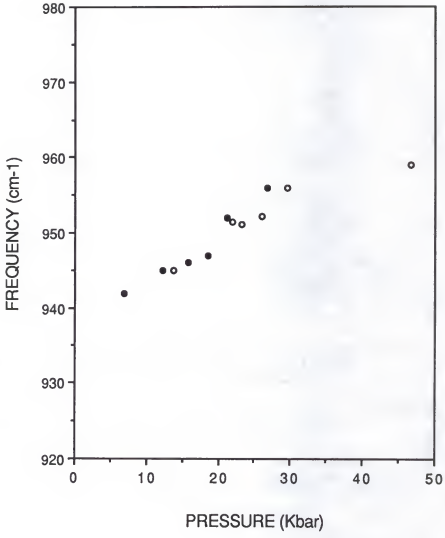

Figure 5.52 Variation of peak position with pressure for 8% titania-silica gel-glass. (b) peak at 940 cm-1.

gel-glass. The bending mode at 470 cm^{-1} is reported to decrease with increase in pressure.

The infrared active vibrations studied under pressure may be considered to be of two types: stretching and bending modes. Among the stretching, the absorption band at ~1100 cm^{-1} is associated with the Si-O stretching vibration within the tetrahedra, while the band at ~800 cm^{-1} is related to the stretching between the tetrahedra. Among the bending, one mode is related to the Si-O-Si bending and the other mode is associated with the O-Si-O bending. As the force constants associated with the stretching modes are larger than that with the bending modes, one would expect the Si-O bond within the tetrahedra to be less sensitive to the pressure. Experimentally, the stretching vibration at ~1100 cm^{-1} is observed to be insensitive to the pressure in the present study whether the sample contains TiO_2 or not. This indicates that the individual SiO_4 tetrahedra are not significantly affected by the pressure. Thus, compaction of the structure under pressure occurs along the network whereby the tetrahedra move in closer to each other. This is indicated by the increase in wavenumber with increasing pressure for both the 815 cm^{-1} and 940 cm^{-1}.

The Grüneisen parameter, γ_i, contributed from vibration mode i has been defined as [122]:

$$\gamma_i = -(d\ ln\ \upsilon_i)/(d\ ln\ V) = (K_T/\upsilon_i)\ (d\ \upsilon_i/\ d\ p)_T \qquad (5.16)$$

where K_T is the isothermal bulk modulus and υ_i is the frequency for vibration mode i. This γ_i gives a measure of the anharmonic interaction arising from vibrational mode i.

Thermodynamically, the coefficient of volume thermal expansion, β, is related to the Grüneisen parameter, γ, through the Grüneisen relation:

$$\beta = \gamma\ (\chi\ C_v/V) \qquad (5.17)$$

where

$$\gamma = (\Sigma \gamma i\ Ci)/\Sigma\ Ci \qquad (5.18)$$

is the summation from each vibration mode, χ is the isothermal compressibility and C_v is the heat capacity.

Thus, based on the amount of peak position shift under pressure, corresponding Grüneisen gamma for each mode of vibration can be calculated through Equation 5.16. A positive Grüneisen gamma contributes positively to the thermal expansion of the material and a negative one contributes negatively.

Table 5.3 showed the pressure infrared results and the calculated Grüneisen parameter, γ_i, from Ferraro et al.

Table 5.3 Results from high pressure IR study

Material	Vi (cm-1)	dVi/dP (cm-1/kb)	Gamma
Silica [121]	475	-0.07	-0.05
	815	0.17	0.07
	1095	No Shift	0
Silica (0% TiO2-SiO2)	475	N/A	N/A
	815	0.66	0.27
	1095	No Shift	0
3% TiO2-SiO2	475	N/A	N/A
	815	0.66	0.25
	940	0.59	0.21
	1095	No Shift	0
8% TiO2-SiO2	475	N/A	N/A
	815	0.40	0.16
	940	0.62	0.21
	1095	No Shift	0

[121] as well as the results on the sol-gel derived silica and titania-silica obtained in collaboration with Dr. Jiri Jonas's group at the Department of Chemistry, University of Illinois at Urbana Champaign. Changes in the 475 cm^{-1} peak position as a function of pressure can not be ascertained at the present. The changes under pressure for the 815 cm^{-1} and 1095 cm^{-1} peaks from the present work are similar to that reported by Ferraro et al. [121] While the vibration band at ca. 815 cm^{-1} increases with increasing pressure, the vibration mode near 1095 cm^{-1} shows no change, within experimental error, with increasing pressure. The value of gamma, however, for the 815 cm^{-1} mode is several times higher than that reported by Ferraro et al. It has been stated recently that the pressure measurements made by Ferraro et al. are incorrect with a maximum pressure of approximately 16 kbar being obtained instead of 58.8 kbar claimed [123]. Taking this into account, the gamma value in Ferraro et al. was recalculated to be 0.26 for the 815 cm^{-1} peak which is close to the present study. The γ_i for the peak at 475 cm^{-1} is recalculated to be -0.18.

Vitreous silica has a much lower thermal expansion than its crystalline form, quartz. This low thermal expansion has been attributed to the transverse vibration of oxygen atom in the Si-O-Si network, i.e. the bending

mode [124,125]. In other words, the increase in the Si-O bond length with increasing temperature is accompanied by a folding-up of the structure. This is in agreement with the value of γ_i reported by Ferraro et al. for the peak at 475 cm^{-1}.

Vitreous silica containing a small quantity of titania has a thermal expansion lower than that of pure silica. With the addition of titania, one sees that the Grüneisen gamma for the 815 cm^{-1} peak decrease which suggests a less positive contribution to the thermal expansion. The sign of the Grüseisen gamma for the 940 cm^{-1} peak in the TiO_2-SiO_2 gel-glass, however, is also positive. This means the vibration mode also contributes positively to the thermal expansion of the material. This suggests that the origin of the low thermal expansion of the titania-silica glass is the same as that of vitreous silica, i.e. the transverse vibration of the oxygens between neighboring SiO_4 tetrahedra (negative Grüneisen gamma for the 475 cm^{-1} peak in the vitreous silica [121]). It is possible that because of the longer Ti-O bond length, the oxygen between neighboring SiO_4 and TiO_4 tetrahedra can move transversely more easierly (a shift of ~14 cm^{-1} toward lower wavenumber is observed, see Figure 5.49) which contributes negatively to the thermal expansion by pulling tetrahedra closer together. With the increase in the titania content, there

are more neighboring SiO_4 and TiO_4 tetrahedra, thus, the thermal expansion decreases as long as the titanium substitutes for the silicon iso-structurally. However, due to present experimental limitations, the exact change in peak position with increasing pressure can not be ascertained for the 475 cm^{-1}.

5.3.4 Raman Spectroscopy

Figure 5.53 shows the Raman spectrum of a dried 8wt% titania-silica gel. Because the sample contains organic impurities, the spectrum was obscured due to florescence. The Raman spectra for 3 wt% and 8 wt% titania-silica gel-glasses partially densified at 615°C are shown in Figures 5.54 and 5.55, respectively. These samples contain the characteristic bands at ca. 430, 490, 605, 805, 950, and 1100 cm-1. Earlier studies indicate that the bands at ca. 430, 490, 605 and 805 cm^{-1} are associated with the vibrational modes for the SiO_4 structural unit, while the bands at ca. 950 and 1100 cm^{-1} are associated with the presence of titanium ions in the glass network [126-128].

The bands at 490 and 605 cm^{-1} have been attributed to the defect structures (3-membered and 4-membered rings) in the glass network. The band at 805 cm^{-1} has been assigned to network Si-O-Si symmetric bond stretching vibrations.

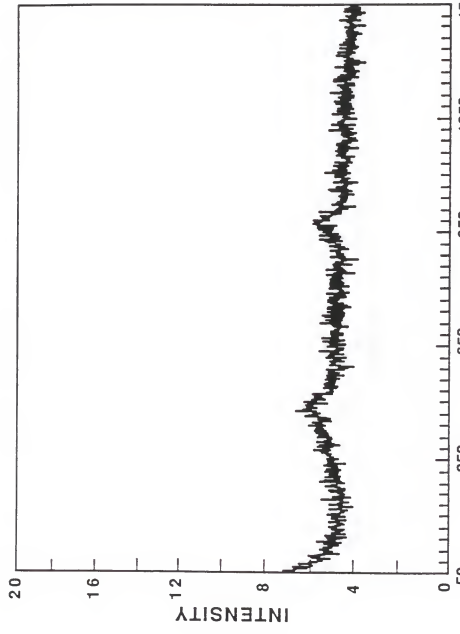

Figure 5.53 Raman spectra for dried 8% titania-silica gel.

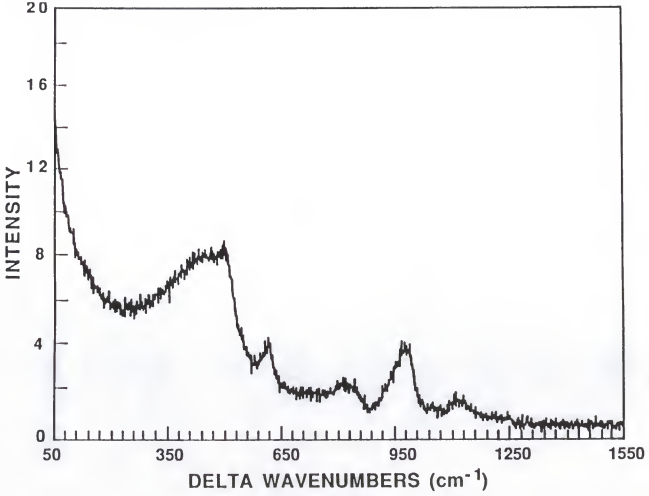

Figure 5.54 Raman spectra for 3% titania-silica gel previously densified at 615°C.

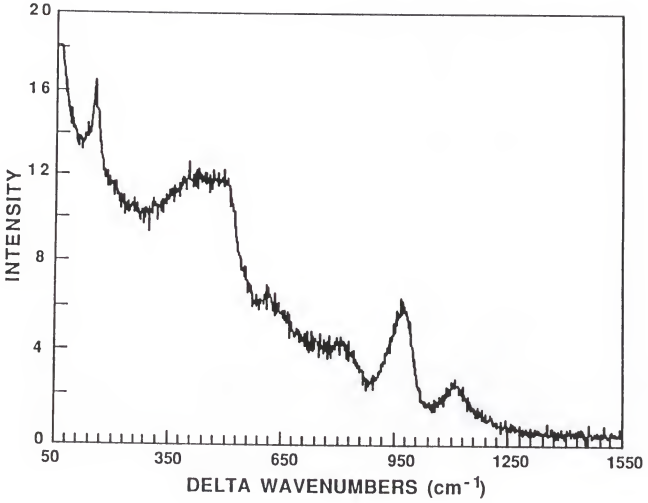

Figure 5.55 Raman spectra for 8% titania-silica gel previously densified at 615°C.

The bands at ca. 950 cm^{-1} and 1100 cm^{-1} have been assigned to the network Si-O-Ti asymmetric bond stretching vibrations [127].

As the titania content increases, the bands at ca. 950 and 1100 cm^{-1} are observed to gain intensity. With the increase in titania, more Si-O-Ti bridges form; thus the intensities at 950 and 1100 cm-1 should increase. It is interesting to note that the band at ca. 605 cm^{-1} loses intensity as the titania content increases, i.e., the formation of Si-O-Ti bridges decreases the number of defect structures in the silica network. This implies that upon addition of titanium ions, the more strained 3-membered ring structure will open up in order to accommodate the larger titanium ions.

5.3.5 UV/VIS/NIR Spectroscopy

Figure 5.56 shows the UV/VIS/NIR spectrum for a dried 5% titania-silica gel. Spectra for dried gels with higher titania contents are very similar to that shown in this figure. The peaks evident in this spectrum are summarized in Table 5.4. These peaks are primarily associated with the hydroxyl groups present on the surface of the gel which are in good agreement with that reported for porous gel-silica [39]. The comparison is shown in Table 5.4.

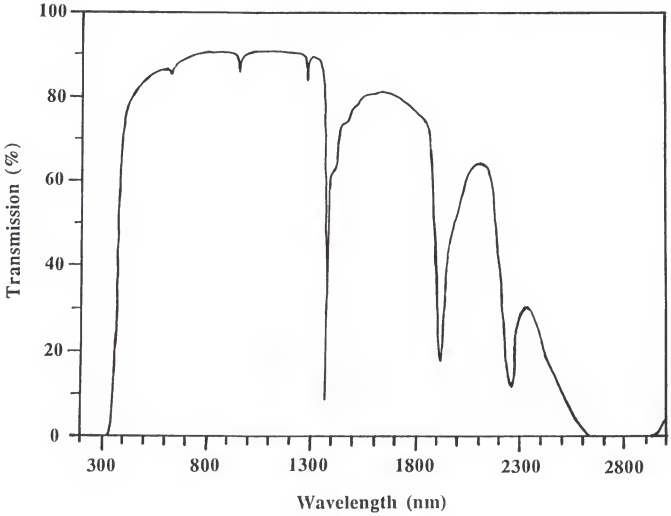

Figure 5.56 UV/VIS/NIR spectrum for a dried 5%% titania-silica gel monolith.

Table 5.4 UV/VIS/NIR peak assignment.

Wavelength (nm)	Type	Observation (in SiO_2)	Observation (in TiO_2-SiO_2)
2919.7	υ_4	a broad peak on a broad band	under a broad band
2816.8	υ_3	a tiny peak on a broad band	under a broad band
2732.2	υ_2	combination of two peaks	under a broad band
2668.8	υ_1	a sharp symmetric peak	under a broad band
2262.6	$\upsilon_3+\upsilon_{OH}$	a broad band	a broad band
1890.3	$\upsilon_3+2\upsilon_{OH}$	a asymmetric peak	a broad asymmetric peak
1408.4	$2\upsilon_3$	a small peak on a broad band	a small peak on a broad band
1366.1	$2\upsilon_2$	a sharp symmetric peak	a sharp symmetric peak
1237.8	$2\upsilon_2+2\upsilon_3$	a small peak	a small peak
938.9	$3\upsilon_3$	a small peak	a small peak
704.2	$4\upsilon_4$	a tiny peak	a tiny peak

υ_{OH} : an out of plane bending vibration of Si-O-H bond.

υ_1 : stretching vibration of an isolated Si-O-H bond.

υ_2 : stretching vibration of an adjacent Si-O-H bond.

υ_3 : stretching vibration of a Si-O-H bond which is hydrogen beonded to water.

υ_4 : stretching vibration of adsorbed water.

The main difference in the UV/VIS/NIR spectra for dried gels with various titania contents appears in the UV region, as shown in Figure 5.57. Figure 5.58 shows the UV-cutoff value as a function of the titania content for dried gels. It is observed that as the titania content increases, the UV-cutoff increases. Compared with pure silica, the UV-cutoff for dried titania-silica occurred at longer wavelength.

Curves in Figure 5.59 show the UV-VIS-NIR spectra of 5% titania-silica gel monoliths heated in ambient air up to the designated temperature. Compared with Figure 5.56, peaks at 704 nm, 938 nm and 1131 nm have completely disappeared when the sample was heated to 800°C. As shown in this figure, overtone and vibrational peaks are observed at 2207 nm, 1890 nm, 1408 nm and 1366 nm. There is a strong and broad band occurring between 2700 nm and 3200nm. As the temperature increases, the intensities for all the peaks decrease. The peaks at 1366 nm and 1890 nm have been eliminated completely while that at 1408 nm are negligible when the sample was heated to 1050°C. It is obvious that the sample still has residual hydroxyl groups in it.

In addition to the change in peak intensity, it is noted the UV-cutoff also changes as a function of densification temperature. This is shown in Figure 5.60.

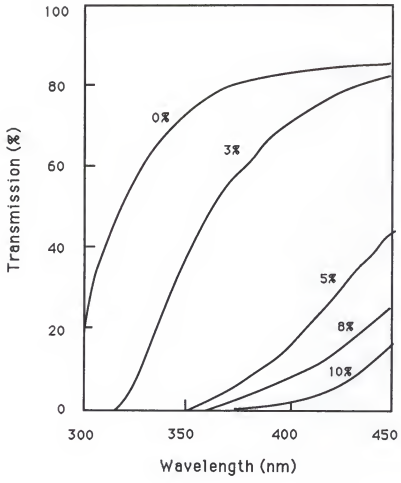

Figure 5.57 Variation of UV transmission with titania content for dried gels.

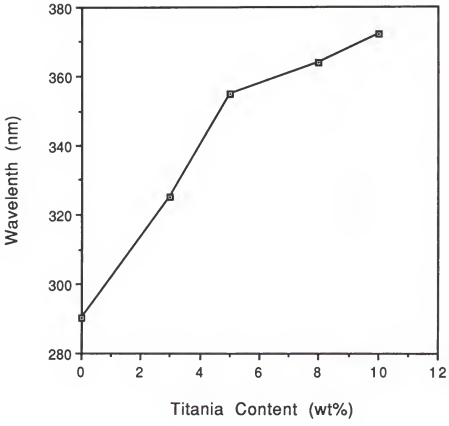

Figure 5.58 Variation of UV cut-off with titania content for dried gels.

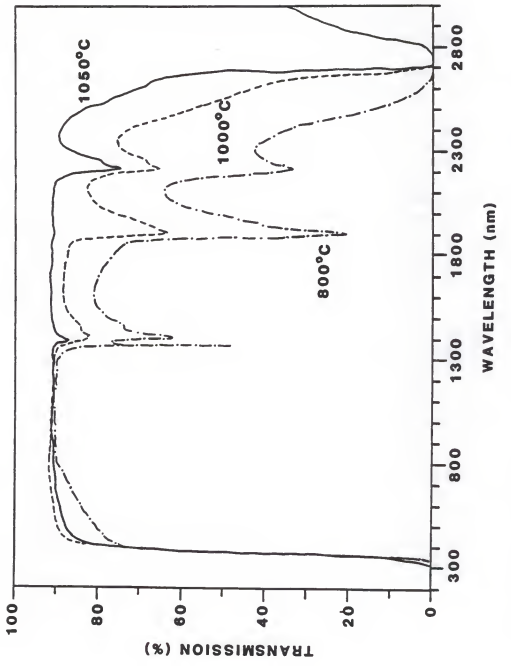

Figure 5.59 Variation of UV/VIS/NIR spectra for a set of 5% titania-silica gels densified to various temperature.

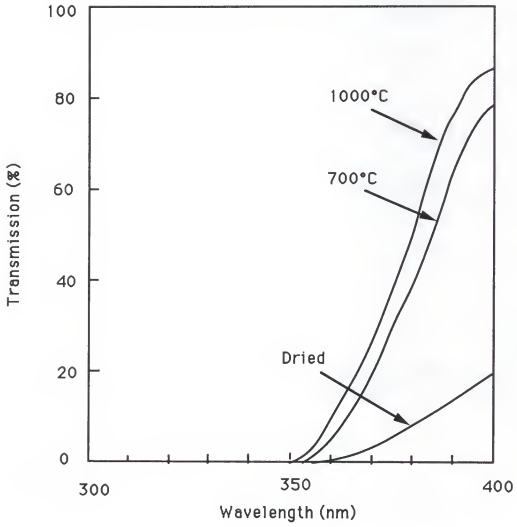

Figure 5.60 Variation of UV transmission for 5% titania-silica gels densified to various temperatures.

The optical transmission near the UV absorption end increases while the UV-cutoff shifts to lower wavelengths as the temperature of thermal treatment increases. This results from the progressive elimination of water from the high temperature samples, which is similar to the results reported in pure silica gel system [39].

CHAPTER VI
QUANTUM CALCULATIONS

6.1 Introduction

The main objective of any theory of molecular structure is to provide some insight into the various physical laws governing the chemical nature of molecules. In principle, the theory of molecular structure can give a precise quantitative description of the structure of molecules and their chemical properties. In practice, however, the mathematical and computational complexities make this goal difficult to achieve. Thus, one must usually resort to approximate methods which generally provide a sufficiently good approximate description. In many physical and chemical problems though, this qualitative or semi-quantitative knowledge of the structure is sufficient to extract the necessary information to interpret or predict physical or chemical properties and behavior.

The central feature for full analytical calculation of the molecular orbitals involves the calculation and diagonalization of an effective interaction energy matrix for the system. For many-electron molecules, this

calculation may be reduced to a purely mathematical problem. The *ab initio* method for computing the molecular wavefunctions is developed directly from the fundamental equations of quantum mechanics. The semiempirical technique, on the other hand, uses a simplified formalism as a framework for parameterization.

There are two approaches for the approximate molecular orbital theory. One involves choosing appropriate values for the elements of the interaction energy matrix from empirical considerations. The other approach is based explicitly on the mathematical formalism which involves introducing approximations for the atomic and molecular integrals that are needed for the expression of the elements in the energy interaction matrix. This latter approach is referred to as the approximate self-consistent field theory.

Recently, Burgraff and Davis [129] have studied hydrolysis and polycondensation reactions of silica using quantum mechanical calculations. They applied the AM1 semiempirical program to examine the formation of pentacoordinate silicic acid complexes with hydroxide ion and fluoride ion. They also calculated reaction paths for water elimination from silicic acid complexes with hydroxide ion. Their results indicate that a hypervalent silicon complex forms as an intermediate state in the

polycondensation reaction. This pentacoordinated silicon has no activation energy for water removal. This is important in understanding how water is eliminated as the polymerization proceeds. Experimental evidence for the existence of the pentacoordinated silicon were reported by Zerda and Hoang [130] using pressure Raman spectroscopy. Their results confirm a series of theoretical calculations.

An Intermediate Neglect of Differential Overlap (INDO) molecular orbital model was used in the calculations done by West et al. [131] on silica clusters designed to model sol-gel silica system. The silica structures evaluated contained from 1 to 6 silica tetrahedra. To each silicon, two bridging oxygens and two non-bridging oxygens are bonded. One hydrogen is bonded to each of the non-bridging oxygens to terminate the structure and to balance the charge. Figure 6.1 and 6.2 show the chain and ring structure of 4 silica tetrahedra used by West et al. [131]. The upper part of the figure shows the two dimensional projection of the cluster while the lower part shows the corresponding atomic designations. The relative stability of these clusters was evaluated by comparing their molecular energies. The more negative the energy, the more stable the structure. There is a difference in the number of atoms between chains and rings, i.e. the

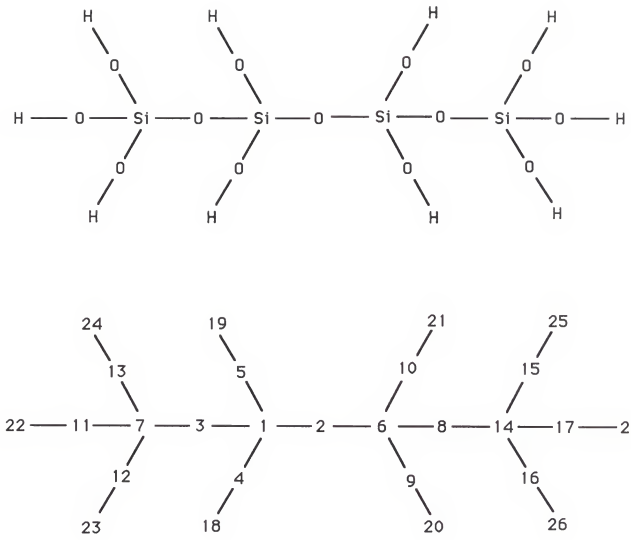

Figure 6.1 2-D projection of chain structure of four silica tetrahedra.

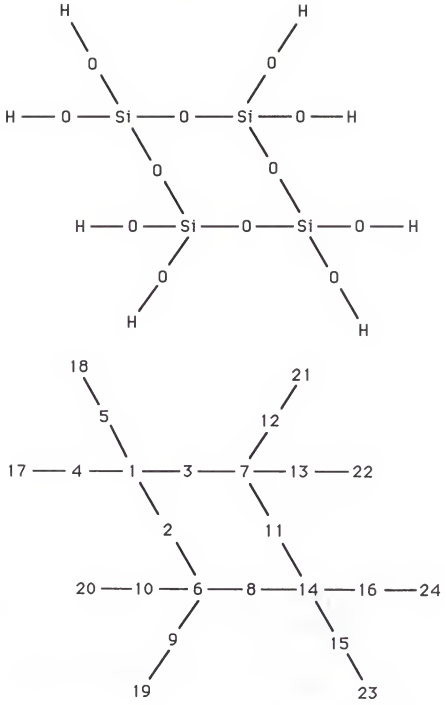

Figure 6.2 2-D projection of ring structure of four silica tetrahedra.

water content. A chain has one extra water molecule when it is compared to a ring. Thus, the energy of free water must be excluded from that of the chain when comparing the energies of rings and chains. The results [131] show that the chain structures are more stable than the rings for small number of silica tetrahedra. This has been observed experimentally by Klemperer and Ramamurthi [132] and Orcel and Hench [133,134] using NMR spectroscopy.

In order to evaluate the effect of titanium ions on the structure of silica, a titanium ion was added to both the ring and chain structure of 4 silica tetrahedra to replace one silicon atom. The following sections discuss the results from the quantum calculation of these titania silica clusters. These calculation was performed using an INDO program from the Quantum Theory Project of the University of Florida [135].

6.2. Structure of the Titania Doped Silica

In order to evaluate the effect of a titanium ion on the silica clusters, chain and ring structures similar to those shown in Figures 6.1 and 6.2 were used with one silicon being replaced by titanium. Thus, of the four tetrahedra in the structure, three are made of silica and one is made of titania. Table 6.1 summarizes the results

Table 6.1 INDO Energies of titanium doped structures

Chain Structure		Ring Structure	
Ti Position	INDO Energy	Ti Position	INDO Energy
6	-222.0136	6	-222.0182
14	-221.9468	14	-222.0175

of INDO energy calculations in order to compare the relative stability of the INDO structure. As shown in this table, the position of the titanium ion in the ring and/or chain structure does not affect the calculated INDO energy. The ring and the chain clusters have approximately the same energy with the energy for ring being slightly lower. Note that the INDO energies shown in this table for chain structures have been corrected for the extra water molecule in chains. In the case of pure silica [131], chain structures are more stable than the rings for small number of tetrahedra. The relative stability of chains compared to rings decreases as the number of silica tetrahedra increases. The energy difference between chains and rings reaches zero as the number of tetrahedra reaches about 5, when the driving force for forming rings becomes more favorable than for chains. With titanium doped structures, this cross-over energy shifts to 4 tetrahedra, as shown in Figure 6.3. Similar results have been reported for fluorine doped clusters [77]. This suggests that addition of titanium ions limit the growth of chains and favors the formation of rings (i.e. promotes cross-linking of the structure) which may explain why gelation time decreases as titania content increases (Figure 3.2).

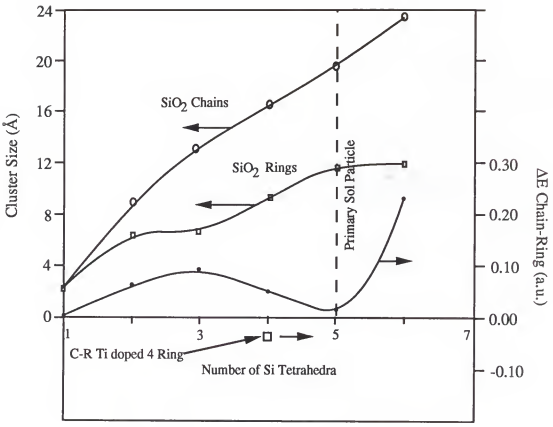

Figure 6.3 INDO calculations.

The ring structure shown in Figure 6.4 with atomic designations is used to evaluate the change in interatomic distances when the titanium is doped into silica. Table 6.2 and Table 6.3 show the individual bond lengths and bond angles for this structure and that of the corresponding silica structure shown in Figure 6.2. It is observed that as titanium enters the structure, the average O-H, bridging Si-O and non-bridging Si-O distances all increase. This indicates a structural dilation when titanium is added in place of a silicon. The increase in the Si-O bond length infers a decrease in the bond strength, i.e. a smaller force constant. This is consistent with the experimental observation (see Figure 5.49).

Specifically, the average Ti-O bond length is 1.9584 Å and the Si-O distance is 1.6874 Å from the INDO calculation. Experimentally, Greegor et al. [66], using EXAFS, has determined the Ti-O and Si-O bond distance to be 1.83 Å and 1.62 Å respectively when the titanium ions are four-fold coordinated with the oxygen. The results from the INDO calculation are larger in absolute value than the experimental value. However, one must keep in mind that the structure in Figure 6.4 is a small one with much less boundary constraint compared to the real glass structure. Therefore, a larger bond distance is expected.

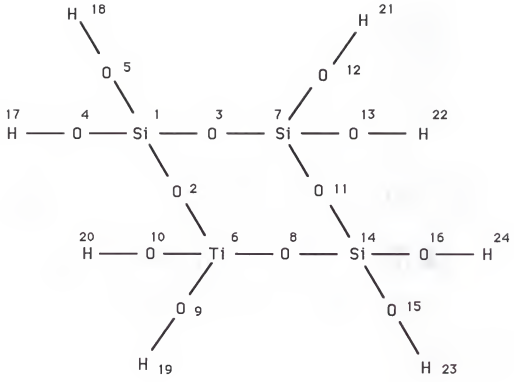

Figure 6.4 2-D projection of titanium doped ring structure.

Table 6.2 Bond Distance of Ring Structure

Ti-Doped Ring			Silica Ring	
Bond Type	Distance (Å)	Atomic Designation	Distance (Å)	Bond Type
O-Si	1.6785	(2- 1)	1.6891	O-Si
O-Si	1.6800	(3- 1)	1.6770	O-Si
O-Si	1.6970	(4- 1)	1.6928	O-Si
O-Si	1.6948	(5- 1)	1.6941	O-Si
Ti-O	1.9582	(6- 2)	1.6885	Si-O
Si-O	1.6773	(7- 3)	1.6726	Si-O
O-Ti	1.9630	(8- 6)	1.6819	O-Si
O-Ti	1.9523	(9- 6)	1.6930	O-Si
O-Ti	1.9596	(10- 6)	1.6931	O-Si
O-Si	1.6724	(11- 7)	1.6811	O-Si
O-Si	1.6965	(12- 7)	1.6933	O-Si
O-Si	1.6947	(13- 7)	1.6959	O-Si
Si-O	1.6778	(14- 8)	1.6774	Si-O
Si-O	1.6767	(14-11)	1.6801	Si-O
O-Si	1.6971	(15-14)	1.6919	O-Si
O-Si	1.6941	(16-14)	1.6966	O-Si
H-O	1.0214	(17- 4)	1.0185	H-O
H-O	1.0221	(18- 5)	1.0166	H-O
H-O	1.0206	(19- 9)	1.0198	H-O
H-O	1.0216	(20-10)	1.0198	H-O
H-O	1.0210	(21-12)	1.0180	H-O
H-O	1.0201	(22-13)	1.0203	H-O
H-O	1.0221	(23-15)	1.0175	H-O
H-O	1.0213	(24-16)	1.0233	H-O

Table 6.3 Bond Angle of Ring Structure

Ti-Doped Ring			Silica Ring	
Type	Angle	Designation	Angle	Type
O-Si-O	93.180	(2- 1- 3)	107.476	O-Si-O
O-Si-O	101.832	(2- 1- 4)	110.894	O-Si-O
O-Si-O	130.203	(2- 1- 5)	110.052	O-Si-O
O-Si-O	142.665	(3- 1- 4)	109.317	O-Si-O
O-Si-O	109.250	(3- 1- 5)	110.940	O-Si-O
O-Si-O	86.703	(4- 1- 5)	108.174	O-Si-O
Si-O-Ti	143.601	(1- 2- 6)	144.790	Si-O-Si
Si-O-Si	147.687	(1- 3- 7)	149.736	Si-O-Si
Si-O-H	128.481	(1- 4-17)	110.096	Si-O-H
Si-O-H	135.403	(1- 5-18)	115.597	Si-O-H
O-Ti-O	137.725	(2- 6- 8)	111.858	O-Si-O
O-Ti-O	106.959	(2- 6- 9)	108.854	O-Si-O
O-Ti-O	96.853	(2- 6-10)	110.253	O-Si-O
O-Ti-O	95.471	(8- 6- 9)	109.372	O-Si-O
O-Ti-O	112.922	(8- 6-10)	107.309	O-Si-O
O-Ti-O	102.563	(9- 6-10)	109.153	O-Si-O
O-Si-O	133.980	(3- 7-11)	108.864	O-Si-O
O-Si-O	85.756	(3- 7-12)	111.707	O-Si-O
O-Si-O	105.185	(3- 7-13)	109.822	O-Si-O
O-Si-O	115.265	(11- 7-12)	108.321	O-Si-O
O-Si-O	100.363	(11- 7-13)	108.407	O-Si-O
O-Si-O	117.208	(12- 7-13)	109.645	O-Si-O
Ti-O-Si	136.621	(6- 8-14)	144.971	Si-O-Si
Ti-O-H	120.540	(6- 9-19)	113.293	Si-O-H
Ti-O-H	112.343	(6-10-20)	109.622	Si-O-H
Si-O-Si	161.364	(7-11-14)	146.707	Si-O-Si
Si-O-H	119.015	(7-12-21)	110.964	Si-O-H
Si-O-H	109.043	(7-13-22)	105.684	Si-O-H
O-Si-O	93.175	(8-14-11)	104.500	O-Si-O
O-Si-O	109.864	(8-14-15)	107.741	O-Si-O
O-Si-O	145.226	(8-14-16)	118.796	O-Si-O
O-Si-O	143.246	(11-14-15)	114.838	O-Si-O
O-Si-O	90.388	(11-14-16)	104.780	O-Si-O
O-Si-O	86.456	(15-14-16)	106.555	O-Si-O
Si-O-H	132.760	(14-15-23)	106.041	Si-O-H
Si-O-H	140.867	(14-16-24)	106.523	Si-O-H

Nevertheless, the structure in Figure 6.4 should represent the local structure when the titanium ion replaces silicon isostructurally. When one takes the ratio of the Si-O bond distance to that of the Ti-O distance, a value of 0.862 is obtained from the INDO calculations while that from the experimental results is 0.885. The difference between these two values is only 2.60%, which is within experimental accuracy. Thus, results from quantum mechanical calculations compare quite favorably to the experimental observations.

In addition to the bond length increase when titanium ion enters a silica tetrahedron, the average M-O-M' angle also increases as indicated in Table 6.3. The increase in both the bond angle and bond distance implies an increase in the molar volume when titania is doped into the vitreous silica. Using the structures shown in Figure 6.2 and Figure 6.4, the densities for the silica ring and titanium doped silica ring structures are calculated to be 1.94 and 1.98 g/cm^3 respectively. The difference is about 2 %. Therefore, the weight increase from the heavier titanium ions is offset by the molar volume increase and experimentally a constant density is observed for the titania-silica glasses.

6.3. Quantum Calculations of UV-Cutoff for Titania-Silica

After the cluster shown in Figure 6.4 was geometrically optimized using the INDO calculation, its molecular orbitals were computed using configurational interaction INDO calculations. The HOMO-LUMO energy gap, i.e. the energy difference between the Highest Occupied Molecular Orbital (HOMO) and the Lowest Unoccupied Molecular Orbital (LUMO), is determined and the corresponding UV-cutoff wavelength is then calculated. For a ring structure of 4 silica tetrahedra, the HOMO-LUMO bandgap is 0.4725 a.u. which corresponds to an UV-cutoff wavelength of 114.3 nm. For the titanium doped ring structure, the HOMO-LUMO bandgap is 0.3888 a.u. which corresponds to an UV-cutoff wavelength of 138.9 nm. Thus, the INDO calculation predicts an increase in the UV-cutoff wavelength when titanium enters the ring structure isostructurally. This is consistent with the experimental observation, as shown in Figure 5.55.

6.4. Quantum Calculations of Water Adsorption onto Titania-Silica

There is roughly an equal distribution of 3-fold, 4-fold, 5-fold and 6-fold rings of silica tetrahedra present in silica gels as in the case of fused silica as reported

in Klemperer et al. [132,136] West et al. [74,131] used the 4-fold ring structure shown in Figure 6.2 to study the theoretical effect of water on silica ring clusters. The water was hydrogen bonded to the silica cluster as indicated by Takahashi [137]. The cluster was geometrically optimized with and without the presence of the adsorbed water molecules using the INDO molecular orbital theory developed by Zerner et al. [138] Figure 6.5 shows the silica ring structure with the presence of water. It is reported [74] that the ring structure without water adsorption is uniform with the diagonal Si-Si distance nearly equal. With the adsorption of water, the ring elongated along the axis without the adsorbed water. Also, the average silicon-silicon distance for neighboring atoms increases. In average, the 4-fold silica ring structure is predicted to expand 0.84% upon the water adsorption. Experimentally, the expansion of a silica gel monolith in an ambient atmosphere has been reported by Hench and West [32].

In order to study the effect of water on titanium doped silica, a ring structure with the addition of one hydrogen bonded water molecule was used as shown in Figure 6.5. The cluster was again geometrically optimized using INDO molecular orbital theory. Table 6.4 shows the results of the calculations for the structural change of

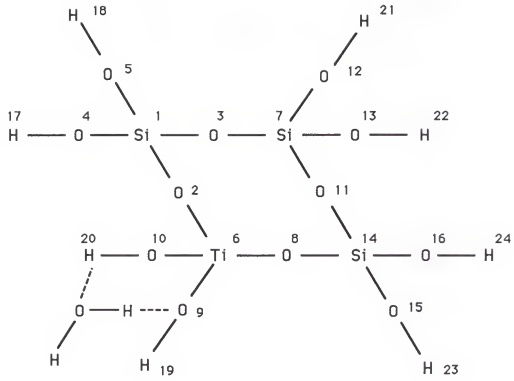

Figure 6.5 2-D projection of titanium doped ring structure with a hydrogen bonded water.

Table 6.4 Dilation of titanium doped silica structure.

4 Fold Ring	Diagonal Metal-Metal Distance (Å) (1)-(14)	(6)-(7)	Average Neighbor Metal-Metal Distance (Å)
Without Water	4.800017	4.779820	3.388492
With Water	4.777038	4.652012	3.339780

the 4-fold ring structure in the presence of a bonded water molecule. The distance between the diagonal metal atoms are reported. As shown in the table, the cluster without water is nearly uniform with the diagonal metal-metal distance roughly the same. With the presence of water abduct, the diagonal metal-metal distance along the axis of water is shorter than that without water. This is similar to the results of pure silica (West et al. 1990). However, it is noted that the average diagonal metal-metal distance decreases with the presence of water. In addition, the neighboring metal-metal distance also decreases. On the average, the quantum calculation predicts that there is nearly 1.4 % structural shrinkage when one water is added to the titanium doped 4-fold ring structure.

As stated in West et al. [74], in an amorphous silica structure, there should be a random orientation of the structural elongation. Some of the elongation will occur in regions where contraction of the ring will compensate. On the average, however, it is predicted that there is small expansion when the water is adsorbed onto the structure.

In an amorphous titania-silica system, one can expect that there shall be structural dilation and contraction arising from the silica and the titanium doped silica

clusters respectively when the water is bonded to the structure. With the small amount of titania in the amorphous structure (less that 7%), it is predicted that the expansion upon water adsorption for the titania-silica is less than that for the pure silica. This is consistent with the experimental data observed in Figure 4.14.

CHAPTER VII
CONCLUSIONS AND FUTURE DIRECTIONS

The recent development in sol-gel processing offers a new approach for the preparation of glasses that are difficult to make by traditional methods. The objective of this dissertation is to develop an alkoxide based sol-gel method for the preparation of titania-silica gels and to study the evolution of thermal, physical and chemical properties for the gels derived as a function of densification.

The monolithic, titania-silica xerogels were successfully derived using nitric acid as catalyst and tetramethylorthosilicate and titanium isopropoxide as the metal metal precursors. The sols gelled in one day and drying of the gels can be accomplished in less than four days. The method developed for gel preparation does not require addition of alcohol as solvent.

The physical properties of the dried titania-silica gels, i.e. microhardness, specific surface area, pore radius and pore volume, are nearly the same as those reported for pure silica gels with an average pore radius of 12 Å, also derived using nitric acid as the catalyst.

These physical properties do not vary as a function of the TiO_2 content. However, optical properties, i.e. refractive index and UV cut-off, increase as the titania content increases.

Below 600 °C, the physical properties of the TiO_2-SiO_2 gel-glass with various titania contents do not change significantly and their values are comparable with those of a pure silica gel-glass. Above 600 °C, these physical properties increase rapidly with densification temperature. Thus, a range of desired physical properties can be achieved through proper thermal treatment.

For gel-glass with low TiO_2 content, the sample remains amorphous even after heating for 15 hours at 900 °C, while for high TiO_2 content, precipitation of anatase crystals occurs. The boundary between amorphous and anatase precipitation regions has been established.

The linear thermal expansion coefficient of the alkoxide derived TiO_2-SiO_2 glasses decreases with increasing titania content, as is known for flame hydrolysis derived titania-silica glasses. In addition, the expansion values and their dependence upon composition for the sol-gel derived titania-silica glasses are consistent with the data reported for glasses prepared by flame hydrolysis method.

The structural densities of the titania-silica gel-glasses increase as the densification temperature increases and approach those of flame hydrolysis derived titania-silica glasses at a temperature above 900 °C. No maximum in the structural density is observed in the temperature range ~800 °C, contrary to reports for the pure silica gel-glasses. This probably arises from the elimination of the strained defect structure as titanium is doped into the structure.

The gels with higher titania content are more difficult to sinter due to foaming. This arises from the decrease in viscosity with increasing titania content, since flow in the system should initiate from the weaker Ti-O bonds. Using a topological analysis, the onset temperature of pore closure is determined to decrease linearly with increasing titania content. This is similar to the decrease in strain point and annealing point as titania content increases.

The structure of a porous titania-silica gel-glass dilates upon water adsorption. The amount of expansion progressively decreases with increasing densification temperature. The amount of structural dilation is smaller for porous TiO_2-SiO_2 gel-glasses than for pure silica monoliths.

XPS results indicate the gel-glasses prepared in this study have better homogeneity than that reported in literature for pure silica made by sol-gel methods. This indicates the importance of structural control at the early stage of processing for single component and especially for multi-component systems such as titania-silica. The binding energy for the tetrahedrally coordinated titanium is determined to be 460.6 eV which is 1.9 eV higher than the octahedrally coordinated titanium present in TiO_2.

Characteristic peaks observed in the UV/VIS/NIR spectra are those associated with water present in the network. With an increase in the densification temperature, peak intensities are observed to decrease. This is similar to the pure silica system. The UV cut-off wavelength is observed to increase with increasing titania content.

The refractive index of the gel-glass is observed to increase with increasing titania content. This arises from the higher electronic polarizability of the titanium ions. The refractive index of the gel-glass is also observed to increase with increase in density, as reported in the pure SiO_2 system.. Within the experimental error, the Lorenz-Lorentz relationship is followed.

In summary, a successful and reliable processing sequence has been developed in this work for the preparation of alkoxide derived titania-silica gel monoliths. Variation with densification of the physical and chemical properties of the porous gel monoliths have been characterized using various techniques. There are several problems, though, that are brought up by this work that deserve further study:

(1) The obvious problem is to achieve full dehydration and densification of the titania-silica gel-glasses. A feasible process, using chlorination, has been developed for the sol-gel derived pure silica although it is elaborate and time consuming. A similar approach should apply to the titania-silica gel system, though more research is needed to develop proper control of the processing parameters as well as to improve and decrease the cost of processing.

(2) For use with doping and impregnation applications, gel monoliths with relatively large pore size are preferred. This can be accomplished, as in the case of pure silica, by using different acid as catalyst, e.g. hydrofluoric acid, as well as by using hydrothermal treatment. A comprehensive study on the structural and physical properties of these materials is then necessary.

(3) The skeletal density of the titania-silica gel-glass increases with increasing densification temperature. No maximum in the structural density is observed in the temperature range ~800 °C which is contrary to that reported for the pure silica gel-glasses. As mentioned in Chapter V, this probably arises from the elimination of the strained defect structures as titanium is doped into the structure. It would be an interesting study to investigate, using Raman spectroscopy, the variation of the structural changes with densification for gel-glasses with various titania contents, and to correlate the results with that of the pure silica gel-glasses.

(4) Further work on the pressure IR study is needed in order to determine the Grüneisen parameter, γ_i, for the bending mode at 470 cm-1. This is important in explaining the low thermal expansion of the titania-silica glasses.

REFERENCES

[1] C.L. Rathmann, G.H. Mann and M.E. Nordberg, Appl. Opt., 7, (1968), 819.

[2] R.C. DeVries, R. Roy and E.F. Osborn, Trans. Brit. Ceram. Soc., 53, (1954), 525.

[3] M. Ebelmen, Ann. Chimie Phys, 16, (1846), 129.

[4] M. Ebelmen, C. R. Acad. Sci., 25, (1847), 854.

[5] T. Graham, J. Chem. Soc., 17, (1864), 318.

[6] D.M. Roy and R. Roy, Am. Mineral., 39, (1954), 957.

[7] R. Roy, J. Am. Ceram. Soc., 39, (1956), 145.

[8] R. Roy, J. Am. Ceram. Soc., 52, (1969), 344.

[9] G.J. McCarthy, R. Roy and J.M. McKay, J. Am. Ceram. Soc., 54, (1971), 637.

[10] R.K. Iler, The Chemistry of Silica, Wiley, New York, 1955.

[11] W. Stöber, A. Fink and E. Bohn, J. Colloid. Interface Sci., 26, (1968), 62.

[12] J. Phalippou, M. Prassas and J. Zarzycki, J. Non-Cryst. Solids, 48, (1982), 17.

[13] M. Prassas, J. Phalippou and J. Zarzycki, Int. Conf. Glasses, 13th, Hamburg, Germany, 1985.

[14] B.E. Yoldas, Bull. Am. Ceram. Soc., 54, (1975), 286.

[15] J.D. Mackenzie, J. Non-Cryst. Solids, 41, (1982), 1.

[16] J.D. Mackenzie, in *Ultrastructure Processing of Ceramics, Glasses and Composites*, L.L. Hench, D.R. Ulrich Eds., Wiley, New York, 1984, 15.

[17] L.L. Hench, S. Wang and J.L. Noguès, in *Multifunctional Materials*, R.J. Gunshor Ed., SPIE, Bellingham, W.A., 1988, Vol. 878, 76.

[18] L.L. Hench, M.J.R. Wilson, C. Balaban and J.L. Noguès, *Sol-Gel Processing of Large Silica Optics, Proceedings of 4th International Conference on Ultrastructure Processing of Ceramics, Glasses and Composites*, Tucson, AZ, 1989.

[19] S. Wang, C. Campbell and L.L. Hench, in *Ultrastructure Processing of Advanced Ceramics*, J.D. Mackenzie, D.R. Ulrich Eds., Wiley, New York, 1988, 145.

[20] J.T. Davis and E.K. Rideal, in *Interfacial Phenomena*, Academic Press, New York, 1963.

[21] P.J. Flory, *Principles of Polymer Chemistry*, Cornell University Press, Ithaca, New York, 1953, Chapter IX.

[22] R.K. Iler, in *Science of Ceramic Chemical Processing*, L.L. Hench, D.R. Ulrich Eds., Wiley, New York, 1986, 3.

[23] T.K. Sherwood, Ind. Eng. Chem., 21, (1929), 12.

[24] T.K. Sherwood, Ind. Eng. Chem., 22, (1930), 132.

[25] T.K. Sherwood, Ind. Eng. Chem., 21, (1929), 976.

[26] R.W. Ford, *Ceramics Drying*, Pergamon, New York, 1986.

[27] G.W. Scherer, *Proceedings of 4th International Conference on Ultrastructure Processing of Ceramics, Glasses and Composites*, Tucson, AZ, 1989.

[28] T. Kawaguchi, J. Jura, N. Taneda, H. Hishikura and Y. Kokuba, J. Non-Cryst. Solids, 82, (1986), 50.

[29] R.K. Dwivedi, J. Mater. Sci. Lett., 5, (1986), 373.

[30] H.H. Macey, Tran. Brit. Ceram. Soc., 41, (1942), 73.

[31] F.H. Clews, *Heavy Clay Technology*, Academic Press, New York, 1969.

[32] L.L. Hench and J.K. West, Chem. Rev., 90, (1990), 33.

[33] C.J. Brinker and G.W. Scherer, *Sol-Gel Science*, Academic Press, New York, 1989.

[34] G. Hetherington, K.H. Jack and J.C. Kennedy, Phys. Chem. Glasses, 5, (1964), 130.

[35] T.A. Gallo and L.C. Klein, J. Non-Cryst. Solids, 82, (1986), 198.

[36] M.E. Nordberg, U.S. Patent 2,326,059 (1943).

[37] A.Dietzel, Naturwissenschaften, 31, (1943), 22.

[38] P.C. Schultz and H.T. Smyth, *Amorphous Materials*, R.W. Douglas and B. Ellis Eds., Wiley, New York, 1972, 452.

[39] S. Wang, Ph.D. Dissertation, University of Florida, 1988.

[40] K. Kamiya, S. Sakka and Y. Tatemichi, J. Mater. Sci., 15, (1980), 1765.

[41] A. Hardy, G. Gowda, T. McMaham, R.E. Riman, W.E. Rhines and H.K. Bowen, in *Ultrastructure Processing of Advanced Ceramics*, J.D. Mackenzie, D.R. Ulrich Eds., Wiley, New York, 1988, 407.

[42] H. Schmidt, J. Non-Cryst. Solids, 100, (1988), 51.

[43] H. Dislich, J. Non-Cryst. Solids, 80, (1986), 115.

[44] N. Tohge, G.S. Moore and J.D. Mackenzie, J. Non-Cryst. Solids, 63, (1984), 95.

[45] B.E. Yoldas, J. Non-Cryst. Solids, 38/39, (1980), 81.

[46] K. Kamiya and S. Sakka, J. Mater. Sci., 15, (1980), 2937.

[47] K. Kamiya and S. Sakka, J. Non-Cryst. Solids, 52, (1982), 357.

[48] S. Sakka and K. Kamiya, J. De Physique, 43, (1983), 235.

[49] K. Kamiya and S. Sakka, J. Chem. Soc. Jpn., 10, (1981), 1571.

[50] T. Hayashi, T. Yamada and H. Saito, J. Mater. Sci., 18, (1983), 3137.

[51] M. Emili, L. Incoccia, S. Mobilio, G. Fagherazzi and M. Guglilmi, J. Non-Cryst. Solids, 74, (1985), 129.

[52] M. Yamane, S. Inoue and K. Nakazawa, J. Non-Cryst. Solids, 48, (1982), 153.

[53] H. Morikawa, T. Osuka, F. Marumo, A. Yasumore, M. Yamane and M. Momura, J. Non-Cryst. Solids, 82, (1986), 97.

[54] C.J.R. Gozalez-Oliver, P.F. James and H. Rawson, J. Non-Cryst. Solids, 48, (1982), 129.

[55] L. Yuan and G. Yao, J. Non-Cryst. Solids, 100, (1988), 309.

[56] J. Cheng and D. Wang, J. Non-Cryst. Solids, 100, (1988), 288.

[57] C.P. Scherer and C.G. Pantano, J. Non-Cryst. Solids, 82, (1986), 246.

[58] Z. Deng, E. Breval and C.G. Pantano, J. Non-Cryst. Solids, 100, (1988), 364.

[59] W.T. Minehan, G.L. Messing and C.G. Pantano, J. Non-Cryst. Solids, 108, (1988), 163.

[60] M. Ramirez-Del-Solar, N. de la Rosa-Fox, L. Esquivias and J. Zarzycki, J. Non-Cryst. Solids, 121, (1990), 84.

[61] P.C. Schultz, J. Am. Ceram. Soc., 59, (1976), 214.

[62] D.L. Evans, J. Am. Ceram. Soc., 53, (1970), 418.

[63] L.L. Hench, at the 3rd International Conference on Ultrastructure Processing of Ceramics, Glasses and Composites, San Diego, February, 1987.

[64] J.E. Shelby, J. Am. Ceram. Soc., 55, (1972), 195.

[65] J.L. Bland, Acta. Cryst., 14, (1961), 875.

[66] R.B. Greegor, F.W. Lytle, D.R. Sandtrom, J. Wong and P. Schultz, J. Non-Cryst. Solids, 55, (1983), 27.

[67] D.R. Sandtrom, F.W. Lytle, P.S.F. Wei, R.B. Greegor, J. Wong and P. Schultz, J. Non-Cryst. Solids, 41, (1980), 201.

[68] C.F. Smith, Jr., R.A. Condrate Sr. and W.E. Votava, Appl. Spectroscopy, 29, (1975), 79.

[69] R.V. Ramaswamy, T. Chia, R. Srivastava, A. Miliou and J. West, *Proceedings of Society of Photo-Optical Instrumentation Engineer's Symposium on Innovative Science & Technology*, LA, CA, 1988.

[70] J.L. Noguès, S. Majewski, J.K. Walker, M. Bowen, R. Wojcik and W.M. Moreshead, J. Am. Ceram. Soc., 71, (1988), 1159.

[71] V.Y. Davydoo, L.T. Zhuravlev and A.V. Kieselev, Trans. Faraday Soc., 60, (1964), 2254.

[72] W.L. Vasconcelos, Ph.D. Dissertation, University of Florida, August, 1988.

[73] F. Wang, M.S. Thesis, University of Florida, 1988.

[74] J.K. West, B.F. Zhu, Y.C. Cheng and L.L. Hench, J. Non-Cryst. Solids, 121, (1990), 51.

[75] M.L. Lakhanpal and B.R. Puri, Nature, 172, (1953), 917.

[76] S. Wallace and L.L. Hench, in *Proceedings of 4th International Conference on Ultrastructure Processing of Ceramics, Glasses and Composites*, Tucson, AZ, 1989.

[77] E.A. Elias, M.S. Thesis, University of Florida, 1989.

[78] T. Demediuk and W.F. Cole, J. Am. Ceram. Soc., 43, (1960), 359.

[79] J.L. Woolfrey and M.J. Bannister, J. Am. Ceram. Soc., 55, (1972), 390.

[80] W.S. Young, S.T. Rasmussen and I.B. Cutler, in *Ultra-Fine Grain Ceramics*, J.J. Burke, N.L. Reed and V. Weiss Eds., Syracuse University Press, Syracuse, New York, 1970.

[81] W.S. Young and I.B. Cutler, J. Am. Ceram. Soc., 53, (1970), 659.

[82] M.J. Bannister, J. Am. Ceram. Soc., 51, (1968), 548.

[83] C.J. Brinker, G.W. Scherer and E.P. Roth, J. Non-Cryst. Solids, 72, (1985), 345.

[84] C.J. Brinker, G.W. Scherer and W.D. Drotning, in *Better Ceramics Through Chemistry*, C.J. Brinker, D.E. Clark and D.R. Ulrich, Eds., Elsevier, North Holland, New York, 1984.

[85] L.C. Klein and T.A. Gallo, J. Non-Cryst. Solids, 121, (1990), 119.

[86] C.J. Brinker and G.W. Scherer, J. Non-Cryst. Solids, 70, (1985), 301.

[87] C.J. Brinker and S.P. Mukherjee, J. Mater. Sci., 16, (1981), 1980.

[88] S. Brunauer, R.Sh. Mikhail and E.E. Bodor, J. Colloid and Interface Sci., 26, (1968), 54.

[89] W. Cao, R. Gerhardt and J.B. Watchman Jr., J. Am. Ceram. Soc., 71, (1988), 1108.

[90] S.P. Mukherjee, J.F. Cordaro and J.C. Debsikdar, Adv. Ceram. Mater., 3, (1988), 463.

[91] W. Vasconcelos, R.T. DeHoff and L.L. Hench, in *Proceedings of 4th International Conference on Ultrastructure Processing of Ceramics, Glasses and Composites*, Tucson, AZ, 1989.

[92] S. Wallace and L.L. Hench, Private Communication, 1989.

[93] M.F. Best and R.A. Condrate Sr., J. Mater. Sci. Lett., 4, (1985), 994.

[94] J. Arndt, J. Am. Ceram. Soc., 52, (1969), 285.

[95] S. Lowell and J.E. Schields, *Powder Surface Area and Porosity*, 2nd Ed., Champion and Hall, London, 1984.

[96] F.N. Rhines, Plansee Proceedings, 3rd Seminar, Reutte, Tyrol, (1958), 38.

[97] P.B. Macedo and T.A. Litovitz, J. Chem. Phys., 42, (1965), 245.

[98] D. Turnbull and M.H. Cohen, J. Chem. Phys., 34, (1961), 120.

[99] P.B. Macedo and A. Napolitano, J. Chem. Phys., 49, (1968), 1887.

[100] A.K. Doolittle, J. Appl. Phys., 22, (1951), 471.

[101] A.K. Doolittle and D.B. Doolittle, J. Appl. Phys., 26, (1957), 907.

[102] H. Vogel, Phys. Z., 22, (1921), 645.

[103] G.S. Fulcher, J. Am. Ceram. Soc., 8, (1925), 339.

[104] J.F. Bacon, A.A. Hasapis and J.W. Whooley, Phys. Chem. Glasses, 1, (1960), 90.

[105] R.W. Douglas and J.O. Isard, J. Soc. Glass Technol., 35, (1951), 206.

[106] J.D. Mackenzie, J. Am. Ceram. Soc., 46, (1963), 461.

[107] J. Arndt, Phys. Chem. Glasses, 24, (1983), 104.

[108] G.A. Pavlova and A.N. Amatuni, Inorg. Mater., 11, (1975), 1443.

[109] W.D. Kingery, H.K. Bowen and D.R. Uhlmann, *Introduction to Ceramics*, 2nd Ed., Wiley, New York, (1976), 658.

[110] L.L. Hench and J.K. West, *Electronic Principles of Ceramics*, Wiley, New York, 1990.

[111]M. Prassas, J. Phalippou and J. Zarzycki, in *Science of Ceramic Chemical Processing*, L.L. Hench and D.R. Ulrich, Eds., Wiley, New York, (1986), 156.

[112]G.J. Young, J. Colloid Sci., 13, (1958), 67.

[113]A.V. Kieselev, *Structure and Properties of Porous Materials*, Colston Papers, Butterworth, London, 10, (1958), 9.

[114]R.S. McDonald, J. Chem. Phys., 62, (1958), 1168.

[115]S. Hofmann, Surf. Interf. Sci., 9, (1986), 3.

[116]M. Anpo, H. Nakaya, S. Kodama, Y. Kubokawa, K. Domen and T. Qnishi, J. Phys Chem., 90, (1986), 1633.

[117]K. Shibata, T. Kiyoura, J. Kitagawa, T. Sumiyoshi and K. Tanabe, Bull. Chem. Soc. Jpn., 46, (1973), 2985.

[118]M. Laczka, W. Beier and L. Stoch, Glastech. Ber., 62, (1989), 9.

[119]E.R. Lippicott, A. Van Valkenburg, C.E. Weir and E.N. Bunting, J. Res. Natn. Bur. Stand., 61, (1958), 61.

[120]T.C. Chia, Private Communication, University of Florida, 1989.

[121]J.R. Ferraro, M.H. Manghnani and A. Quattrochi, Phys. Chem. Glasses, 13, (1972), 116.

[122]E. Grüneisen, Ann. Phys., 39, (1926), 257.

[123]P.T.T. Wong, F.L. Baudais and D.J. Moffatt, J. Chem. Phys., 84, (1986), 671.

[124]H.T. Smyth, J. Am. Ceram. Soc., 38, (1955), 140.

[125]A.J. Leadbetter, Phys. Chem. Glasses, 9, (1968), 1.

[126]H.R. Chandrasekhar and M. Chandrasekhar, Solid State Commun., 31, (1979), 329.

[127]B.G. Varshal, V.N. Denisov, B.N. Mavrin, G.A. Pavlova, V.B. Podobedov and Kh.E. Sterin, Opt. Spectrosc. (USSR), 47, (1979), 344.

[128]M.F. Best and R.A. Condrate Sr., J. Mat. Sci. Lett., 4, (1985), 994.

[129]L.W. Burggraj and L.P. Davis in *Better Ceramics Through Chemistry II*, C.J. Brinker, D.E. Clark and D.R. Ulrich Eds., Materials Research Society, Pittsburgh, PA, 73, (1986), 529.

[130]T.W. Zerda and G. Hoang, J. Non-Cryst. Solids, in press.

[131]T.K. West, S. Wallace, L.L. Hench and C.R. Lishawa, Quantum Calculations of Sol-Gel Silica Structure, in *Proceedings of 4th International Conference on Ultrastructure Processing of Ceramics, Glasses and Composites*, Tucson, AZ, 1989.

[132]W.G. Klemperer and S.D. Ramamurthi, in *Better Ceramics Through Chemistry III*, C.J. Brinker, D.E. Clark and D.R. Ulrich Eds., Materials Research Society, Pittsburgh, PA, 121, (1988), 1.

[133]G. Orcel and L.L. Hench, in *Science of Ceramic Chemical Processing*, L.L. Hench and D.R. Ulrich, Eds., Wiley, New York, (1986), 224.

[134]G. Orcel and L.L. Hench, J. Non-Cryst. Solids, 79, (1986), 177.

[135]Quantum Theory Project, University of Florida, Pgm No. 010183.

[136]W.G. Klemperer, V.V. Mainz, S.D. Ramamurthi and F.S. Rosenberg, in *Better Ceramics Through Chemistry III*, C.J. Brinker, D.E. Clark and D.R. Ulrich Eds., Materials Research Society, Pittsburgh, PA, 121, (1988), 15.

[137]K. Takahashi, J. Chem. Soc. Faraday Trans. I., 78, (1982), 2059.

[138]M.C. Zerner, G.H. Loew, R.F. Kirchner and U.T. Mueller-Westerhoff, J. Am. Chem. Soc., 102, (1980), 589.

BIOGRAPHICAL SKETCH

Yeu-Chyi Cheng was born August 25, 1959 in Tainan, Taiwan, Republic of China. She received her primary and secondary education in Taichung, Taiwan, R.O.C. In 1978, she graduated from Taichung Municipal Girl's Senior High School and entered National Tsing-Hua University in Hsin-Chu, Taiwan, Republic of China. She received her Bachelor of Science degree in materials science and engineering in 1981. In 1982, she was admitted to University of Florida, Department of Materials Science and Engineering, for her graduate study. She received her Master of Science degree in materials science and engineering in 1985. She entered the Ph.D program in Department of Materials Science and Engineering in 1986.

I certify that I have read this study and that in my opinion it conforms to acceptable standards of scholarly presentation and is fully adequate, in scope and quality, as a disseratation for the degree of Doctor of Philosophy.

Larry L. Hench, Chair
Graduate Research Professor
of Materials Science and
Engineering

I certify that I have read this study and that in my opinion it conforms to acceptable standards of scholarly presentation and is fully adequate, in scope and quality, as a disseratation for the degree of Doctor of Philosophy.

Joseph H. Simmons, Cochair
Professor of Materials
Science and Engineering

I certify that I have read this study and that in my opinion it conforms to acceptable standards of scholarly presentation and is fully adequate, in scope and quality, as a disseratation for the degree of Doctor of Philosophy.

David E. Clark
Professor of Materials
Science and Engineering

I certify that I have read this study and that in my opinion it conforms to acceptable standards of scholarly presentation and is fully adequate, in scope and quality, as a disseratation for the degree of Doctor of Philosophy.

Brij M. Moudgil
Professor of Materials
Science and Engineering

I certify that I have read this study and that in my opinion it conforms to acceptable standards of scholarly presentation and is fully adequate, in scope and quality, as a disseratation for the degree of Doctor of Philosophy.

Dinesh O. Shah
Professor of Chemical
Engineering

This dissertation was submitted to the Graduate Faculty of the College of Engineering and to the Graduate School and was accepted as partial fulfillment of the requirements for the degree of Doctor of Philosophy.

May, 1991

for Winfred M. Phillips
Dean, College of Engineering

Madelyn M. Lockhart
Dean, Graduate School